



Universitetet
i Stavanger

FACULTY OF SCIENCE AND TECHNOLOGY

MASTER'S THESIS

Study programme/specialisation: Biological Chemistry	Spring semester, 2018 Restricted Access
Author: Cecilie Lindseth	<i>Cecilie Lindseth</i> (signature of author)
Programme coordinator: Supervisor(s):	Peter Ruoff Hanne R. Hagland & Martin Watson
Title of master's thesis: Metabolic and Epithelial-To-Mesenchymal Transition Assessment of Colon Cancer Cell Lines	
Credits: 60 ECTS	
Keywords: biologisk kjemi, molekylær og cellebiologi, colorectal cancer, colon cancer cell line, cancer metabolism, oxidative phosphorylation, glycolysis, epithelial to mesenchymal transition, EMT, biomarkers, qPCR, gene expression	Number of pages: 96 + supplemental material/other: 19 Stavanger, 11.06.2018 date/year

UNIVERSITY OF STAVANGER

MASTER THESIS

**Metabolic and
Epithelial-To-Mesenchymal Transition
Assessment of Colon Cancer Cell Lines**

by

Cecilie Lindseth

A thesis submitted in partial fulfillment for the
degree of Master of Science in Biological Chemistry

in the

Department of Mathematics and Natural Sciences
Faculty of Science and Technology

Faculty Supervisor: Hanne R. Hagland

Co-supervisor: Martin Watson

June 2018

Declaration of Authorship

I, Cecilie LINDSETH, declare that this thesis titled, 'Metabolic and Epithelial-to-Mesenchymal Transition Assesment of Colon Cancer Cell Lines' and the work presented in it are my own. I confirm that:

- This work was done wholly or mainly while in candidature for a research degree at this University.
- Where any part of this thesis has previously been submitted for a degree or any other qualification at this University or any other institution, this has been clearly stated.
- Where I have consulted the published work of others, this is always clearly attributed.
- Where I have quoted from the work of others, the source is always given. With the exception of such quotations, this thesis is entirely my own work.
- I have acknowledged all main sources of help.
- Where the thesis is based on work done by myself jointly with others, I have made clear exactly what was done by others and what I have contributed myself.

Signed: Cecilie Lindseth

Date: 11/6-18

“Science is not meant to cure us of mystery, but to reinvent & reinvigorate it.”

Robert Sapolsky

Abstract

BACKGROUND: Cancer have varying dependency on oxidative phosphorylation and glycolysis, and cancer metastasis decreases the patient 5-year survival rate. Epithelial to mesenchymal transition (EMT) are demonstrated to increase the chances of metastasis. The purpose of this study was to characterize colon cancer cell lines and colorectal cancer patient samples by qPCR. To assess how the cells were affected in different glucose conditions and evaluate the development of cancer using a multimarker panel.

METHODS: Cell culture assay were used to check how glucose (high (4.5 g/L) and physiological (1.0 g/L)) affected the cell viability, proliferation and invasiveness. A multimarker panel consisting of metabolic and EMT markers were used to analyze cell cultures that had been cultured in different glucose concentrations, and patient samples from FFPE tissue blocks by qPCR. The multimarker panel was selected based on previous literature and analysis on cell lines. Multiplex PCR was done to analyze the patients DNA samples by checking if any EMT and MSI markers could be considered unstable.

RESULTS: Wound healing test showed that SW948 changed morphology and formed multilayers after applied tests, while SW1116 slowly began to heal by forming a monolayer. GLUT1 and LDHA yielded significantly upregulation of relative gene expression, while MCT4 yielded significantly downregulation of relative expression. Some of the EMT markers (N-cadherin, ZEB1, TWIST1, and Vimentin) only are expressed in the mesenchymal-like CCD-18Co cell, while E-cadherin are only expressed in the epithelial cells (SW1116 and SW948).

CONCLUSIONS: Glucose condition were found to affect the cells relative gene expression. GLUT1, LDHA, and MCT4 yielded significantly relative expression, and could be used as biomarkers for understanding the cell's metabolic profile. E-cadherin, N-cadherin, ZEB1, TWIST1 and Vimentin could be used as biomarkers to identify the cells phenotype, epithelial or mesenchymal.

Acknowledgements

First and foremost I would like to express my sincere gratitude to my main supervisor, Prof. Hanne R. Hagland, who has supported and encouraged me over the last few months. Her office door was always open when I ran into problems about my research or writing. She helped improve my knowledge and understanding of a subject I was not completely familiar with, and have given advises, insights and suggestions for my work. Also, appreciations to my co-supervisor Martin Watson, who have answered my endless number of questions, been patient with my lack of self-confidence while pushing me to work independent. He have given me a lot of guidance, explained the conventional analytic and technical aspect of the work, and trained my technical skills.

Thanks to my fellow master students, Sam Danby, Alexandra Szwedó and Hina Ahmad for making the whole laboratory work a pleasant experience, and being wonderful friends and colleagues with support through the year. A special thanks to Ansooya Bokil who have helped me with academic and moral support, and given complements and encouraging words, thereby helping me through tough times.

I would like to acknowledge and thank the academic staff at the Centre for Organelle research (CORE), who graciously helped with assistance in different laboratory work, answered questions, and taught me a few laboratory techniques. You all made it a great place to work, and I am grateful to everyone. Also I would like to thank the staff at the molecular biology lab and pathology lab (Stavanger University Hospital) for creating a welcoming work environment.

A profound gratitude to my friends and family for providing me with endless support and interest in my work. My parents and by brother have always been there for me, giving continuous encouragement throughout my years of study, and help me reach my goals. Finally, my deepest thank you to my beloved Reidar, you have been so understanding and supportive of my work, your patience and care means everything to me. Your support made this accomplishment possible, and I am lucky to have you.

Contents

Declaration of Authorship	i
Abstract	iii
Acknowledgements	iv
List of Figures	ix
List of Tables	xi
Abbreviations	xii
1 Introduction	1
1.1 Cancer	1
1.1.1 Colorectal Cancer	1
1.1.2 Pathogenesis in Colorectal Cancer	2
1.1.2.1 Chromosomal Instability (CIN)	2
1.1.2.2 Microsatellite instability and Elevated Microsatellite Alterations at Selected Tetranucleotide Repeats	3
1.1.2.3 CpG Island Methylator Phenotype (CIMP)	4
1.1.2.4 Wnt signaling pathway	4
1.1.2.5 TP53 Mutation and Loss of Heterozygosity (LOH)	5
1.1.2.6 PI3K/AKT/mTOR Pathway and PTEN	5
1.1.2.7 Reactive Oxygen Species (ROS)	5
1.1.3 Cancer Metabolism	6
1.1.4 Epithelial to Mesenchymal Transitions in Cancer	7
1.1.5 Cancer and Metformin	7
1.2 Biomarkers in Colorectal Cancer	8
1.2.1 Metabolic Biomarkers	8

1.2.2	Survivin as a Biomarker	10
1.2.3	Epithelial to mesenchymal biomarkers	11
1.3	Aim and Objectives	13
2	Materials and Methods	14
2.1	Materials	14
2.1.1	Cell Culture	14
2.1.2	Patient samples	15
2.1.3	Prepared solutions	15
2.1.4	Kits	16
2.1.5	Primers and probes for multiplex PCR and qPCR	16
2.1.6	Reagents and equipment	19
2.2	Methods	21
2.2.1	Cell Culture	21
2.2.1.1	Aseptic Technique	21
2.2.1.2	Resuscitation of Frozen Cell Lines	21
2.2.1.3	Subculture of Adherent Cell Lines	21
2.2.1.4	Cell Quantification	22
2.2.1.5	Cryopreservation of Cell Lines	23
2.2.1.6	Cell Viability and Proliferation assay	23
2.2.1.7	Wound healing assay	24
2.2.1.8	RNA extraction	24
2.2.2	DNA/RNA Extraction from FFPE with QIAcube	25
2.2.3	Precipitation of RNA with EtOH	26
2.2.4	Nucleic Acid Quantification	26
2.2.5	cDNA Synthesis	27
2.2.6	Multiplex PCR and Fragment analysis	28
2.2.7	Relative Gene Expression Analysis	29
2.2.7.1	Pre-Amplification	29
2.2.7.2	Real-time quantitative PCR (RT-qPCR)	29
2.2.8	Reference gene Stability	30
2.2.9	Amplification Efficiency	31
2.2.10	RNA Analysis	31
2.2.11	Data analysis	32

2.2.11.1	Relative Gene Expression (RGE)	32
2.2.11.2	Statistical Analysis	32
3	Results	33
3.1	Cell Culture assays	33
3.1.1	Cell lines Proliferation and Viability	34
3.1.2	Cell lines Wound Healing	38
3.2	Multiplex PCR of Patient Samples	42
3.3	Validation of Quantitative PCR	43
3.3.1	Cell line Expression of Markers	44
3.3.2	Stability analysis of Reference Genes	44
3.3.3	Amplification Efficiency of SYBR Green markers	46
3.3.4	Amplification Efficiency of TaqMan assays	48
3.4	Quantitative PCR Gene Expression	48
3.4.1	Relative Gene Expression of Cell lines	48
3.4.1.1	High and Low Glucose for 48 hours	48
3.4.1.2	High and Low Glucose for 72 hours	49
3.4.2	Applied Wound Healing	50
3.4.3	Metformin Treatments	51
3.4.3.1	Cell culturing as 2D and 3D	53
3.4.4	Relative Gene Expression of Patient Material	54
3.4.4.1	Patient Sample Quality	55
3.4.5	Pre-Amplification	56
4	Discussion	57
4.1	Cell Culture	57
4.1.1	Viability and Proliferation Related to Glucose Levels	57
4.1.2	Wound Healing Related to Glucose Levels	58
4.2	Multiplex PCR	59
4.3	Reference genes stability analysis	60
4.4	Validation of Quantitative PCR analysis	60
4.5	Quantitative PCR analysis	61
4.5.1	Cell Samples	61
4.5.2	Patient Samples	65
4.6	Future Perspectives	65

5 Conclusion	67
References	82
Appendix A	83
Appendix B	85
Appendix C	91
Appendix D	92
Appendix E	96
Appendix F	100

List of Figures

1.1	Development of colorectal cancer from a normal cell to cancer metastasis	2
1.2	Metabolic pathway, including metabolic biomarkers	9
1.3	Electron transport chain (ETC)	10
1.4	Epithelial to mesenchymal transition (EMT)	11
1.5	AXL (tyrosine kinase membrane receptor)	12
2.1	Counting cells with Bürker heamocytometer	22
2.2	RNeasy Mini kit workflow	25
2.3	QuantiTect Reverse Transcription kit workflow	27
3.1	Methods workflow used in this study	33
3.2	Cells viability	34
3.3	Cell growth of SW1116 (P14) at 24, 48 and 73 hours	35
3.4	Proliferation of SW1116 (P14, P16, P23) at 48 and 72 hours	35
3.5	Cell growth of SW948 (P17) at 24, 48 and 72 hours	36
3.6	Proliferation of SW948 (P15, P16, P20, P25) at 48 and 72 hours	36
3.7	Cell growth of CCD-18Co (P16) at 24, 48 and 72 hours	37
3.8	Proliferation of CCD-18Co (P14, P16) at 48 and 72 hours	38
3.9	Wound healing over time for SW1116 (P19)	39
3.10	Measured wound area over time for SW1116 (P18, P19, P14)	39
3.11	Wound healing over time for SW948 (P26)	40
3.12	Measured wound area over time for SW948 (P25, P26, P13)	40
3.13	Wound healing over time for CCD-18Co (P16)	41
3.14	Measured wound area over time for CD-18Co (P16)	42
3.15	Expression of markers in cell lines	44
3.16	Distribution of Cq values for reference genes	45

3.17	Average expression stability (M)	46
3.18	Amplification efficiency of SYBR Green assays.	47
3.19	Relative gene expression for cells cultured for 48 hours	49
3.20	Relative gene expression for cells cultured for 72 hours	50
3.21	Relative gene expression for cells extracted after wound healing assay	51
3.22	Relative gene expression for SW948 treated with metformin	52
3.23	Relative gene expression for SW1116 treated with metformin	53
3.24	Relative gene expression for SW948 and SW1116 (2D and 3D)	54
3.25	Cq differences for pre-amplification	56
1	Population and viability profiles	83
2	EMAST positive for ACRO067	86
3	EMAST negative for ACRO157	87
4	MSI-High for ACRO067	89
5	Microsatellite stable (MSS) for ACRO067	90
6	Standard curves for SYBR green markers amplification efficiencies (1).	93
7	Standard curves for SYBR green markers amplification efficiencies (2).	94
8	Standard curves for SYBR green markers amplification efficiencies (3).	95
9	Standard curves for TaqMan assays amplification efficiencies	95
10	RNA integrity analysis	101

List of Tables

2.1	Information about cell lines	14
2.2	Kits, manufacturer, catalog number and their uses.	16
2.3	EMAST markers used for instability analysis with multiplex PCR . . .	17
2.4	MSI markers used for instability analysis with multiplex PCR	17
2.5	SYBR Green Gene Expression Primers	18
2.6	TaqMan Gene Expression Assays.	19
2.7	Reagents and equipment used in experiments	19
2.8	Cell suspension dilution table	23
2.9	Reagents used and their position in QIAcube.	26
2.10	Reverse Transcription reaction master mix	28
2.11	Reaction mix volumes for RT-qPCR with SYBR Green.	29
2.12	RT-qPCR cycling mode for SYBR Green.	30
3.1	Result of EMAST and MSI analysis	43
3.2	Amplification efficiency (E) for SYBR Green markers	47
3.3	Amplification efficiency of TaqMan Assays (E).	48
3.4	Bioanalyzer result for normal tissue samples	55
3.5	Bioanalyzer result for tumor tissue samples	55
1	Wound healing measurements	84
2	Average expression stability (M) value and coefficient of variation (CV)	91
3	Relative gene expression of cell lines after 48 hours	97
4	Relative gene expression of cell lines after 72 hours	98
5	Relative gene expression of cell lines after wound healing assay	99

Abbreviations

AMP;ADP;ATP	Adenosine mono;di;tri-phosphate
cDNA	Complementary DNA
CIMP	CoG island methylator phenotype
CIN	Chromosomal instability
CRC	Colorectal Cancer
DNA	Deoxyribonucleic acid
ECM	Extracellular matrix
EGFR	Epidermal growth factor receptor
EMAST	Elevated microsatellite alterations at selected tetranucleotide repeats
EMT	Epithelial to Mesenchymal Transition
ETC	Electron transport chain
FAD	Flavin adenine dinucleotide
GLUT	Glucose transporter
KRAS	Kirsten rat sarcoma viral oncogene homolog
LDH	Lactate dehydrogenase
LOH	Loss of Heterozygosity
MCT	Monocarboxylate transporter
MET	Mesenchymal to Epithelial Transition
MMR	DNA mismatch repair system
MSI	Microsatellite instability
MSS	Microsatellite stable
NAD	Nicotinamide adenine dinucleotide
OXPHOS	Oxidative phosphorylation
PI3K	Phosphoinositide 3-kinase
PTEN	Phosphatase and tensin homolog
RGE	Relative Gene Expression
RNA	Ribonucleic acid
ROS	Reactive oxygen species
RTP	Receptor tyrosine kinase
RT-qPCR	Real-time quantitative Polymerase Chain Reaction
SUCLA	Succinate-CoA ligase ADP-forming beta subunit
T2D	Type 2 Diabetes
TCA	Tricarboxylic acid cycle
UCP	Uncoupling Protein
WNT	Wingless-type MMTV integration site family

*Dedicated to those who have been there for me,
offering unconditional love and support.*

Chapter 1

Introduction

1.1 Cancer

Cancer is a collective term for diseases that exhibit uncontrolled growth. Common cancer are lung, breast, blood, skin and colon [1]. With more than 8 million cancer deaths each year (2012), it is considered a global health concern, with colorectal cancer (CRC) as one of the most predominant cancer types worldwide [2].

The word cancer comes from the Greek word *karcinos*, meaning “crab”, and is a process of uncontrolled cell mutations that produce a tumor which in turn produce new colonies of cancer cells at adjacent tissues and metastasize [3]. Earlier cancer was thought to be a single illness, but now it is considered to be several diseases with multiple causes and therefore, available treatments are generally drastic, poorly selective and in many situation not curative. In the seventeenth century, a milestone in cancer research treatment arose, when Wilhelm Fabricius provided adequate descriptions of operations for several cancer types [4]. The ability to diagnose cancer at an early stage, allows for more effective treatments and increases the survival rate.

1.1.1 Colorectal Cancer

Colorectal cancer in Norway has approximately 4000 new cases and 1500 deaths per year [5]. Mortality records for CRC are substantially lower than the number of incidents per year, in less developed regions the mortality rate of CRC is however significantly higher [2].

Colorectal cancer risk factors are similar to general cancer risk factors like health, environment and lifestyle. Lifestyle factors such as obesity, heavy alcohol consumption and smoking increase the chance of CRC to develop. Additionally, genetic risk factors such as chromosomal instability (CIN), microsatellite instability (MSI) and inherited syndromes like Lynch syndrome and familial adenomatous polyposis (FAP) also impacts the development of the disease [6, 7].

Detection and diagnosis at an early stage increases the overall survival rate due to improved treatments, however, approximately half of the patients with CRC will experience metastasis, either at time of diagnosis or as a recurrent disease. Nearly 90 % of all cancer deaths are caused by development of metastasis. Patients with cancer metastasis are not suited for normal treatments, and thus have a poorer 5-year survival rate [8]. The most common metastatic sites for colorectal cancer are liver and lungs, but carcinomas from CRC can metastasize to almost any organ in the body [9].

1.1.2 Pathogenesis in Colorectal Cancer

Most of colorectal cases occur sporadically (approximately 75%). Sporadic CRC usually develops by CIN, but can also be developed by MSI or CpG Island Methylator phenotype (CIMP). Other known mutations increases the risk of CRC, like mutations in APC, KRAS and p53 (Figure 1.1) and different pathways like Wnt signaling and PI3K/AKT [10].

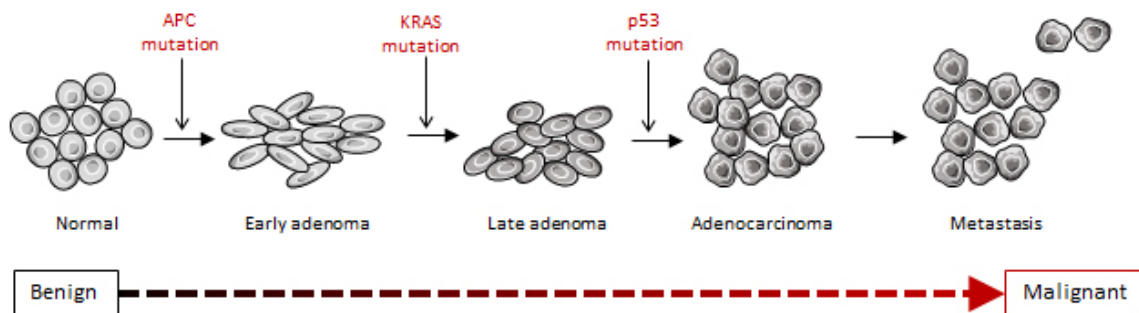


FIGURE 1.1: Development of colorectal cancer from a normal cell to cancer metastasis. Black downwards arrows represent mutation causing error in growth and repair mechanism of cells, thus inducing metastasis.

1.1.2.1 Chromosomal Instability (CIN)

The chromosomal instability pathway is the first distinct pathway in genomic instability that is recognized in colorectal cancer. Genomic changes occur at a chromoso-

mal level, and may include insertions, inversions, deletions and rearrangements with the activation of KRAS and the inactivation of different tumor suppressor genes (such as APC, p53 and loss of heterozygosity (LOH)) [10, 11].

1.1.2.2 Microsatellite instability and Elevated Microsatellite Alterations at Selected Tetranucleotide Repeats

The microsatellite instability is the second genomic instability phenotype determined for colorectal cancer. DNA sequences composed of mono-, di-, tri-, or tetranucleotide repeats are named microsatellites, but are often referred to as short tandem repeats (STRs). Mismatch repair (MMR) deficiency in sporadic CRC is mainly due to epigenetic silencing of the MMR genes by CpG methylation [11, 12].

DNA polymerase are enzymes that build DNA and proofread for errors during DNA replication. Human DNA mismatch repair (MMR) system functions to repair single nucleotide miss-pairs and slippage mistakes at the sequences [13]. If a few errors are not detected by DNA polymerase, MMR system tries to repair the DNA. Deficiency in MMR system will leave nucleotide sequences longer or shorter, called MSI and EMAS [10].

The MMR system are comprised of several proteins that interact to repair the DNA (Mut S homologue (MSH2, MSH3, MSH6), Mut L homologue (MLH1 and MLH3) and post-meiotic segregation (PMS1 PMS2)). MSH2 forms heterodimer with MSH6 (MutS α) and with MSH3 (MutS β), these complexes have different abilities to bind to DNA mismatches, MutS α recognizes single base-pair mismatches and single insertion-deletion loops (LDLs), and MutS β have increased ability to bind to larger LDLs [14, 15].

A panel of five mono- or tetranucleotide microsatellites are used to characterize tumors. The panel consisting of mononucleotides are shown to be quasimonomorphic in normal DNA, and are selective for MSI mutations [16], while the panel consisting of tetranucleotide microsatellites are shown to be highly polymorphic in their DNA, and are selective for EMAS mutations. Bethesda Guidelines are used for identification of MSI mutations (no marker unstable, microsatellite stable (MMS, one marker unstable, MSI-L (low frequency), more than one marker unstable MSI-H (high-frequency)) [16, 17]. EMAS guidelines are similar, EMAS- (negative) if one or no markers are unstable, and EMAS+ (positive) if more than one marker are unstable. EMAS causes frameshift mutations from tetranucleotides, and believed to be a result of MSH3 dysfunction, with its MutS β complex [13, 14].

1.1.2.3 CpG Island Methylator Phenotype (CIMP)

Cytosine-phosphate-Guanine (CpG) Island Methylator Phenotype, are the third and last genetic instability phenotype recognized in CRC. Epigenetics of CIMP are related to modification of nucleic acid and chromatin components other than mutations, and have potential to alter gene expression by silencing [11]. Nucleotides with high frequency of CpG sites, called CpG islands, and are often located in the promoter area of human genes [11]. In healthy cells CpG sites often are methylated, while they are unmethylated in cancer, however, they may become hypermethylated, causing inappropriate silencing of gene expression. The process is thought to deregulate expression of important genes, causing cancer development [18]. The classic panel for CIMP positive tumors can be divided into two types, CIMP-high (BRAF mutations and MLH1 methylation) and CIMP-low (KRAS mutations and MSS) [12].

1.1.2.4 Wnt signaling pathway

The Wnt signaling pathway is one of the key regulators in crucial aspects of cell fate determination, migration, polarity, neural patterning and organogenesis during the development of embryos [19]. Wnt pathway are associated with cancer development, due to mutations that promote constitute activation of Wnt signaling [20]. The pathway are commonly divided into canonical (Wnt/ β -catenin) and independent or non-canonical signaling (Planar Cell Polarity pathway and Wnt/ Ca^{2+} pathway) [19, 21].

A mutation of the Wnt pathway increase signal activity, and mutations can be inherited or acquired. In colorectal cancer the most commonly mutated gene is the Adenomatous polyposis coli (APC). The gene is classified as a tumor suppressor gene that produces APC protein, which controls β -catenin concentrations and interacts with E-cadherin [21]. An inherited inactivating mutation in APC gene causes Familial adenomatous polyposis (FAP), and increases the risk of colorectal cancer. APC mutation leads to accumulation of β -catenin and β -catenin mutations that prevent degradation, both leads to excessive cell proliferation that favor tumor cell over normal epithelial cells [22]. Wnt/ β -catenin relies on the transcriptional co-factor β -catenin a protein found interacting with cytoplasmic tails of cadherins in the cell membrane.

1.1.2.5 TP53 Mutation and Loss of Heterozygosity (LOH)

A common mutated gene is TP53 which is involved in control of cell cycle and apoptosis. p53 protein induces cell cycle arrest and DNA repair prior to DNA replication, and if necessary induces cell death [10]. The mutation is believed to occur in the transition from adenoma to cancer, and are found to undergo missense mutations in tumors. In these mutation a single nucleotide are substituted by another type [23].

Loss of heterozygosity are loss of one of the two alleles of a gene, and remaining allele are often mutated. LOH in chromosome 18q21 are frequently observed in advanced CRC. The deleted in colorectal carcinoma (DCC) gene are located on the long arm of chromosome 18, and encodes a transmembrane protein, which is a conditional tumor suppressor gene. DCC contributes to normal processes of apoptosis, and when mutated an abnormal cell survival is a common result [10].

1.1.2.6 PI3K/AKT/mTOR Pathway and PTEN

Phosphoinositide 3-kinases (PI3K)/AKT/mammalian target of rapamycin (mTOR) is an intracellular EGFR (epidermal growth factor receptor) mediating signal pathway important for cell cycle. PI3K activates AKT through phosphorylation; once AKT (protein kinase B) is activated it phosphorylates and activates mTOR and many other proteins [10]. In various cancer this pathway is overactive, therefore allowing proliferation of cancer cells and reducing apoptosis. Phosphatase and tensin homolog (PTEN) gene regulates the PI3K/AKT signaling pathway by inhibition of AKT via hyperactivation of PI3K signaling. PTEN gene is activated in cancer, and therefore negatively regulates the signaling pathway [10].

1.1.2.7 Reactive Oxygen Species (ROS)

Reactive oxygen species (ROS) is a byproduct of mitochondrial oxidative phosphorylation. An excel in nutrient uptake without converting to aerobic glycolysis, could lead to increased ROS formation [24]. ROS are short lived unstable molecules, which cause cellular damage by reacting rapid and spontaneous with other molecules. Reactive oxygen species damages DNA, and activate signaling pathways which may lead to cancer progression [25].

1.1.3 Cancer Metabolism

Gene and protein expression of cancer cells may be highly diverse, even though they have some commonalities. In 2000, Hanahan and Weinberg published a paper called “Hallmarks of Cancer”, which include six biological traits that characterize the development and progression of malignant tumors [26]. These traits are sustaining proliferative signaling, evading growth suppressors, resisting apoptosis, enabling replicative immortality, inducing angiogenesis, and activating invasion and metastasis [26]. Hanahan and Weinberg later published a follow-up article with two additional hallmarks (deregulating cellular energetics and avoiding immune destruction) and two characteristics of neoplasia (Genome instability and mutation and tumor-promoting inflammation) [27]. One of these traits, metabolic reprogramming (deregulating cellular energetics), support that cancer cells have changed its metabolism to sustain a rapid uncontrolled cell growth, is important for a wider understanding of all the other traits published.

Healthy cells have their primary energy production through mitochondrial oxidative phosphorylation (OXPHOS) during aerobic conditions, producing 36 adenosine triphosphate (ATP) molecules per glucose molecule. While tumor cells mostly rely on glycolysis for energy production even under aerobic conditions, glycolysis is less efficient in terms of ATP production (producing 2 ATP molecule per glucose), termed the Warburg effect [28]. Warburg thought that the increased glycolysis was caused by defective mitochondrial machinery [29]. This have in more recent publications been disproven, and research have shown important links between cancer cell metabolism involving the mitochondria and its tumor growth abilities [30, 31]. The Warburg effect is considered as a result of mutations in oncogenes and tumor suppressor genes that are responsible for malignant transformation, and not the cause. These changes in metabolism are a fundamental cause of cancer and are known as the Warburg hypothesis.

Mitochondrial dysfunctions are identified in various human diseases, including diabetes mellitus, cardiomyopathy, kidney failure and cancer. Mutations or changes to the mitochondria can cause tumorigenesis, suppressed mitochondrial respiration by stimulated glycolysis, and thereby facilitate tumor progression [32, 33]. Facilitating tumor progression may be done by at least three different means. First, solid tumor cells seems to build up hypoxic microenvironment, and therefore the cells will have reduced oxygen requirements, second, reactive oxygen species as a byproduct of OXPHOS, a shift to glycolysis may reduce the formation of ROS, and third, the glycolytic phenotype increases lactate formation, and acidifying the tumor environment [32].

1.1.4 Epithelial to Mesenchymal Transitions in Cancer

Elizabeth Hay researched how cells assemble into functional tissue to shape the embryo, which in 1967 led to realization of the importance of EMT in the embryonic development [34]. Epithelial to mesenchymal transition (EMT) was first recognized and described as a distinct process in 1982 by Greenberg and Hay [35]. EMT is a process where epithelial cells lose their cell polarity and the adherens junctions, thereby gaining migratory and invasive properties as mesenchymal cells. Mesenchymal to epithelial transition (MET) describe the reverse process of EMT, and it occurs at different stages of morphogenesis. The junctions keep the epithelial cells tightly bound to neighbor cells, and when connection is lost, cells can invade and migrate through the extracellular matrix (ECM) [36]. Cells experience profound changes in their cytoskeleton architecture, needed for migratory properties. The transition is important for various processes, such as germ formation and neural tube (precursor to the central nerve system) formation, wound healing, but also plays an important role in initiation of cancer metastasis [37].

Three distinct biological types of EMT were proposed at Cold Spring Harbor Laboratories in 2008, classified depending on the phenotype output [38]. Type 1 EMT generates various cell types that share common mesenchymal phenotypes and generate organs, as well as affecting implantation and embryo formation. Type 2 EMT is part of a repair-associated event to generate fibroblast to reconstruct tissues, and therefore associated with wound healing, tissue regeneration and organ fibrosis. Type 3 EMT involves progression of primary cancer cells to metastatic cells, leading to cancer progression [38, 39].

The EMT process represses E-cadherin, a cell adhesion molecule and induces mesenchymal markers like vimentin and N-cadherin to acquire a mesenchymal phenotype with mobility. During CRCs later stages, cancer acquire cancer cells to be more aggressive, invasive and metastatic, which is why EMT are proposed as an important step [12]. Transforming growth factor- β (TGF- β) turn out to be responsible for inducing EMT, but also the Wnt/ β -catenin signaling pathway and loss of E-cadherin are considered as major effectors of epithelial to mesenchymal transition [12].

1.1.5 Cancer and Metformin

Metformin is an insulin-sensitizer oral antidiabetic drug used for treatment of type 2 diabetes (T2D). A possible connection between diabetes and cancer were made in 1934 by Marble [40]. During the last two decades, different studies have shown that

patients with T2D have higher incidences of tumor development, are less sensitive to chemotherapy and have a higher mortality risk compared with a healthy person [41–44]. Metformin treatment studies within epidemiology show a significant decrease compared with diabetics treated with insulin or sulfonylureas, for both incidences of tumors and mortality rate. Metformin is demonstrated to have positive effect on tumors, both *in vitro* and *in vivo*, by repressing proliferation of cancer cells and inducing apoptosis [44, 45].

1.2 Biomarkers in Colorectal Cancer

The National Cancer Institute (NCI) defines biomarker as: “a biological molecule found in blood, other body fluids, or tissues that is a sign of a normal or abnormal process, or of a condition or disease. A biomarker may be used to see how well the body responds to a treatment for a disease or condition. Also called molecular marker and signature molecule” [46]. Biomarkers can be used to help diagnose cancer at an early stage, determine how aggressive the disease is, and identify which drug will respond to the patients [47]. They can also offer quantitative ways to determine if individuals are predisposed to a particular cancer type, making them a popular area of cancer research.

1.2.1 Metabolic Biomarkers

GLUT, also known as Solute carrier family 2 facilitated glucose transporter member 1 (SLC2A1), is a protein that is embedded in the outer membrane of a cell. It transports glucose molecules into the cells from the blood, and starts the process of converting it to energy. Several studies have demonstrated over-expression of GLUT1 in various carcinomas [48–51]. It therefore appear as cancer cells alter GLUT1 expression levels in correlation to increased hypoxic stress [51].

Cancerous cells produce their energy through a high rate glycolysis according to Warburg’s effect, which would lead to a build up of lactic acid. Lactic acid is an important metabolite in the body, and must rapidly be transported out of the cells after production [28, 52]. Monocarboxylate transporter 4 (MCT4), also known as solute carrier family 16 member 3 (SLC16A3), catalyzes the transport of excess lactate out of the cell membrane.

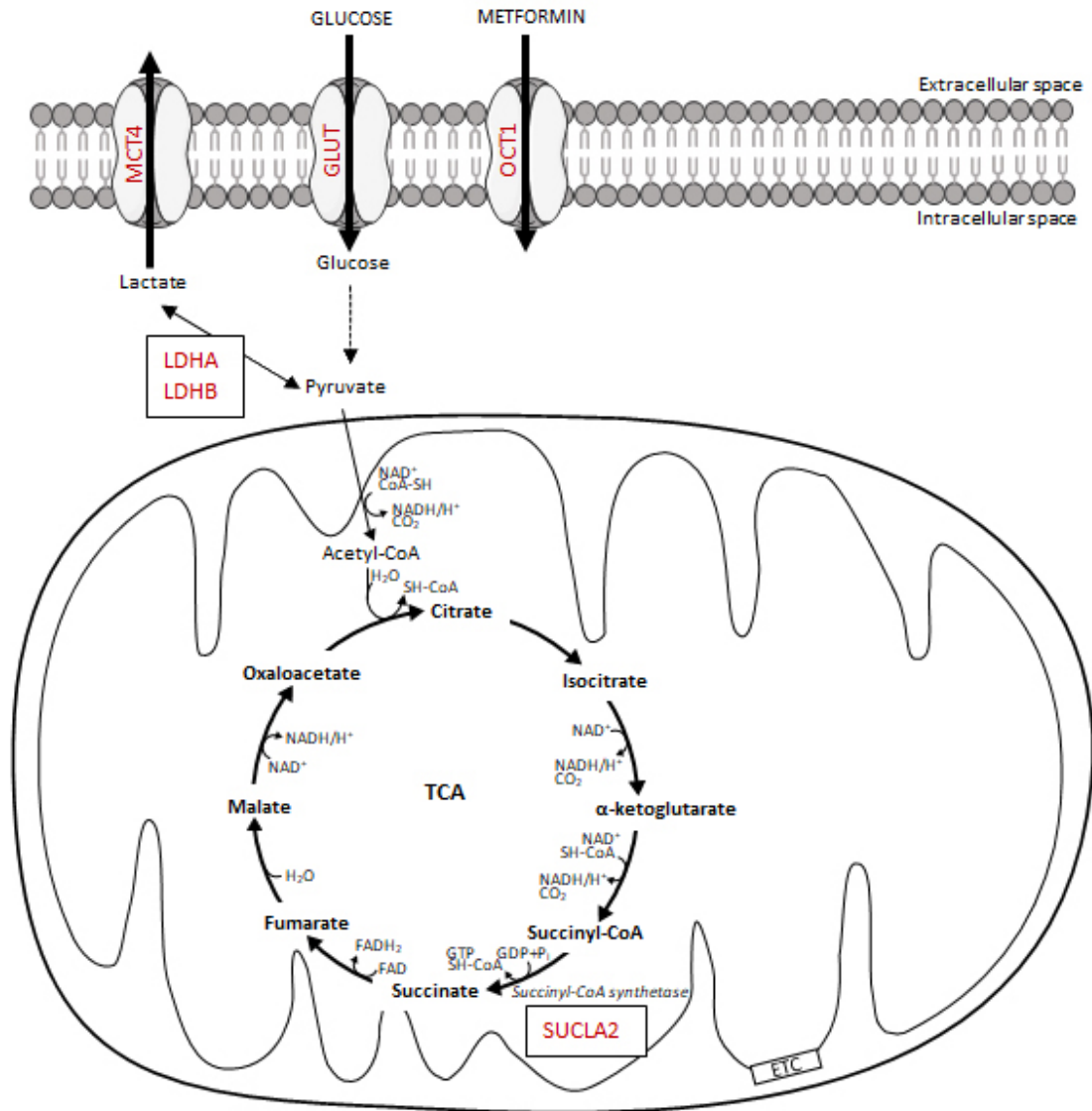


FIGURE 1.2: Metabolic pathway, including metabolic biomarkers. Membrane transporter proteins (MCT4, GLUT1 and OCT1), carries molecules in and out of the cell, lactate dehydrogenase (LDHA and LDHB), breaks down pyruvate to lactate, tricarboxylic acid (TCA) cycle is the location where SUCLA2 convert succinyl-CoA to succinate, and placement of ETC in the mitochondrial membrane.

Lactate dehydrogenase (LDH) is an enzyme that catalyzes the interconversion of pyruvate and lactate with concomitant interconversion of NADH and NAD⁺ [53]. Various combinations of LDHA and LDHB make up different forms of the enzyme, which is important for chemical reactions to produce energy through the body. Pyruvate is the end product of glycolysis, and during absence of oxygen is converted to lactate, with high lactate concentrations the enzyme exhibit feedback inhibition so the rate of conversion is decreased [53].

During the tricarboxylic acid (TCA) cycle, Succinyl-CoA ligase (SUCL) converts succinyl-CoA to succinate, while forming ATP or GTP [54]. Succinate-CoA ligase

ADP-forming beta subunit (SUCLA2) makes up a beta subunit of SUCL. Mutations are associated with mitochondrial dysfunctions, like genetic defects and ontogenetic signaling [54].

An organic cation transport (OCT) protein mediates transport of organic cations, such as the oral insulin-sensitizing drug, metformin [55, 56]. OCT1 belongs to the solute carrier family 22 member 1 (SLC22A1). Previously published articles shows that OCTs could be associated with developmental mechanisms for tumors and could indicate cancer advancement [55].

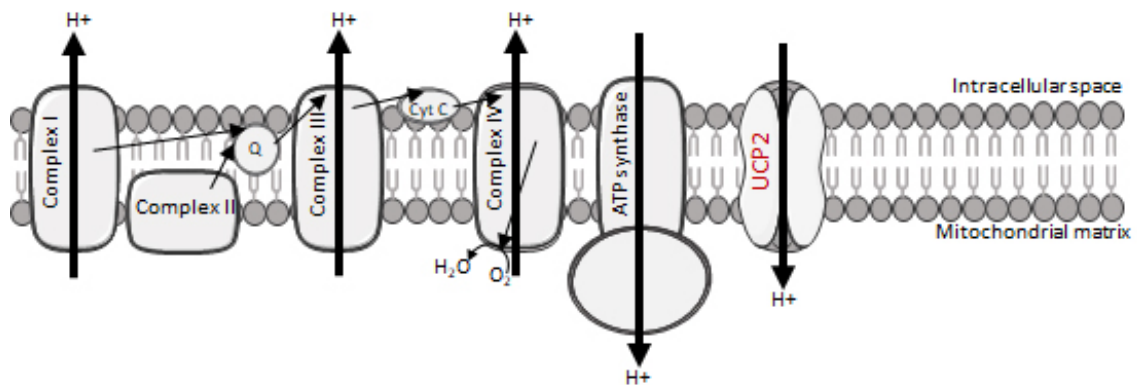


FIGURE 1.3: Electron transport chain (ETC). Different complexes are presented alongside the uncoupling protein 2 (UCP2) transporter, which reduces the membrane potential and ATP formation via ATP synthase.

Uncoupling proteins (UCP) are encoded by UCP2 gene, and located in mitochondrial inner membrane as a regulated proton channel or transporter, probably alongside ATP synthase proton channel. Uncoupling proteins reduce the mitochondrial membrane potential by allowing flow of protons into the inner mitochondrial membrane, thus reducing membrane potential and ATP formation due to formation of energy as heat [57]. It has been suggested that UCP2 is involved in pathogenesis of diabetes, obesity and cancer. Elevated UCP levels are shown to be present in various aggressive human cancer, increases chemoresistance and serves as a tumor promoter during early tumorigenesis [57, 58].

1.2.2 Survivin as a Biomarker

Survivin, also known as Baculoviral IAP repeat containing 5 (BIRC5) is a member of the inhibitor of apoptosis (IAP) family. Survivin inhibits caspase activation, thereby preventing apoptosis or programmed cell death, but it is also highly expressed during mitosis of the cell cycle [59]. Gene expression is high in transformed cell lines and most human tumors [60].

1.2.3 Epithelial to mesenchymal biomarkers

BIRC5 is a target gene of Wnt pathway and upregulated by β -catenin (CTNNB1). β -catenin acts as an intracellular signal transducer in Wnt signaling pathway. It is a subunit of cadherin protein complex and has a dual role in EMT by linking cadherins to cytoskeleton and being a transcriptional activator with T cell factor [61]. Mutations in this gene give rise to many cancer types, including colorectal carcinoma [62]. Gene expression associated with EMT are controlled by the β -catenin/TCF/LEF complex [61].

Cadherins, or calcium-dependent adhesion are a type of cell adhesion molecule (CAM) or surface marker, and is important for the adherens junctions that bind cells together. Different members of the cadherin family are found on different locations, CDH1, are found in epithelial tissues (E-cadherin) and CDH2, are found in neurons (N-cadherin). During cancer progression cadherin switches between expression of E- and N-cadherin, varying the cells from epithelial to mesenchymal types [63]. Loss of E-cadherin functions promotes EMT [61].

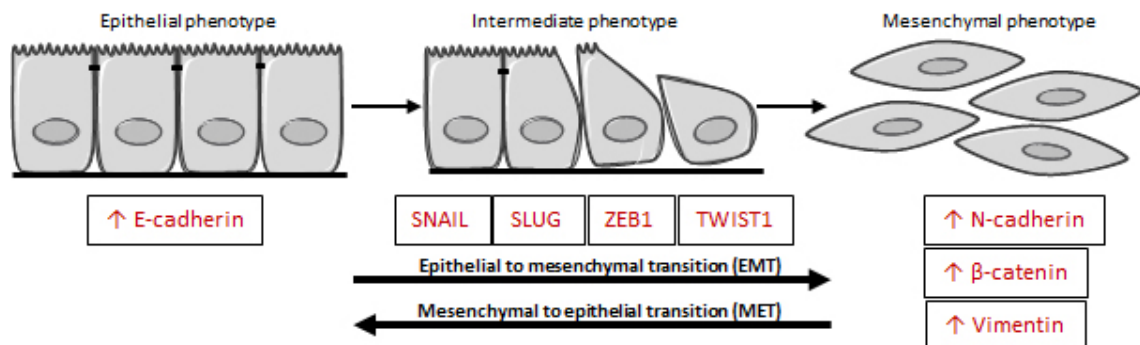


FIGURE 1.4: Epithelial to mesenchymal transition (EMT). Includes a few EMT markers used in this study (CDH1/2, SNAI1/2, ZEB1, TWIST1, VIM and CTNNB1).

Zink finger proteins, SNAI1 (often referred to as SNAIL) and SNAI2 (often called SLUG) are members of the Snail family. Both of them are transcriptional repressors that are important mediators of EMT and are involved in tumor progression [64]. Both SNAI1 and SLUG recruit proteins to the E2 boxes of target genes to form a transcriptional repression complex that suppresses the transcription of SNAI1 target genes [65]. SNAI1s main action mode is inducing EMT by suppression of E-cadherin transcription, responsible for cell adhesion and migratory properties. Repression via silencing RNA results in decreased tumor metastasis, immunosuppression, and increased T-cell response in tumors due to suppression of SNAI1 [66]. SLUG have similar activities, including E-cadherin transcriptional repression and anti-apoptotic activities, and it plays a crucial role in organogenesis and neutralization [66].

Zinc finger E-box binding homeobox 1 (ZEB1) is a zinc finger transcription factor, responsible for DNA binding. ZEB1 can induce EMT in carcinoma cells and thereby promote tumor invasion and metastasis. This is done by binding to the E-box located in the encoding E-cadherin promoter, leading to repression of CDH1 transcription [67].

TWIST1 gene encodes a basic helix loop helix (bHLH) transcription factor, which forms hetero- and homodimers that bind to DNA E-box sequences and regulate transcription of genes involved in cranial structure closure. In various types of cancers this gene is hypermethylated and overexpressed, and the encoded protein promotes tumor cell invasion and metastasis by suppressing expression of E-cadherin and inducing EMT [68].

VIM gene encodes type III intermediate filament protein called vimentin. The protein are responsible for maintaining cell shape and integrity of the cytoplasm and stabilizing cytoskeleton interactions. The cytoskeleton interactions are made by intermediate filament, microtubules and actin microfilaments. Vimentin is overexpressed during EMT, and increases tumor growth and invasion, linking VIM to a metastatic phenotype with poor prognosis [69].

The protein encoded by AXL receptor tyrosine kinase is a member of the Tyro-Axl-Mer (TAM) receptor tyrosine kinase (RTK) subfamily. AXL binds to growth arrest-specific 6 (Gas6), and transduce signals from the extracellular matrix to the cytoplasm, presented in Figure 1.5 [70]. AXL are involved in several cellular processes critical for cell growth, development, migration and invasion caused by EMT. The genes relevance to cancer, makes the cancer more aggressive, and correlates to poorer outcome, due to metastasis [71].

The metabolic elements described and presented in Figure 1.2 and Figure 1.3 could be used to predict response to metabolism-targeting drugs, and determine the metabolic profile of cancer cells. The epithelial-mesenchymal transition elements described and presented in Figure 1.4 and Figure 1.5 could characterize what type of transition the cancer cell are in, and if a patient have a higher risk of cancer metastasis.

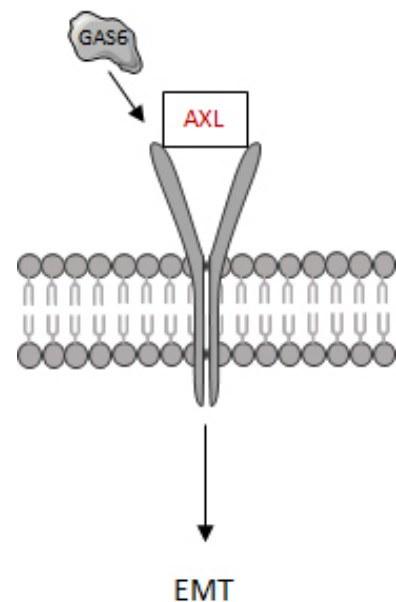


FIGURE 1.5: AXL (tyrosine kinase membrane receptor). Overexpression of AXL gene, coupled with Gas6, can induce EMT

1.3 Aim and Objectives

The overall aim of this project was to assess if metabolic phenotype in colon cancer cell lines correlated to their ability for epithelial to mesenchymal transition. The objectives of this project was to:

- study whether different glucose growth conditions (high (4.5 g/L) and physiological (1.0 g/L)) affect metabolic phenotype and EMT,
- check whether glucose growth conditions affect the cell lines invasiveness,
- multiplex PCR for identifying EMASST and/or MSI mutations in normal versus tumor tissue samples,
- gene expression with comparison between high and physiological glucose conditions for cell lines with metabolic and EMT markers,
- gene expression with metabolic and EMT markers to check for differences between normal and tumor patient samples, and
- investigate potential differences or associations between the glucose growth conditions.

Chapter 2

Materials and Methods

2.1 Materials

2.1.1 Cell Culture

Three different cell cultures are used in this study, SW1116, SW948, and CCD-18Co. The European Collection of Authenticated Cell Cultures (ECACC) catalog numbers and the American Type Culture Collection (ATCC) number are listed in Table 2.1.

TABLE 2.1: Information about cell lines. ECACC and ATCC number for cell lines, as well as their primary sources and morphology.

Cell Line	ECACC #	ATCC #	Primary Source	Morphology
SW1116	87071006	CCL-233	A grade II adenocarcinoma of the colon of a 73 year old Caucasian male	Epithelial
SW948	91030714	CCL-237	A grade III adenocarcinoma of the colon of an 81 year old Caucasian female	Epithelial
CCD-18Co	90070503	CRL-1459	A biopsy colon tissue of a black female infant	Fibroblast

Of the two colorectal cancer cell lines researched in this study, SW948 have shown to have a highly glycolytic profile, while SW1116 have a more OXPHOS dependent profile. These profiles are established through previously unpublished work from research group at CORE, with group leader and thesis supervisor Hanne R. Hagland.

The different cell lines have been grown in nutrient rich and growth factor supplemented medium of high (4.5 g/L) and physiological (1.0 g/L) glucose levels. Normal

glucose levels in blood ranges from 4-11 mM, and 1.0 g/L are approximately 5.6 mM, thereby physiological condition. The high glucose medium contains 4.5 g/L glucose and are approximately 22.2 mM, which is within the range (11.2-25 mM) of normal culture conditions for cancer metabolism studies. The high glucose levels gives the cells hyperglycemic growth conditions, similar to diabetes mellitus conditions. The two different environments for cells were used to assess the effect of glucose related to growth, and their genetic expression with qPCR.

In this experiment, cells were kept in recommended medium (Dulbecco's Modified Eagle Medium (DMEM)) that contained 2mM L-glutamine, and no sodium bicarbonate, 10% fetal bovine serum (FBS) and 5% antibiotics (penicillin/streptomycin). Cells were constantly incubated at 37°C with 5% CO₂ in a humidified incubator (SANYO CO2 incubator (MCO-18AIC), SANYO Electric Co., Japan). The different cell lines were cultured to 70% confluence before passaging for continued growth or culture assays.

2.1.2 Patient samples

Approximately 200 patients diagnosed with colorectal cancer were supposed to be analyzed in this study. One tumor and one normal samples were obtained from each patient, and stored as formalin-fixed, paraffin-embedded (FFPE) tissue sample blocks. The FFPE tissue samples have been operated surgically, analyzed by experienced pathologists, and belongs to the regional ethics committee (REC) biobank.

DNA and RNA have been extracted from patients FFPE tissue samples, and different comparative analysis have been conducted. The DNA have been checked for EMAS^T and MSI mutations, by comparing tumor sample to the normal sample. RNA where to be measured with qPCR to check gene expression with a multimarker panel consisting of metabolic and EMT markers.

2.1.3 Prepared solutions

Medium for cell lines:

- 500 ml Dulbecco's Modified Eagle Medium (DMEM)
- 10 % Fetal bovine serum (FBS)
- 2 mM L-Glutamine

- 5 U/ml Penicillin/streptomycin

1x PBS, 500 ml

- 1 PBS tablet
- 500 ml ddH₂O

1 M Glucose, 50 ml

- 9.01 g Glucose
- 50 ml ddH₂O

1x Tris-EDTA (TE) buffer, 100 ml

- 1 ml 100x TE buffer
- 99 ml ddH₂O

2.1.4 Kits

A few different kits have been used in this study; their catalog number and use are listed in Table 2.2 below.

TABLE 2.2: Kits, manufacturer, catalog number and their uses.

Kit	Manufacturer	Catalog Number	Use
Count & Viability Kit	MUSE	MCH600103	Cell count
RNeasy mini kit	QIAGEN	74104/06	RNA extraction
AllPrep DNA/RNA FFPE kit	QIAGEN	80234	Extract DNA/RNA
Type-it Microsatellite PCR kit	QIAGEN	206241/43/46	Multiplex PCR
Quantitect Reverse transcription kit	QIAGEN	205313	Reverse transcription
Agilent RNA 6000 Nano Kit	Agilent Technologies	5067-1511	RNA quality analysis
SSOAdvanced PreAmp Supermix	BIORAD	172-5160	Pre-amplification
Power Up SYBR Green Master Mix	Applied Biosystems	A25742	Real-time qPCR
TaqMan Fast Advanced Master Mix	Applied Biosystems	4444557	Real-time qPCR

2.1.5 Primers and probes for multiplex PCR and qPCR

Multiplex PCR analysis are conducted with five different markers for each of the stability analysis; EMASST markers are described in Table 2.3 and MSI markers are

described in Table 2.4. Both tables shows the forward and reverse sequence of the primer, amplicon length and the 5' fluorescent label.

TABLE 2.3: EMAST markers used for instability analysis with multiplex PCR. Forward and reverse sequences, amplicon length and 5' fluorescent label.

Marker		Sequence (5'-3')	Amplicon length	Label
NR-27	Fwd.	AAC CAT GCT TGC AAA CCA CT	85 bp	VIC
	Rev.	CGA TAA TAC TAG CAA TGA CC		
NR-21	Fwd.	GAG TCG CTG GCA CAG TTC TA	105 bp	6-FAM
	Rev.	CTG GTC ACT CGC GTT TAC AA		
NR-24	Fwd.	GCT GAA TTT TAC CTC CTG AC	124 bp	PET
	Rev.	ATT GTG CCA TTG CAT TCC AA		
BAT-25	Fwd.	TAC CAG GTG GCA AAG GGC A	146 bp	VIC
	Rev.	TCT GCA TTT TAA CTA TGG CTC		
BAT-26	Fwd.	CTG CGG TAA TCA AGT TTT TAG	178 bp	NED
	Rev.	AAC CAT TCA ACA TTT TTA ACC C		

TABLE 2.4: MSI markers used for instability analysis with multiplex PCR. Forward and reverse sequences, amplicon length and 5' fluorescent label.

Marker		Sequence (5'-3')	Amplicon length	Label
D20S85	Fwd.	TGG GAG TAT CCA GAG AGC TAT T	146 bp	VIC
	Rev.	CCA CTG TAC TCC AGC ATG AAT		
MYCL1	Fwd.	TGG CGA GAC TCC ATC AAA G	181 bp	6-FAM
	Rev.	CCT TTT AAG CTG CAA CAA TTT C		
D8S321	Fwd.	GAT GAA AGA ATG ATA GAT TAC AG	237 bp	PET
	Rev.	ATC TTC TCA TGC CAT ATC TGC		
D20S82	Fwd.	GCC TTG ATC ACA CCA CTA CA	249 bp	VIC
	Rev.	GTG GTC ACT AAA GTT TCT GCT		
D9S242	Fwd.	GTG AGA GTT CCT TCT GGC	178 bp	NED
	Rev.	ACT CCA GTA CAA GAC TCT G		

SYBR Green Primer Assays were used for gene expression analysis of different cell lines, with RRN-18S, ACTB and HSP90AB as reference genes, and 17 different target genes, described in Table 2.5. All these assays are supplied lyophilized from QIAGEN and are reconstituted with 1.1 ml TE buffer.

TaqMan Gene Expression Assays are used for gene expression analysis for 2D and 3D cultured SW948 and SW1116. ACTB and POLR2 are reference genes, SUCLA2 is a target genes, all described in Table 2.6.

TABLE 2.5: SYBR Green Gene Expression Primers

Gene Symbol	Gene Aliases	Gene Name	QuantiTect Assay	Primer	Catalog number	Amplicon Length
ACTB	BRWS1; PS1TP5BP1	Actin, beta	Hs_ACTB_2_SG		QT01680476	104 bp
RRN18S		18S ribosomal RNA	Hs_RRN18S_1_SG		QT00199367	149 bp
HSP90AB1	HSP84; HSPC2; HSPCB; D6S182; HSP90B	heat shock protein 90kDa alpha family class B member 1	Hs_HSP90AB1_2_SG		QT01679790	81 bp
CDH1	UVO; CDHE; ECAD; LCAM; Arc-1; BCDS1; CD324	Cadherin 1, type 1, E-cadherin (epithelial)	Hs_CDH1_1_SG		QT00080143	84 bp
CDH2	CDHN; NCAD; CD325; CDw325	Cadherin 2, type 1, N-cadherin (neuronal)	Hs_CDH2_1_SG		QT00063196	102 bp
SNAIL	SNA; SNAH; SNAIL; SLUGH2; SNAIL1; dJ710H13.1	Snail family zinc finger 1	Hs_SNAI1_1_SG		QT00010010	131 bp
SNAIL2	SLUG; WS2D; SLUGH; SLUGH1; SNAIL2	Snail family zinc finger 2	Hs_SNAI2_1_SG		QT00044128	119 bp
AXL	ARK; UFO; JTK11; Tyro7	AXL receptor tyrosine kinase	Hs_AXL_1_SG		QT00067725	110 bp
ZEB1	BZP; TCF8; AREB6; FECD6; NIL2A; PPCD3; ZFHEP; ZFH1A; DELTAEF1	Zinc finger E-box binding homeobox 1	Hs_ZEB1_2_SG		QT01888446	105 bp
TWIST1	CRS; CSO; SCS; ACS3; CRS1; BPES2; BPES3; SWCOS; TWIST; bHLHa38	Twist family bHLH transcription factor 1	Hs_TWIST1_1_SG		QT00011956	127 bp
CTNNB1	EVR7; CTNNB; MRD19; armadillo	catenin (cadherin-associated protein), beta 1, 88kDa	Hs_CTNNB1_1_SG		QT00077882	130 bp
VIM	CTRCT30, HEL113	Vimentin	Hs_VIM_1_SG		QT00095795	94 bp
SLC2A1	CSE; PED; DYT9; GLUT; DYT17; DYT18; EIG12; GLUT1; HTLVR; GLUT-1; SD-CHCN; GLUTIDS	Solute carrier family 2 (facilitated glucose transporter), member 1	Hs_SLC2A1_1_SG		QT00068957	77 bp
SLC16A1	MCT3; MCT4; MCT 3; MCT 4; MCT-3; MCT-4	Solute carrier family 16 (monocarboxylate transporter), member 3	Hs_SLC16A3_1_SG		QT00085855	140 bp
SLC22A1	OCT1; HOCT1; oct1_cds	Solute carrier family 22 (organic cation transporter), membrane 1	Hs_SLC22A1_1_SG		QT00019572	120 bp
SUCLA2	A-SCS; A-BETA; MTDPS5; SCS-betaA	Succinate-CoA ligase, ADP-forming, beta subunit	Hs_SUCLA2_1_SG		QT00102788	118 bp
LDHA	LDHM; GSD11; PIG19; HEL-S-133P	lactate dehydrogenase A	Hs_LDHA_1_SG		QT00001687	102 bp
LDHB	LDH-B; LDH-H; LDHBD; TRG-5; HEL-S-281	lactate dehydrogenase B	Hs_LDHB_1_SG		QT00071512	141 bp
UCP2	UCPH; BMIQ4; SLC25A8	Uncoupling protein 2 (mitochondrial, proton carrier)	Hs_UCP2_1_SG		QT00014140	117 bp
BIRC5	API4; EPR-1	baculoviral IAP repeat containing 5	Hs_BIRC5_2_SG		QT01679664	105 bp

TABLE 2.6: TaqMan Gene Expression Assays.

Gene Symbol	Gene Aliases	Gene Name	TaqMan Assay ID	Catalog number	Amplicon Length
<i>ACTB</i>	BRWS1, PS1TP5BP1	actin beta	Hs00357333_g1	4331182	77 bp
<i>POLR2A</i>	POLR2, POLRA, RPB1, RPBh1, RPO2, RPOL2, RpI-ILS, hRPB220, hsRPB1	RNA polymerase II subunit A	Hs00172187_m1	4331182	61 bp
<i>SUCLA2</i>	A-BETA, MT-DPS5, SCS-betaA	succinate-CoA ligase ADP-forming beta subunit	Hs01597886_g1	4351372	89 bp

2.1.6 Reagents and equipment

Reagents and equipment used in experiments for this study are listed in Table 2.7.

TABLE 2.7: Reagents and equipment used in experiments. * denotes Dulbecco's Modification of Eagle's Medium.

Material	Manufacturer	Catalog No.	Use
DMEM* (4.5 g/L glucose)	Corning	15-017-CVR	Cell culture
DMEM* (No glucose)	Corning	17-207-CVR	Cell culture
L-Glutamine 200mM	Corning	25-005-CL	Cell culture
0.25% Trypsin/EDTA	Sigma	T4049-500ML	Cell culture
Fetal Bovine Serum	Biowest	S181H-500	Cell culture
Penicillin-Streptomycin	Biowest	L0018-100	Cell culture
Phosphate-Buffered Saline	Life technologies	18912-014	Cell culture
Dimethyl Sulfoxide (DMSO)	Applichem	A3671.0100	Cell culture
D-(+)-Glucose	Sigma	G7021-1KG	Cell culture
50ml Centrifuge Tubes	VWR	525-0402	Cell culture
15ml Centrifuge Tubes	VWR	525-0400	Cell culture
75cm ² Tissue Culture Flask	Corning	353136	Cell culture
25cm ² Tissue Culture Flask	Corning	353108	Cell culture
Tissue culture 6-well plates	VWR	734-2323	Cell culture
SANYO CO ₂ incubator	SANYO electric Co., Japan	MCO-18AIC	Cell culture
Trypan Blue Solution, 0.4%	Amresco	K940-100ML	Cell count
Count & Viability Assay Kit	MUSE	MCH600103	Cell count
AllPrep DNA/RNA FFPE kit	QIAGEN	80234	Extract DNA/RNA from FFPE tissue samples

Continued on next page

Table 2.7 – Continued from previous page

Material	Manufacturer	Catalog No.	Use
QIAcube	QIAGEN	9001292	DNA/RNA extraction and purification
Rneasy mini kit	QIAGEN	74104	Extract RNA from cells
QIAshredder	QIAGEN	79654	Cell lysate homogenization
Type-it Microsatellite PCR kit	QIAGEN	206243	Multiplex PCR
Genetic Analyzer	Applied Biosystems	3130xl	Fragment analyzer
QuantiTect Reverse transcription kit	QIAGEN	205313	Reverse transcription
T100 Thermal Cycler	Bio-Rad	1861096	Thermal cycler
ImageJ software	National Institutes of Health	V 1.51j8	Microscopy analysis
NanoDrop One/OneC	Thermo Fisher Scientific	ND-ONE-W	RNA quantification
Agilent RNA 6000 Nano Kit	Agilent Technologies	5067-1511	RNA analysis
2100 Bioanalyzer	Agilent Technologies	G2939BA	RNA analysis
TE buffer	Borrowed from a lab at CORE		Reconstitute SYBR green assays
Expert software	Agilent Technologies	G2939BA	RNA analysis
QuantiTect Primer Assays	QIAGEN	249900	qPCR
Power Up SYBR Green Master Mix	Applied Biosystems	A25742	qPCR
TaqMan Fast Advanced Master Mix	Applied Biosystems	4444557	qPCR
SSOAdvanced PreAmp Super-mix	Bio-Rad	172-5160	Pre-amplification
96-well plates	BRAND	781365	qPCR
LightCycler 96	Roche	5815916001	qPCR
LightCycler software	Roche Diagnostics International Ltd	V 1.1.0.1320	qPCR

2.2 Methods

2.2.1 Cell Culture

Three different cell lines (see Table 2.1) were used in this study. A few different assays were done to establish an understanding of the responses mediated by the cell lines under different growth conditions.

2.2.1.1 Aseptic Technique

All techniques used for cell culture was performed according to aseptic technique, to prevent bacteria and fungi contamination and cross contamination with other cell lines. All experiments are done in a dedicated cell culture lab, negatively pressurized relative to the adjoined areas, gowns and shoe covers were required for further protection. Hands were washed thoroughly, gloves were used and sanitized with 70% ethanol solution. A laminar flow cabinet was used for all experiments, and also sterilized with 70% ethanol prior to and after use, followed by UV decontamination. Additionally, equipment and materials (media bottles, pipette tip boxes, racks and solutions) were disinfected (70% ethanol) prior to placing them in the cabinet.

2.2.1.2 Resuscitation of Frozen Cell Lines

A cryotube with frozen cells was removed from the cryotank, and thawed in a 37°C water bath for approximately 2 minutes. The content was then transferred into a T75 flask containing pre-warmed medium and incubated at 37°C with 5% CO₂ in a humidified incubator.

2.2.1.3 Subculture of Adherent Cell Lines

Cell cultures were observed in an inverted microscope to assess the degree of confluency and confirm absence of contaminants. The culture medium was carefully removed, then cells were rinsed with pre-warmed (37°C) 1xPBS (phosphate-buffered saline) to remove any fetal bovine serum (FBS), from culture flask (FBS inactivates trypsin), before removing the PBS. Trypsin/EDTA heated to 37°C was added to the culturing flask and incubated at 37°C for 3-12 minutes, depending on cell line. When cells were detached, they were resuspended with fresh medium (volume higher than trypsin). The suspension was mixed thoroughly by pipetting up and down to

ensure single-cells suspension. A portion of the cell suspension was transferred to a new flask containing fresh media. This volume depends on cell number, which again depends on the rate of growth for the cell lines being passaged.

2.2.1.4 Cell Quantification

Cells were brought into suspension with trypsin/EDTA and resuspended in fresh medium. A small aliquot of suspension was removed to perform cell count with haemocytometer (Figure 2.1) and/or MUSE Count & Viability Assay kit.

HAEMOCYTOMETER: An equal amount of Trypan Blue was added to the suspension (50 μl of each), and mixed gently by pipetting. The haemocytometer was cleaned, the cover slip moisten with water and placed over the chamber. 20 μl cell suspension/Trypan blue mix was used to fill the chambers, and x20 magnification phase contrast was used with an inverted microscope. If possible, >100 viable cells (bright and unstained cells) were counted for each sample, to increase the accuracy of the cell count, dead cells was stained blue, and counted for viability estimate. The following equation was used to calculate cells per ml:

$$\text{Viable cells per ml} = \frac{\text{Number of live cells}}{\text{Number of large squares (1mm)}} \times \text{dilution factor} \times 10,000$$

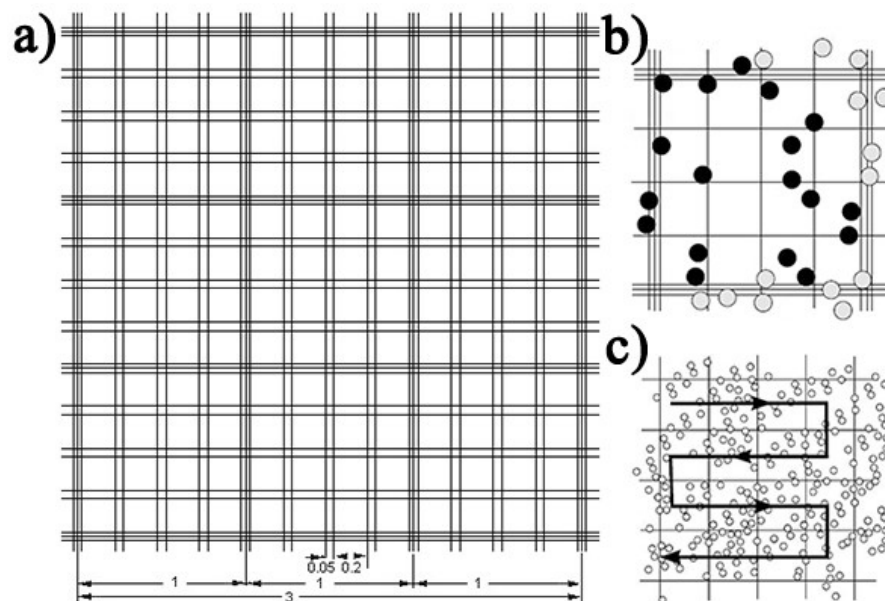


FIGURE 2.1: Counting cells with Bürker haemocytometer. a) Layout and dimension of the counting chamber, b) demonstrate which cells to count for the current square, to avoid recounting, and c) show the order of counting to prevent missing squares (Images: Laboroptik [72]).

MUSE COUNT & VIABILITY ASSAY KIT: According to the concentration of original cell suspension (cells/ml), the recommended volume of Muse Count & Viability reagent was added to each sample tube, followed by the appropriate volume of cell suspension (Table 2.8). The suspension and reagent were incubated for 5 minutes at room temperature, before samples were analyzed with the Muse cell analyser (Merck Millipore) according to the manufacturers protocol [73].

TABLE 2.8: Cell suspension dilution table. *Further dilution may be necessary for highly concentrated cell suspensions.

Concentration of original cell suspension	Dilution factor	Cell suspension volume	Count & viability reagent volume
1x10 ⁵ to 1x10 ⁶ cells/ml	10	50 μ l	450 μ l
1x10 ⁶ to 1x10 ⁷ cells/ml	20	20 μ l	380 μ l
1x10 ⁷ to 2x10 ⁷ cells/ml	40*	20 μ l	780 μ l

2.2.1.5 Cryopreservation of Cell Lines

Cells were harvested with a confluency of at least 70 %. The cells were brought into suspension using trypsin/EDTA and resuspended in fresh medium. A small aliquot of suspension was removed to perform cell count. The suspension remaining after count was centrifuged (5 min, 900 rpm) and the pellet was resuspended in freeze medium (80 % DMEM, 10 % FBS, 10 % DMSO) at a concentration of 1x10⁶ cells/ml. Aliquots of 1 ml were pipetted into cryotubes with correct labeling and placed in freezer (-80°C) overnight, then the cryotubes were transferred to liquid nitrogen storage in the cryotank.

2.2.1.6 Cell Viability and Proliferation assay

Cells with a confluency of >70% were brought to suspension using trypsin/EDTA and resuspended in fresh medium. A small aliquot of suspension was removed to perform cell count, and 1x10⁵ cells/well (6-well plate). The cells were treated with high (4.5 g/L) and physiological (1.0 g/L) glucose medium, and cultured for 48 and 72 hours at 37°C, before the cell number was determined for both live and dead cells. The growth over time has been normalized (Equation 2.1) to the control (0 hours) and put into graphs with cell proliferation in percentage versus time. The

doubling time have been calculated with Equation 2.2.

$$\text{Normalization} = \frac{n_f}{n_i} \times 100 \quad (2.1)$$

where:

n_i = initial cell number

n_f = cell number at 48 and 72 hours

$$\text{Doubling time} = \frac{(t_f - t_i) \times \log(2)}{\log(n_f) - \log(n_i)} \quad (2.2)$$

where:

t_i = initial time

t_f = final time

n_i = initial concentration

n_f = final concentration

2.2.1.7 Wound healing assay

Cells were seeded onto 6-well plates, where each of the wells were marked on the bottom for composition the images at approximately the same place each time. The cells are cultured to confluency in high (4.5 g/L) and physiological (1.0 g/L) glucose levels, and then the cells were scraped with a 200 μ l pipette (one whole line across each well). Images were taken and analyzed (ImageJ, with wound healing tool) after different time intervals (from 0h to cells started growing back together). Analysis are performed to check the cells invasiveness, and RNA was extracted after cells have started growing into the initial scratched area.

2.2.1.8 RNA extraction

Medium was carefully removed from the 6-well plate, with subsequent gentle washing with pre-heated (37°C) 1xPBS before 350 μ l RNeasy Lysis Buffer (RLT) were added to produce RNA lysate. The lysate was homogenized using the QIAshredder homogenizer columns by centrifuging the columns at maximum speed for 2 minutes. Flow through was transferred to RNeasy Mini spin column and purification of total

RNA performed as described by the manufacturer and summarized in Figure 2.2 [74].

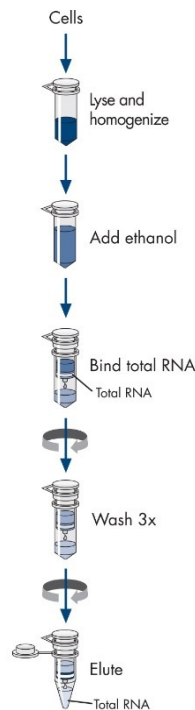


FIGURE 2.2: RNeasy Mini kit workflow [74].

2.2.2 DNA/RNA Extraction from FFPE with QIAcube

Following experienced pathologists inspection, tumor and normal tissue sections were extracted from formalin-fixed paraffin-embedded (FFPE) tissue sample blocks, by cutting excess paraffin off the samples, and slicing the FFPE block to 20 μm thick slices with a microtome. This sample cohort is part of a larger project led by PhD. student M. Watson. The prepared samples were placed in a 1.5 ml Safe-Lock microcentrifuge tube, and the lid was closed.

The paraffin where removed by xylene and step 1-9 were performed according to the protocol in the AllPrep DNA/RNA FFPE Handbook [75], this step gives supernatant for RNA purification and pellet for DNA purification. The supernatant was transferred to a 2 ml safe-lock microcentrifuge tube and placed onto the QIAcube, with the required reagents (Table 2.9, RNA reagents) according to the protocol sheet. The pellet was resuspended in 180 μl Buffer ALT, digested with 40 μl proteinase K and incubated for 1 hour at 56 $^{\circ}\text{C}$ and 2 hours at 90 $^{\circ}\text{C}$ before the lysate was transferred to a 2 ml safe-lock microcentrifuge tube and placed in the QIAcube with the required reagents (Table 2.9, DNA reagents) according to the protocol

sheet.

TABLE 2.9: Reagents used and their position in QIAcube.

Position	RNA reagents	DNA reagents
1	Buffer RLT	-
2	96-100% ethanol	Buffer ALT
3	-	96-100 % ethanol
4	Buffer FRN	Buffer AW1
5	Buffer RPE	Buffer AW2
6	RNase-free water	Buffer ATE

2.2.3 Precipitation of RNA with EtOH

The RNA supernatant obtained after RNA purification with QIAcube, was added 3 NaOAc μ l, which reacts with the nucleotides in the pellets making them precipitate. 100 μ l ice cold 100% ethanol was added to the tube and kept at -80°C for 24 hours. The samples were centrifuged at full speed at 4°C for 30 minutes, followed by 2x washing with ice cold 75% ethanol (20 minutes centrifuging at 4°C). Ethanol was removed, and tubes placed in water bath at 37°C for approximately 10 minutes to ethanol had vaporized. The pellet was resuspended in 30 μ l nuclease free water.

2.2.4 Nucleic Acid Quantification

Before DNA and RNA samples were frozen, they were measured for concentration and quality with NanoDrop 2000c (patient samples) and NanoDrop One (cell cultures), both manufactured by Thermo Fisher Scientific [76].

The NanoDrop spectrophotometers reports nucleic acid concentration and two absorbance purity ratios (A260/A280 and A260/A230). The concentration are based on modified Beer's Law equation using corrected nucleic acid absorbance value and purity ratios. Purity ratios are based on ratios of corrected absorbance at 260 nm to corrected absorbance at 280 nm or 230 nm. An A260/A280 purity ratio of 1.8 is considered pure for DNA, while a ratio of 2.0 is considered pure for RNA. An A260/A230 ratio between 1.8 and 2.2 are generally accepted as pure for both DNA and RNA. The purity ratios are sensitive for contaminants, and if present in the samples it affect the purity ratios with a lower number.

2.2.5 cDNA Synthesis

Extracted RNA was reverse transcribed to produce cDNA for gene expression analysis. The RNA template and reagents in the QuantiTect reverse transcription kit were thawed on ice. The genomic DNA elimination reaction was prepared on ice with a final volume of 14 μ l for each reaction, according to Table 2.10.

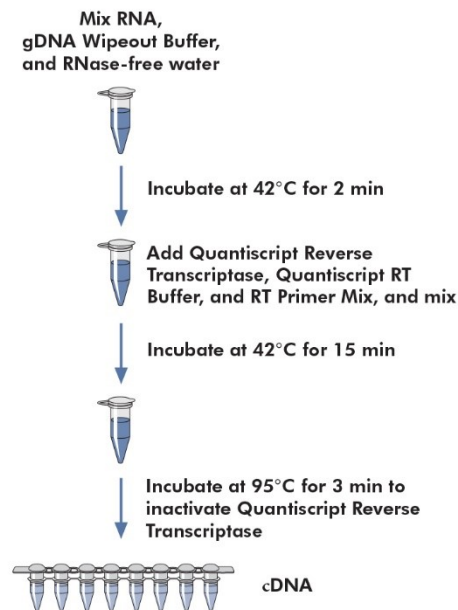


FIGURE 2.3: QuantiTect Reverse Transcription kit workflow [77].

The sample tubes were incubated for 2 minutes at 42°C in a thermal cycler and placed immediately on ice. While the sample was on ice, the reverse-transcription reaction master mix was prepared according to Table 2.10, and added to the sample. The tubes were incubated for 15 minutes at 42°C, followed by 3 minutes at 95°C on the thermal cycler, as described in manufacturers protocol, and presented in the workflow in Figure 2.3. The reverse-transcription reactions were stored at -20°C until qPCR was performed.

TABLE 2.10: Reverse Transcription reaction master mix.^aUp to 1 μg , ^bContains RNase inhibitor, ^cIncludes Mg^{2+} and dNTPs.

Component	Volume
gDNA Wipeout Buffer	2 μl
RNA ^a	variable
RNase-free water	variable
<i>Genomic DNA elimination reaction volume</i>	<i>14 μl</i>
Quantiscript Reverse Transcriptase ^b	1 μl
Quantiscript RT Buffer ^c	4 μl
RT Primer Mix	1 μl
<i>Reverse-transcription reaction master mix volume</i>	<i>6 μl</i>
Total reaction volume	20 μl

2.2.6 Multiplex PCR and Fragment analysis

The extracted DNA (section 2.2.2) was amplified with Type-it Microsatellite PCR reaction mix according to the manufacturer's instructions, with 5' fluorescently labeling of the markers [78]. Five tetranucleotide microsatellite primer pairs (EMAST: D20S85, MYCL1, D8S321, D20S82, D9S242) and five mononucleotide microsatellite primer pairs (MSI: NR-27, NR-21, NR-24, BAT-25, BAT-26) were used. Primers sequences, amplicon sizes and fluorescent dyes are provided in Table 2.3 and Table 2.4. The PCR cycling conditions were 5 min activation at 95°C, 35 cycles at 95°C for 30 s (denaturation), annealing for 40 s at 52°C (EMAST) or 30 s at 55°C (MSI), extension for 30 s at 72°C (EMAST) or 70°C (MSI), followed by a final extension for 30 min at 60°C.

The PCR product was analyzed with a capillary electrophoresis, 3130xl Genetic Analyzer (Applied Biosystems), with GeneMapper software based on their fragment lengths. Tumor and normal samples were compared within the same patient samples. Those showing extra peaks at tetranucleotide markers (EMAST) and/or mononucleotide markers (MSI) were scored as unstable for the specific marker.

Samples showing instability in one out of five markers was scored as EMAST-negative and/or MSI-Low, while instability in at least two out of five markers were scored EMAST-positive and/or MSI-High. If no markers were showing instability, the sample was defined as microsatellite stable (MSS) or EMAST-negative.

2.2.7 Relative Gene Expression Analysis

SYBR Green primer assays (Table 2.5) was used for cell gene expression analysis, while TaqMan Gene Expression assays (Table 2.6) were used for 2D and 3D cell samples.

2.2.7.1 Pre-Amplification

The SsoAdvanced PreAmp Supermix was tested for pre-amplification of the cDNA extracted from FFPE tissue samples, and the protocol followed [79]. All primer assays were pooled and added nuclease free water for a total volume of 500 μl . The pre-amplification reaction mix was made by mixing 25 μl SsoAdvanced PreAmp Supermix, 5 μl pre-amplification assay pool and 20 μl cDNA template to achieve a 50 μl reaction mix. PCR cycling conditions for pre-amplification of the samplers were 3 min at 95°C for polymerase activation and DNA denaturation followed by 12 cycles of denaturation 15 seconds at 95°C and annealing/extension for 4 min at 58°C.

2.2.7.2 Real-time quantitative PCR (RT-qPCR)

PowerUp SYBR Green Master mix are used to run the real-time quantitative PCR for cell samples. The reaction mix are prepared according to Table 2.11, with 10% overage and transferred a 96-well plate, including no template control (NTC) and negative control (RNase free water). Plate was sealed with an optical adhesive cover, and centrifuged briefly (800 rpm, 1 min). Roche LightCycler 96 Real-time PCR program was set to the settings in Table 2.12, with appropriate reaction volume and dye.

TABLE 2.11: Reaction mix volumes for RT-qPCR with SYBR Green.

Component	Volume	Volume
PowerUp SYBR Green Master Mix	5 μl	10 μl
Forward and reverse primers	1 μl	2 μl
DNA template	1 μl	2 μl
Nuclease-Free Water	3 μl	6 μl
Total	10 μl	20 μl

The LightCycler software displays the amplification plot, and calculate the quantification cycles for the amplification curves. Relative quantification was done to

analyze the results.

TABLE 2.12: RT-qPCR cycling mode for SYBR Green.

Step	Temperature	Duration	Cycles
UDG activation	50°C	2 min	Hold
Dual-Lock DNA polymerase	95°C	2 min	Hold
Denature	95°C	15 sec	45
Anneal	55°C	30 sec	
Extend	72°C	30 sec	
Melting curve stage 1:	95°C	10 sec	
Melting curve stage 2:	65°C	1 min	
Melting curve stage 3:	97°C	1 sec	

TaqMan Fast Advanced Master mix are used to run the Real-time quantitative PCR for 2D and 3D cell samples. The reaction mix was made by mixing 10 μ l TaqMan Fast Advanced Master mix, 1 μ l TaqMan assay, 7 μ l of nuclease free water and 2 μ l cDNA template to achieve a 20 μ l reaction mix, and adding a 10 % overage, and transferred to a 96-well plate.

The 96-well plate are sealed with an optical adhesive film, before centrifuged (800 rpm, 1 min), and placed in Roche LightCycler. The qPCR cycling conditions were 2 min UNG incubation at 50°C, 20 s polymerase activation at 95°C, followed by 40 cycles of denaturation and annealing/extension (95°C for 3s and 60°C for 30s, respectfully). The LightCycler software displays the amplification plot, and calculate the quantification cycles (Cq) for the amplification curves. Relative quantification was done to analyze the results.

2.2.8 Reference gene Stability

A stability analysis of the different reference genes was performed with the quantification cycle data obtained from the qPCR. The reference genes were separated according to conditions, high and low glucose and based on cell lines. An determination of expression stability of reference genes were also conducted by geNorm [80]. Specific criteria must be meet for a gene to be defined as a reference or housekeeping gene. Experimental factors should not affect the expression levels of the genes, and different physiological states and tissues should give a minimal variability in expression levels, making reference genes important as internal control of qPCR gene expression [81].

Reference genes used in this study were analyzed for their stability and variance over high and low glucose, for three different cell lines. The Cq values obtained from the different experiments were combined in excel, and used to check the how the Cq was for the different conditions, the same data were analyzed by geNorm to obtain the average expression stability value (M) and the variance between them.

2.2.9 Amplification Efficiency

To test the amplification efficiency of the SYBR Green primer assays, a series of 10-fold dilutions (1:5, 1:50, 1:500 and 1:5000, which correspond to 10 ng, 1 ng, 0.1 ng, 0.01 ng respectfully) were made with the cDNA. The samples were run in triplicates on 96-well plates.

Amplification efficiency of TaqMan gene expression assays, a series of 10-fold dilutions (equal to the one used for SYBR Green) were made with cDNA. The samples were run in duplicates on 96-well plates with both 2D and 3D cell lines (SW1116 and SW9489).

The efficiencies were calculated for all markers with the cell line that showed best expression, by the standard curve produced from Cq values plotted against log concentration. The slope of this curve was used in Equation 2.3 and Equation 2.4:

$$E = 10^{\frac{-1}{slope}} \quad (2.3)$$

Efficiency calculated in percentage:

$$\%E = (10^{\frac{-1}{slope}} - 1) \times 100 \quad (2.4)$$

2.2.10 RNA Analysis

The FFPE tissue RNA sample quality where assessed by on-chip electrophoresis with Agilent 2100 Bioanalyzer as described in the manufacturers protocol [82]. Agilent RNA 6000 Nano kits contains chips, spin filters and reagents (gel matrix, dye concentrate, marker and ladder) for analysis of Eukaryote Total RNA Nano. The RNA samples were diluted to a concentration between 5 and 500 ng/ μ l.

The RNA gel matrix was filtered with spin filter inserted in a centrifuged, and mixed with RNA dye concentrate, and loaded on the chip following manufacturers protocol with the priming station. The RNA marker was loaded into all 12 sample

wells and the ladder well on the chip. The samples were heat denatured at 70°C for 2 minutes, before 1 µl of the samples and ladder were loaded onto the chip in appropriate wells. The chip was vortexed with an adapter and analyzed with the Agilent 2100 Bioanalyzer instrument.

2.2.11 Data analysis

2.2.11.1 Relative Gene Expression (RGE)

Cq values were calculated in the LightCycler software, exported as a text file and imported to excel for analysis and relative gene expression (RGE) calculation.

To calculate the relative gene expression, Equation 2.5 was used for the samples of each assays, according to the $2^{-\Delta\Delta Cq}$ method by Livak *et al.* [83]. The samples were normalized to the average reference genes and high glucose (4.5 g/L) levels were used as control for the samples of the experiment. The equation gives the result as fold change in expression compared to the control cell, which is linear, and does not show negative values, by converting the numbers to logarithm, negative values will represent downregulation, while positive values will represent upregulation of relative gene expression levels.

$$RGE = 2^{-(\Delta Cq_{target(experiment-control)} - \Delta Cq_{reference(experiment-control)})} \quad (2.5)$$

2.2.11.2 Statistical Analysis

Statistical analysis was evaluated for each of the target genes by performing an independent student t-test (also called two sample t-test) on excel of the ΔCq values obtained. The t-test are done for equal or unequal variances depending on the F-value obtained, and the limit for significance used is $p > 0.05$.

Chapter 3

Results

This study are compiled in a workflow (Figure 3.1), which include optimization and calibration test for validity of techniques used.

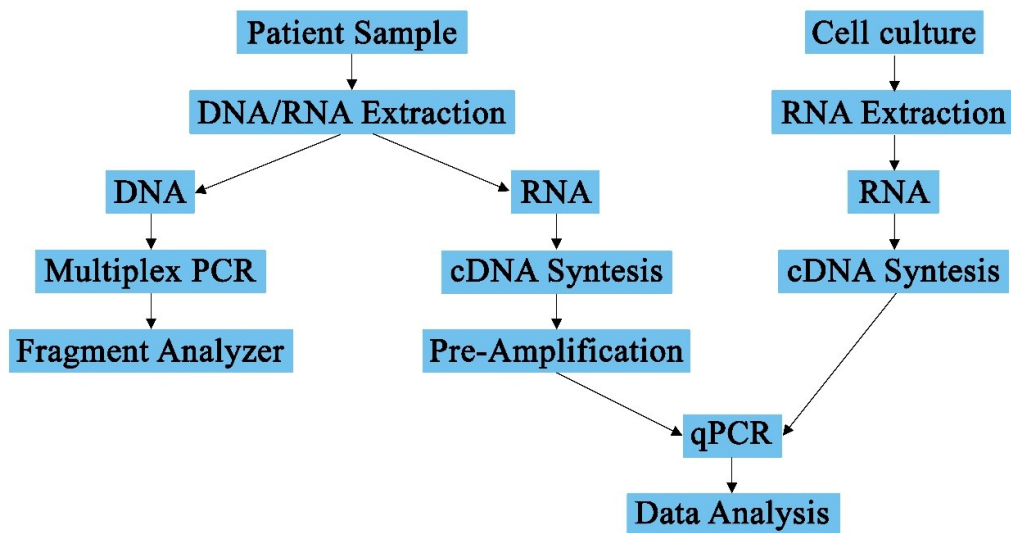


FIGURE 3.1: Methods workflow used in this study. Analysis on cell culture used as a model for gene expression analysis of cell and patient samples. The analysis followed the flow of the diagram RNA and/or DNA was extracted from patients and cell culture, then RNA was reverse transcribed to cDNA, followed by qPCR analysis.

3.1 Cell Culture assays

Cells used in this study are described Table 2.1, and the assays protocols are described in section 2.2.1 Cell Culture.

3.1.1 Cell lines Proliferation and Viability

To understand which growth variance high (4.5 g/L) and physiological (1.0 g/L) glucose that favor proliferation and viability, the doubling time was calculated by Equation 2.2.

Viability are presented in Figure 3.2, with differences in high and low glucose cultured for 48 and 72 hours. CCD-18Co present with the highest viability of 98% for 48 hours, then it decreases to approximately 95%. SW1116 shows the lowest viability, with a range of 79 to 83%. SW948 have around 95% viability for 48 hours measurements, and a small decrease to 93% for 72 hours. Examples of the different cell lines population and viability profiles are located in Appendix A.

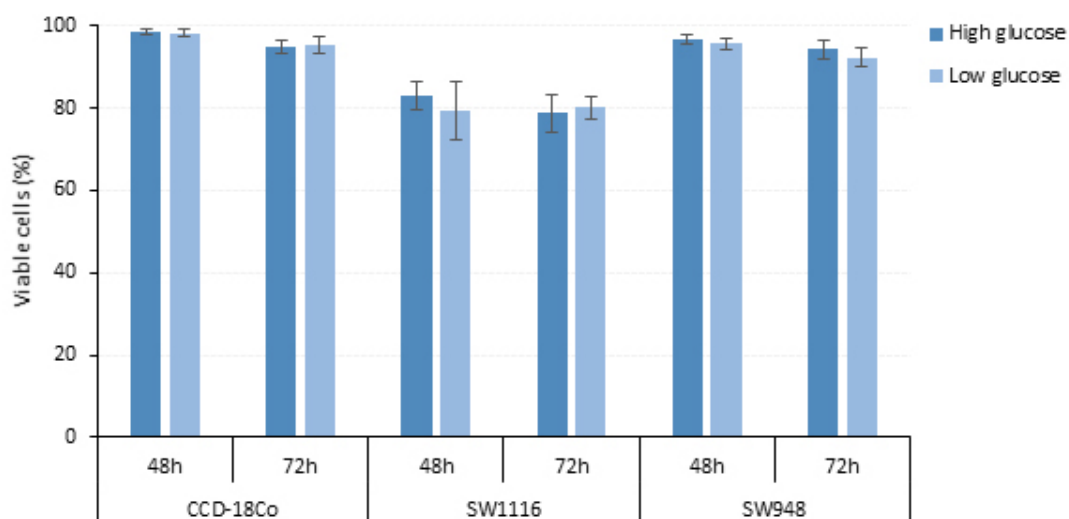


FIGURE 3.2: Cells viability. Cells are cultured in high (4.5 g/l) and low (1.0 g/L) glucose for 48 and 72 hours, and quantified with MUSE Count & viability kit. CCD-18Co (P14, P16, n=9), SW1116 (P14, P15, P22, n=24), and SW928 (P14, P16, P23, n=24 (high glucose), n=22 (low glucose)). Initial seeding number of cells: 1×10^5 cells/well (6-well plate).

SW1116 shows a slow growth the first 48 hours, before they increase over the next 24 hours, the cell culture seems to grow faster in low glucose compared with high glucose medium (Figure 3.4), these results can also be observed in the images Figure 3.3.

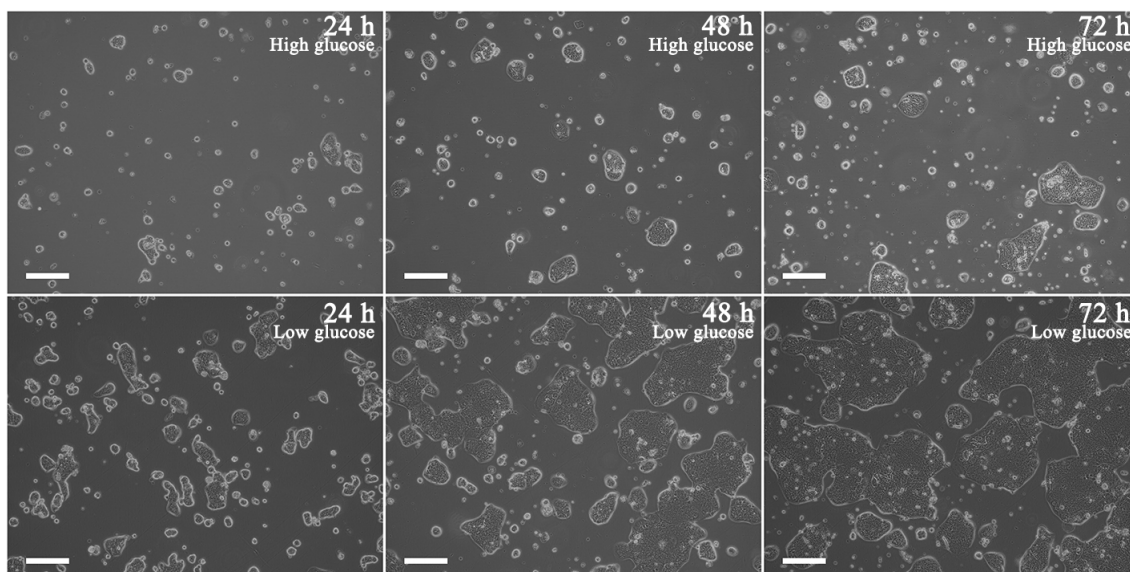


FIGURE 3.3: Cell growth of SW1116 (P14) at 24, 48 and 73 hours. Seeded 1×10^5 cells/well (6-well plate) and cultured in high (4.5 g/L) and physiological (1.0 g/L) glucose. Scale bar: 200 μm (ImageJ).

High glucose present with an increase of 2.52-fold after 72 hours compared to physiological glucose which presents with a 3.35-fold increase. The graph shows that the cells grows a bit faster for low glucose compared to high glucose, which also are calculated by doubling time. Doubling time for high glucose are 2 days, 13 hours and 42 minutes (61.70 hours), and 1 day, 17 hours and 2 minutes (41.03 hours), for low glucose culturing.

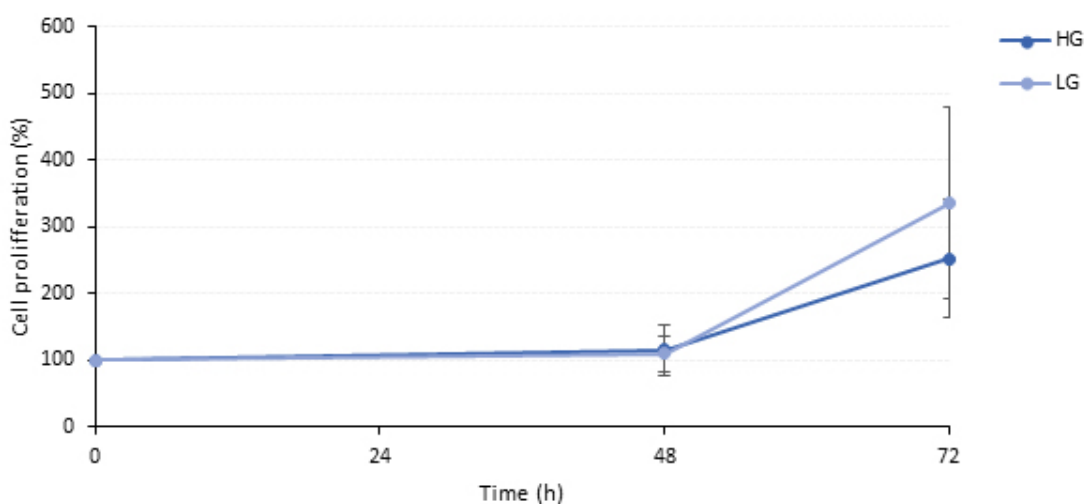


FIGURE 3.4: Proliferation of SW1116 (P14, P16, P23) at 48 and 72 hours. The chart are normalized to high (4.5 g/L) and low (1.0 g/L) glucose at 0 hours (seeded 1×10^5 cells/well), and presented with standard deviations between the replicates ($n=8$).

SW948 shows an increasing growth over the whole time interval, and the increase

for high glucose are a bit higher than for physiological glucose (Figure 3.6). The cell line have been imaged at 24, 48 and 72 hours, and are presented in Figure 3.5.

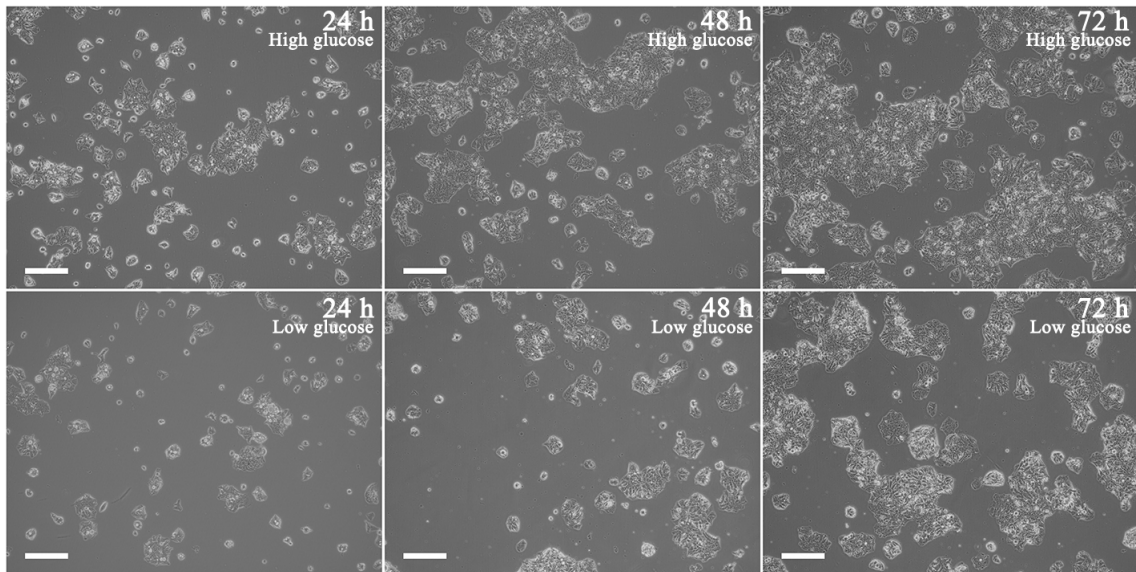


FIGURE 3.5: Cell growth of SW948 (P17) at 24, 48 and 72 hours. Seeded 1×10^5 cells/well (6-well plate) and cultured in high (4.5 g/L) and physiological (1.0 g/L) glucose. Scale bar: 200 μm (ImageJ).

The high glucose present a fold increase 7.70 after 72 hours compared to physiological glucose that had a fold increase of 7.16.

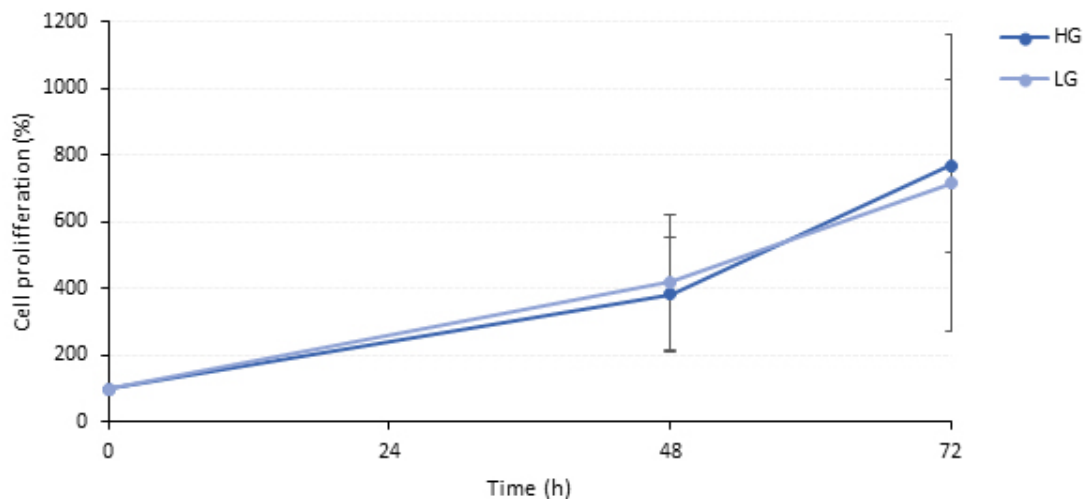


FIGURE 3.6: Proliferation of SW948 (P15, P16, P20, P25) at 48 and 72 hours. The chart are normalized to high and low glucose at 0 hours (1×10^5 cells/well), and presented with standard deviations between the replicates ($n=10$).

The doubling time for SW948 for high and low glucose are only two hours apart. High glucose culturing is 1 day, 2 hours and 19 minutes (26.32 hours) and low glucose

culturing is 1 day, 4 hours and 37 minutes (28.61 hours). Which also are presented in the images (Figure 3.5, and the proliferation graph (Figure 3.6).

CCD-18Co shows a steep growth the first 48 hours, before the cell number decreases to 72 hours (3.8); this is not visible in the images obtain after 24, 48 and 72 hours culturing (Figure 3.7).

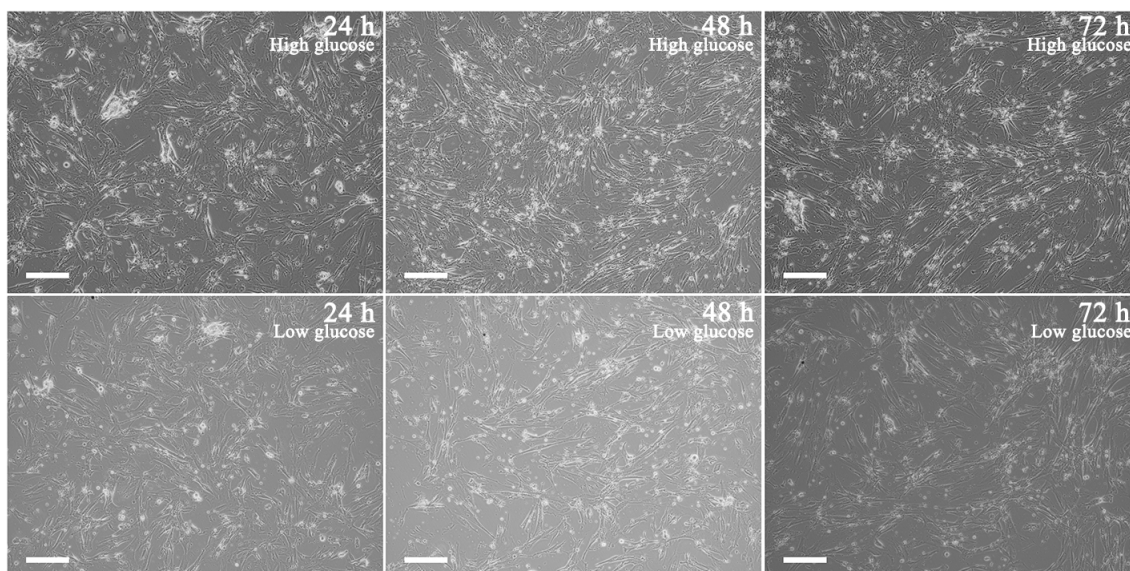


FIGURE 3.7: CCell growth of CCD-18Co (P16) at 24, 48 and 72 hours. Seeded 1×10^5 cells/well (6-well plate) and cultured in high (4.5 g/L) and physiological (1.0 g/L) glucose. Scale bar: 200 μm (ImageJ).

The graph shows that CCD-18Co grows a bit faster and to a higher concentration for low glucose compared to high glucose, and it decreases more for cells cultured in high glucose compared to those cultured in physiological glucose. The decrease are especially observed in high glucose. High glucose present a 3.67-fold increase after 72 hours compared to physiological glucose, which had a 4.95 fold increase after 72 hours.

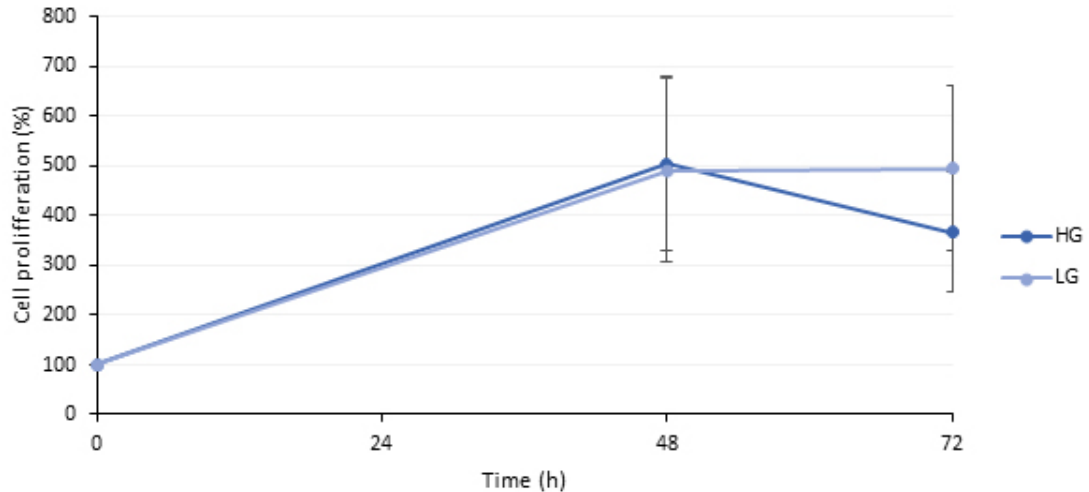


FIGURE 3.8: Proliferation of CCD-18Co (P14, P16) at 48 and 72 hours. The chart are normalized to high and low glucose at 0 hours (1×10^5 cells/well), and presented with standard deviations between the replicates ($n=7$).

The doubling time for CCD18-Co for high and low glucose are a few hours different. Cells cultured in low glucose doubles by 1 day, 11 hours and 16 minutes (35.26 hours), which is a bit faster than cells cultured in high glucose. High glucose cultured cells doubles within 1 day, 20 hours and 25 minutes (44.41 hours).

3.1.2 Cell lines Wound Healing

All three cell lines used for wound healing assay to check the collective cell migration, which is exhibited by epithelial and endothelial monolayers that moves while their intracellular junctions are maintained [84]. To test whether high or low glucose conditions played a role how the slow proliferating cell line SW1116 regrew, a wound healing assay was performed. After the wound was inflicted, it took around one week to the cells started to grow back together; with not much difference between high glucose and physiological glucose (Figure 3.9). Growth medium was changed frequently, to obtain the best growth conditions, and good quality images.

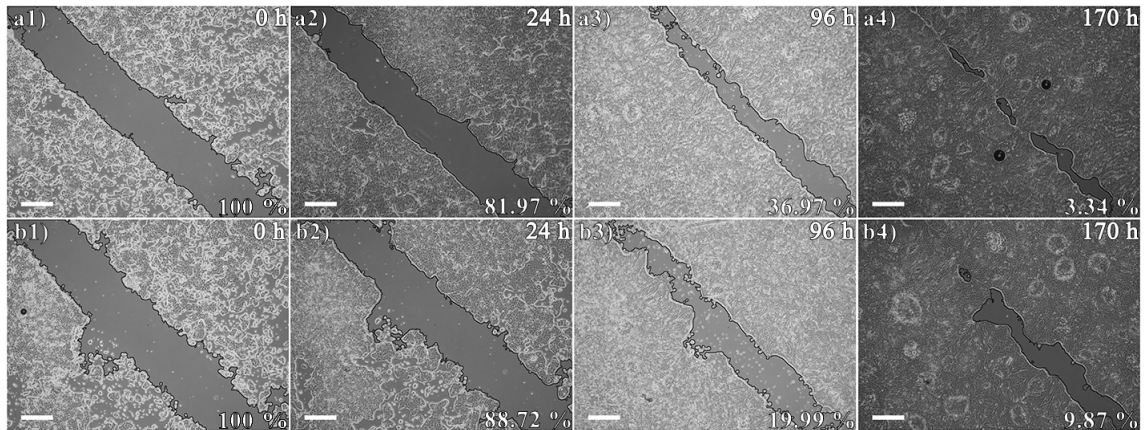


FIGURE 3.9: Wound healing over time for SW1116 (P19). Cultured in high (4.5 g/L, (a1-a4)) and low (1.0 g/L (b1-b4)) glucose. Black area represent scratch applied on cells, and how cells grow back together. Scale bar: 500 μm (ImageJ, wound healing tool).

The MRI Wound healing tool was used to measure the area of the wound and the data collected in an excel sheet and analyzed by normalization to high and low glucose at 0 hours (Figure 3.10, and in Appendix A).

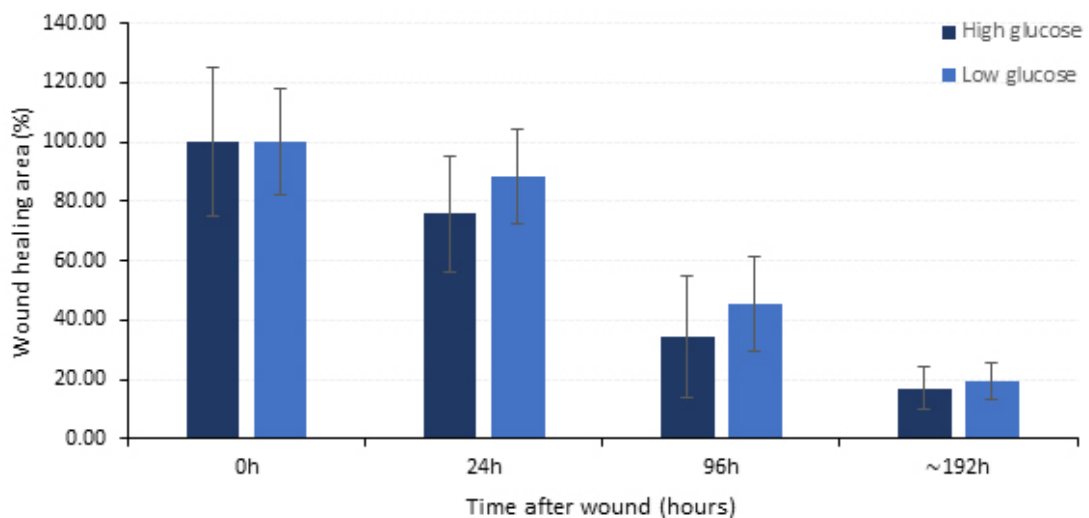


FIGURE 3.10: Measured wound area over time for SW1116 (P18, P19, P14). Cultured in high (4.5 g/L) and low (1.0 g/L) glucose. Bar chart are normalized to initial wound at 0 hours, measured at different time points, and presented with standard deviations between replicates ($n=9$) (ImageJ, wound healing tool).

The bar chart shows that the wound of SW1116 in low glucose grows slower together, than cells cultured in high glucose. The final measurements are an average of all cells that have started growing back together, and they are around 17% closed for high glucose and 19% closed for low glucose.

Wound healing assay was carried out on the fast proliferating cell line SW948 to see

whether high and low glucose conditions play a role on the how well the cell line regrew. The wound healing for SW948 does take around one week to grow back together for the low glucose, while the high glucose is not growing back together (Figure 3.11). The growth medium was changed frequently, to give the cells the best growth conditions possible, and achieve good quality images.

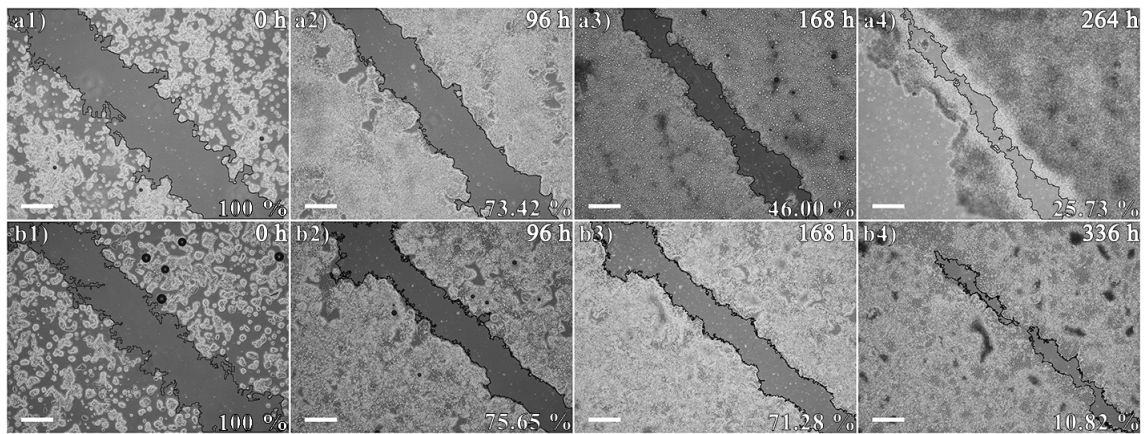


FIGURE 3.11: Wound healing over time for SW948 (P26). Cultured high (4.5 g/L (a1-a4)) and low (1.0 g/L (b1-b4)) glucose. Black area represents measured scratch applied on cells, and how cells grow back together. Scale bar: 500 μm (ImageJ, wound healing tool).

The MRI Wound healing tool gave the area of the scratches and the data was normalization to high and low glucose at 0 hours (Figure 3.12).

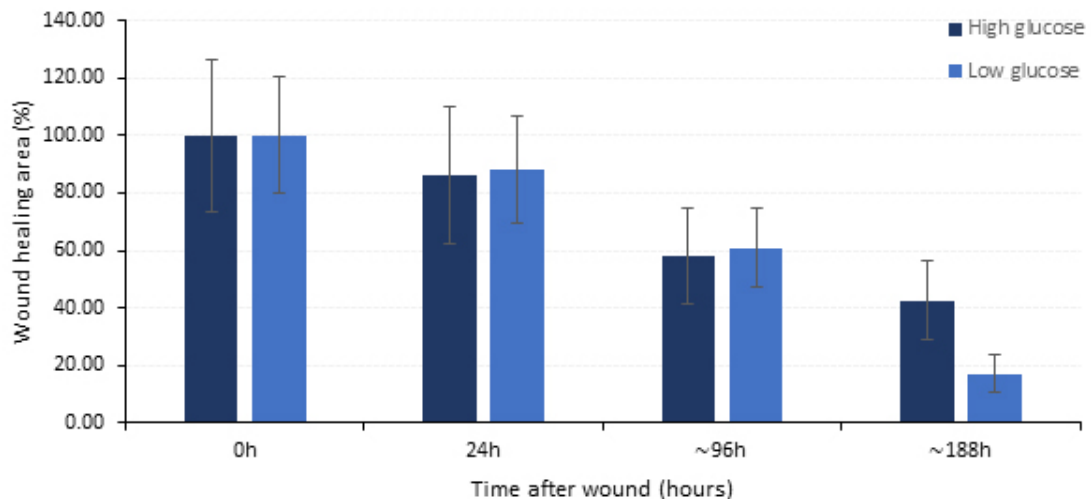


FIGURE 3.12: Measured wound area over time for SW948 (P25, P26, P13). Cultured in high (4.5 g/L) and low (1.0 g/L) glucose. Bar chart are normalized to initial wound at 0 hours, measured at different time points, and presented with standard deviations between replicates (n=9) (ImageJ, with healing tool).

The results are normalized to high and low glucose control at 0 hours, and standard

deviation are added for each of the bars. Low glucose grows slower during the first 96 hours, compared with high glucose conditions. Then the low glucose regrow together, while the high glucose almost stopped growing back together around 188 hours forming multilayers, before they detached from the plate well (Appendix A).

To test whether high or low glucose conditions played a role on how the fibroblastic cell line CCD-18Co regrew, a wound healing assay was performed. After the wound was inflicted on the cell culture, it took less than one day to start to grow back together; with not much difference between high glucose compared to low glucose (Figure 3.13).

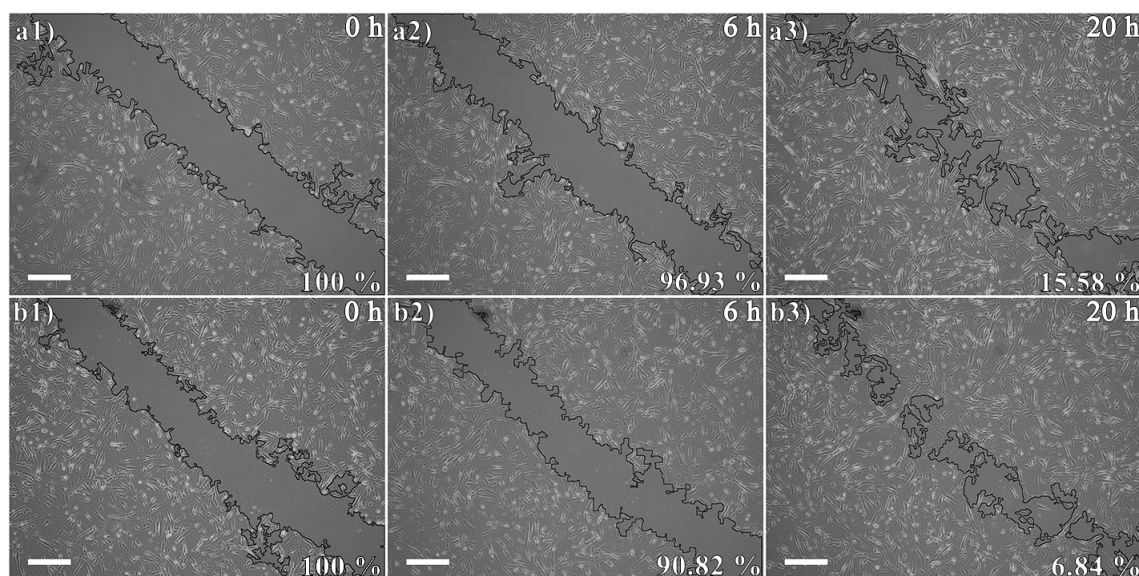


FIGURE 3.13: Wound healing over time for CCD-18Co (P16). Cultured in high (4.5 g/L (a1-a3)) and low (1.0 g/L (b1-b3)) glucose. Black area represents measured scratch applied on cells, and how cells grow back together. Scale bar: 500 μm (ImageJ, wound healing tool).

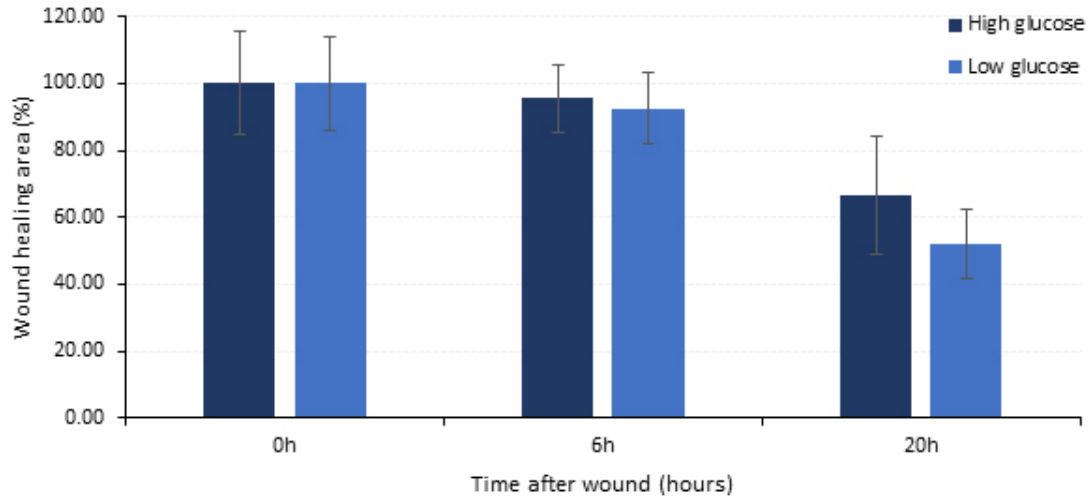


FIGURE 3.14: Measured wound area over time for CD-18Co (P16). Cultured in high (4.5 g/L) and low (1.0 g/L) glucose. Bar chart normalized to initial wound at 0 hours, measured at different time points, and presented with standard deviation between replicates (n=6) (ImageJ, wound healing tool).

The bar chart shows that cells grown in low glucose regrows faster compared to high glucose conditions. Within 20 hours, all the different replicates of CCD-18Co had started growing back together, but as shown in the bar chart above (Figure 3.14), at 20 hours, the low glucose have grown more together than the high glucose.

3.2 Multiplex PCR of Patient Samples

The small sample size (n=26) of the cohort investigated in this study are presented in the Table 3.1, with EMAST (Table 2.3) and MSI (Table 2.4) analysis separated. Normal tissue samples are compared with their corresponding tumor tissue samples.

Microsatellite stable (MSS) are used for MSI when none of the markers were unstable, while EMAST negative represent up to one unstable marker. The samples presented as MSI-H are also EMAST positive for the these results. Four out of 24 EMAST analysis show two or more unstable markers (EMAST+), 7 out of 24 (26 minus two samples N/A) shows one unstable marker, and the rest of EMAST shows no unstable markers (EMAST-). Three out of 23 (26 minus three samples N/A), shows MSI-H and therefore two or more unstable markers, one shows MSI-L with one unstable marker, and the rest presents with no unstable markers and are presented as MSS.

TABLE 3.1: Result of EMAST and MSI analysis. EMAST- (EMAST negative): one or less markers unstable. EMAST+ (EMAST positive): two or more markers unstable. MSS, no makers unstable. MSI-L, one marker unstable. MSI-H: two or more markers unstable. N/A, not analyzed or inclusive analysis.

Sample	EMAST	MSI
35	EMAST-	MSS
43	EMAST-	MSS
67	EMAST+	MSI-H
80	N/A	MSI-H
118	EMAST-	MSS
136	EMAST+	MSS
157	EMAST-	N/A
176	N/A	MSS
180	EMAST-	N/A
181	EMAST-	MSS
182	EMAST-	N/A
183	EMAST-	MSS
184	EMAST-	MSI-L
189	EMAST-	MSS
190	EMAST-	MSS
190(M)	EMAST-	MSS
191	EMAST-	MSS
192	EMAST-	MSS
193	EMAST+	MSI-H
194	EMAST-	MSS
195	EMAST-	MSS
196	EMAST-	MSS
197	EMAST-	MSS
199	EMAST-	MSS
199(M)	EMAST-	MSS
200	EMAST+	MSS

Two layouts of EMAST (patient samples 067N/T and 157N/T), one EMAST positive and one EMAST negatives and two layouts for MSI (patient samples 067N/T and 176N/T), one MSI-H and one MSS are presented in Appendix B.

3.3 Validation of Quantitative PCR

The potential markers of detection of difference in high and low glucose (and tumor and normal tissue samples), had to be highly expressed. Expression of the different genes were evaluated in three colorectal cell lines, two cancerous (SW1116 and SW948) and one normal (CCD-18Co).

3.3.1 Cell line Expression of Markers

	ACTB	RRN18S	HSP90	GLUT1	MCT4	OCT1	SUCLA2	LDHA	LDHB	UCP2
SW948	20.8	17.6	25.0	26.4	29.8	37.5	27.6	35.0	24.5	35.9
SW1116	19.9	17.6	23.7	23.6	30.0	35.7	26.6	32.3	22.2	35.6
CCD-18Co	20.0	18.0	25.2	27.2	29.2	37.1	28.2	33.8	24.5	36.4

	CDH1	CDH2	SNAIL	SLUG	AXL	ZEB1	TWIST	CTNNB1	VIM	BIRC5
SW948	27.1	-	31.4	-	37.6	38.6	-	27.6	-	28.4
SW1116	26.1	-	31.5	-	32.3	38.4	-	26.1	-	27.4
CCD-18Co	-	29.1	32.1	32.7	27.3	29.1	31.4	26.9	21.6	31.5

Cq	17	19	21	23	25	27	29	31	33	35	37	39	-

FIGURE 3.15: Expression of markers in cell lines. Given as average Cq values (n=3). Cell lines cultured in high (4.5 g/L) glucose. No Cq value denotes an undetectable signal or a Cq > 39, a lower Cq value reflects a higher expression of marker.

The cell lines were chosen based on their different phenotype and characteristics. SW1116 and SW948 are epithelial adenocarcinomas. SW1116 are more OXPHOS dependent, and SW948 are more glycolytic dependent, while CCD-18Co is a fibroblast cell line, non-cancerous and motile compared to the other cell line (Table 2.1). RNA was extracted from harvested cell line lysate (section 2.2.1.8), cultured in high (4.5 g/L) or low (1.0 g/L) glucose, before reverse transcribed (section 2.2.5) for cDNA production, and quantified by qPCR (section 2.2.7.2).

The average Cq values of each cell line in high glucose amplified is shown in Figure 3.15. All of these amplifications are done in high glucose, since that is the control environment used for cell lines in this study. The reference genes (ACTB, RRN18S, HSP90AB) are in general similar and evenly expressed between the different cell lines, which is expected. With Cq values around 20 for ACTB, 18 for RRN18S and 25 for HSP90AB. SW948 exhibit the highest expression for SNAI1. SW1116 was the best cell line for CDH1, CTNNB1, SLC2A1, SLC22A1, SUCLA2, LDHA/B, UCP2 and BIRC5. The remaining markers (CDH2, SNAI2, AXL, ZEB, TWIST, VIM, MCT4) were highest expressed in CCD-18Co.

3.3.2 Stability analysis of Reference Genes

The reference genes are supposed to be stable across conditions, therefore an analysis of the quantification cycles (Cq) values have been done of the different reference genes to compare if they are stable over high and low glucose conditions, also separated according to the cell lines (Figure 3.16).

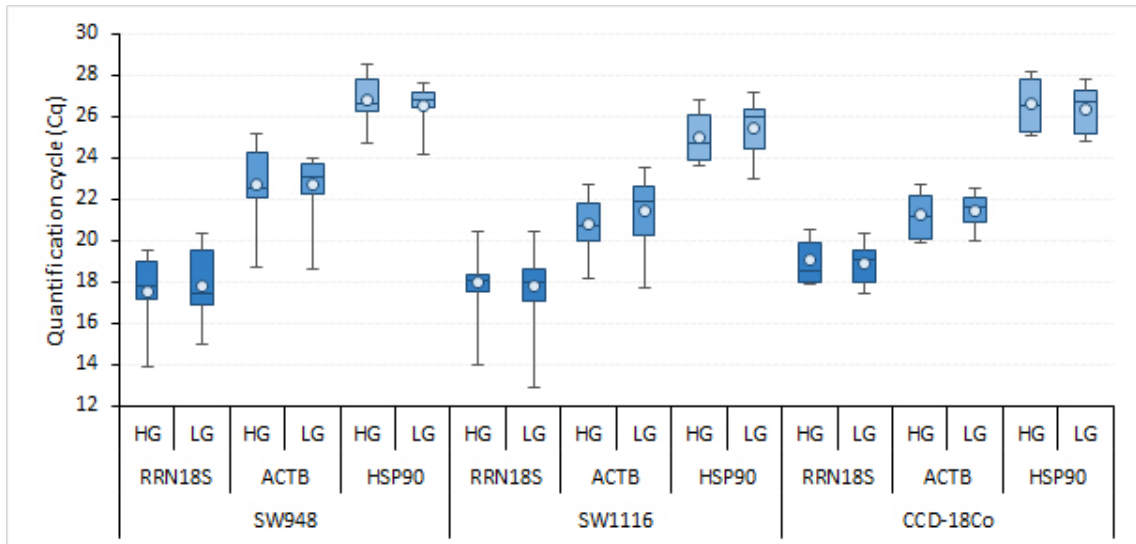


FIGURE 3.16: Distribution of Cq values for reference genes. Separated according to condition (high (4.5 g/L) and low (1.0 g/L) glucose) and cell line (SW948, SW1116, CCD-18Co). Box-and-whisker plots show range of Cq values for each reference genes (RRN-18S, ACTB, HSP90AB). Boxes indicate 75th and 25th percentiles, whiskers indicates largest or smallest Cq value without being an outlier, median are presented as the line within the boxes and average Cq are presented as a dot.

In general, high and low glucose condition do not vary too much between each of the reference genes. They seems to be stable across the condition, also not much different when compared with cell lines, RRN-18S gets amplified first and HSP last in all the different cell lines, while ACTB are somewhere in between the other reference genes. Stability analysis calculated with geNorm (used qBASE+) are presented in Figure 3.17.

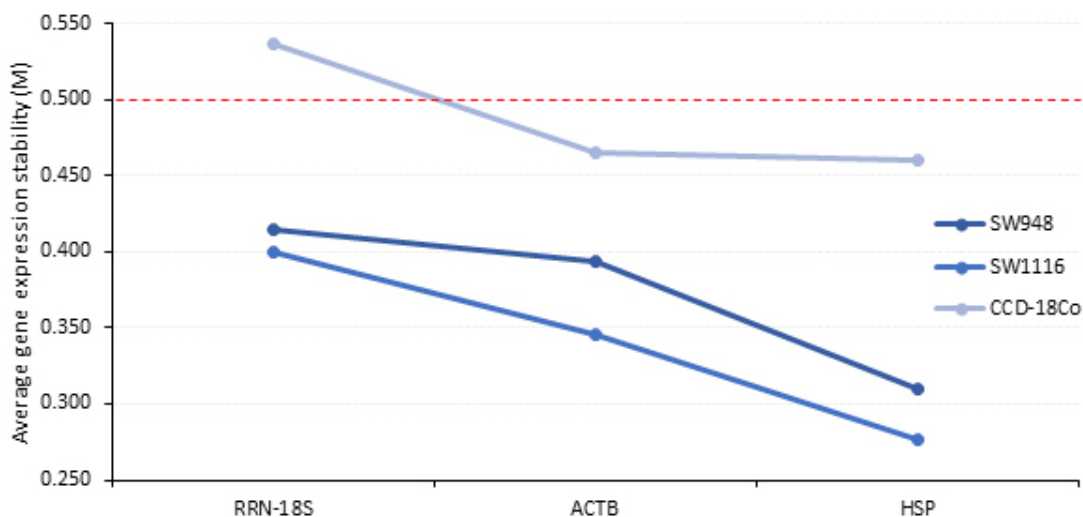


FIGURE 3.17: Average expression stability (M). Calculated with geNorm (qBASE+), with Cq values from qPCR. High (4.5 g/L) relative to low (1.0 g/L) glucose for each of the cell line in this study (SW948, n=10; SW1116, n=13, CCD-18Co; n=6). The lowest average expression stability value are the most stable reference genes. M value should be < 0.5 .

CCD-18Co have the highest stability values over all three reference genes, while all cell line express the highest stability for HSP, and the lowest stability for RRN-18S. The average coefficient of variation (CV) for are 14.8, 13.5 and 20.1, for SW948, SW1116 and CCD-18Co respectfully (Appendix C).

3.3.3 Amplification Efficiency of SYBR Green markers

QuantiTect Primer Assay manufactured by QIAGEN, are designed for SYBR Green expression analysis, and guaranties $100 \pm 10\%$ efficiencies for relative quantification. Efficiency of all markers were tested to confirm this, and validate them (Table 3.2). Extracted cDNA from cell lines (SW1116, SW948, CCD-18Co) with highest expression of the marker tested with qPCR were used for standard curve analysis (Appendix D). The multimarker mRNA panel used in this study can be put in two categories, metabolic and EMT.

Efficiencies for the markers are within this range for most of the markers, with exception of LDHA (74.02%), TWIST1 (82.10%), and SLUG (87.28%) (Table 3.2 and Figure 3.18).

TABLE 3.2: Amplification efficiency (E) for SYBR Green markers. Slope of standard curve and coefficients of determination from linear regression of the standard curve (R^2). *Three points only.

Assay	Slope	R^2	E(%)
RRN-18S	-3.4193	0.985	96.09
ACTB	-3.5643	0.9963	90.79
HSP90AB	-3.4052	0.9989	96.64
E-cadherin	-3.383	0.9986	97.51
N-cadherin	-3.501	0.9936	93.03
SNAIL	-3.3186	0.9741	100.14
SLUG	-3.6699	0.9934	87.28
AXL	-3.5193	0.993	92.38
ZEB1*	-3.54	0.9954	91.64
TWIST1	-3.8417	0.9759	82.1
β -catenin	-3.3703	0.9963	98.02
Vimentin	-3.471	0.9981	94.13
GLUT1	-3.4807	0.9981	93.78
MCT4	-3.3986	0.9667	96.9
OCT1*	-3.1558	0.951	107.43
SUCLA2	-3.4594	0.9942	94.57
LDHA	-4.1564	0.9866	74.02
LDHB	-3.447	0.9958	95.03
UCP2	-3.4783	0.9785	93.86
Survivin	-3.475	0.9778	93.99

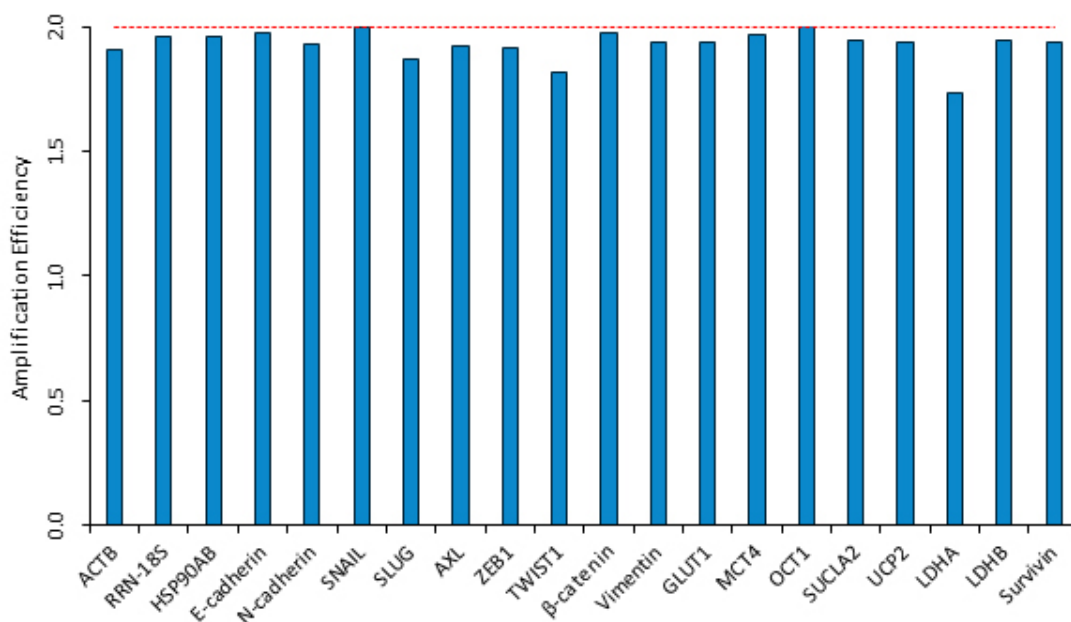


FIGURE 3.18: Amplification efficiency of SYBR Green assays.

3.3.4 Amplification Efficiency of TaqMan assays

SW1116 and SW948 samples, cultured 2D and 3D (spheroids) cells, were used to calculate the efficiency of the TaqMan assays from a dilution series and are presented in Table 3.3 below. In Appendix C are the standard curves used for the efficiency calculation.

TABLE 3.3: Amplification efficiency of TaqMan Assays (E). Coefficients of determination from linear regression of the standard curve (R2). *Three points only.

Assay	Slope	R2	E (%)
ACTB	-3.3865	0.9956	97.37
POLR2A*	-3.26	0.9887	102.65
SUCLA2	-3.4075	0.9937	96.55

3.4 Quantitative PCR Gene Expression

Cell line was cultured as described in section 2.2.1 (Cell Culture) and marker levels quantified by qPCR (section 2.2.7.2) On each plate the reference genes and genes of interest were run in duplicate, and with the two different culturing conditions, high and low glucose. C_q were calculated by the LightCycler and relative gene expression was calculated (section 2.2.11.1).

3.4.1 Relative Gene Expression of Cell lines

RNA have been extracted (section 2.2.1.8) from the cells (SW948, SW1116, and, CCD-18Co), cDNA have been synthesized (section 2.2.5) and qPCR (section 2.2.7.2) have been run to see expression with EMT and metabolic markers depending on their growth condition. Relative gene expression have been calculated according to section 2.2.11.1. In Appendix E, the relative gene expression mean, standard deviation, and threshold value based on 3SD over mean are presented, cell lines cultured in high and low glucose for 48 and 72 hours, 2 weeks, and wound healing assay.

3.4.1.1 High and Low Glucose for 48 hours

The RGE for cells cultured in different glucose conditions for 48 hours are presented in Figure 3.19. The different conditions used are high glucose, containing 4.5 g/L glucose, and low glucose, containing 1.0 g/L glucose.

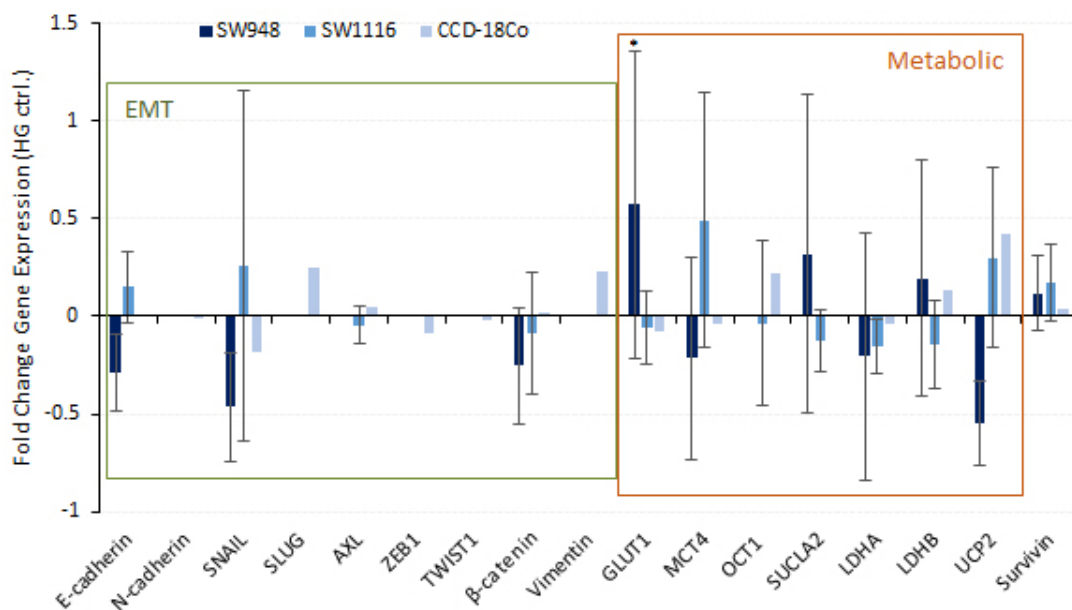


FIGURE 3.19: Relative gene expression for cells cultured for 48 hours. Cells are cultured in high (4.5 g/L) and low (1.0 g/L) glucose medium. The bar chart are normalized to high glucose (control). qPCR data for SW948 (P22, P23, P15) and SW1116 (P20, P22, P17) are shown as RGE means \pm SD from 3 biological replicates, while CCD-18Co (P17) are shown as RGE means (3 technical replicates). *, indicate $p < 0.05$ by Student t-test, not performed for CCD-18Co.

The EMT markers (CDH2, SLUG, ZEB, TWIST and VIM) are not expressed for colon cancer cell lines, while AXL only are expressed SW1116 and CCD-18Co. CDH1/2 gene expression are divided between the cells, the epithelial colon cancer cell lines are up- and downregulated, for SW1116 and SW948, respectfully, and not expressed for CCD-18Co. N-cadherin are downregulated for CCD-18Co, while the other cell lines are not expressed.

With the exception of β -catenin, LDHA and Survivin, all the different markers are expressed different for the two colon cancer cell lines (SW948 and SAW1116). SW948 gene expression of the target gene SLC2A1 (GLUT1) is of statistically significant value, upregulated in low glucose compared high glucose. GLUT1 are on the other hand downregulated for SW1116 and CCD-18Co.

3.4.1.2 High and Low Glucose for 72 hours

Relative gene expression of SW948, SW1116 and CCD-18Co cultured for 72 hours in high and low glucose medium are presented in Figure 3.20.

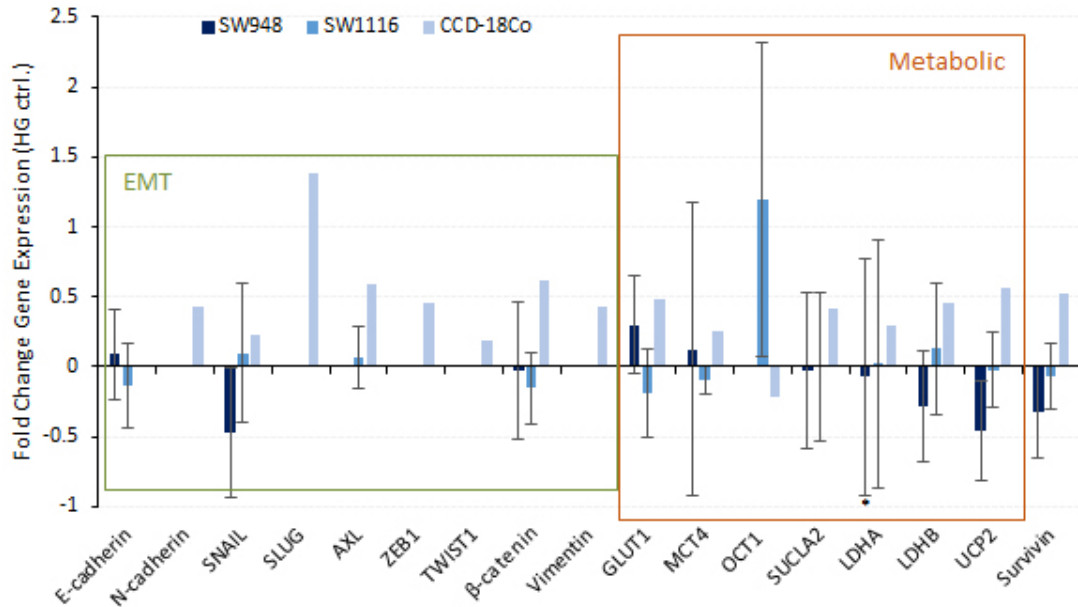


FIGURE 3.20: Relative gene expression for cells cultured for 72 hours. Cells are cultured in high (4.5 g/L) and low (1.0 g/L) glucose. The bar chart are normalized to high glucose (control). qPCR data for SW948 (P22, P23, P15) and SW1116 (P20, P22, P17) are shown as RGE means \pm SD from 3 biological replicates, while CCD-18Co (P17) are shown as RGE means from 3 technical replicates. *, indicate $p < 0.05$ by Student t-test, not performed for CCD-18Co.

CCD-18Co are expressed in all the EMT markers, except for E-cadherin which only is regulated by colon cancer cell lines, SW948 and SW1116. β -catenin are downregulated for both colon cancer cell lines, and AXL are only expressed by SW1116. All markers are expressed in metabolic genes, except for SW948 in OCT1. LDHA gene expression for SW948 is statistically significant between high and low glucose expression according to the Student t-test. This gene is only downregulated for SW948, and upregulated for the other cell lines.

3.4.2 Applied Wound Healing

The relative gene expression of SW1116 and CCD-18Co after wound healing assay (section 2.2.1.7), are calculated (section 2.2.11.1 presented in Figure 3.21, with their RGE means and standard deviation from 3 biological replicates of each cell line.

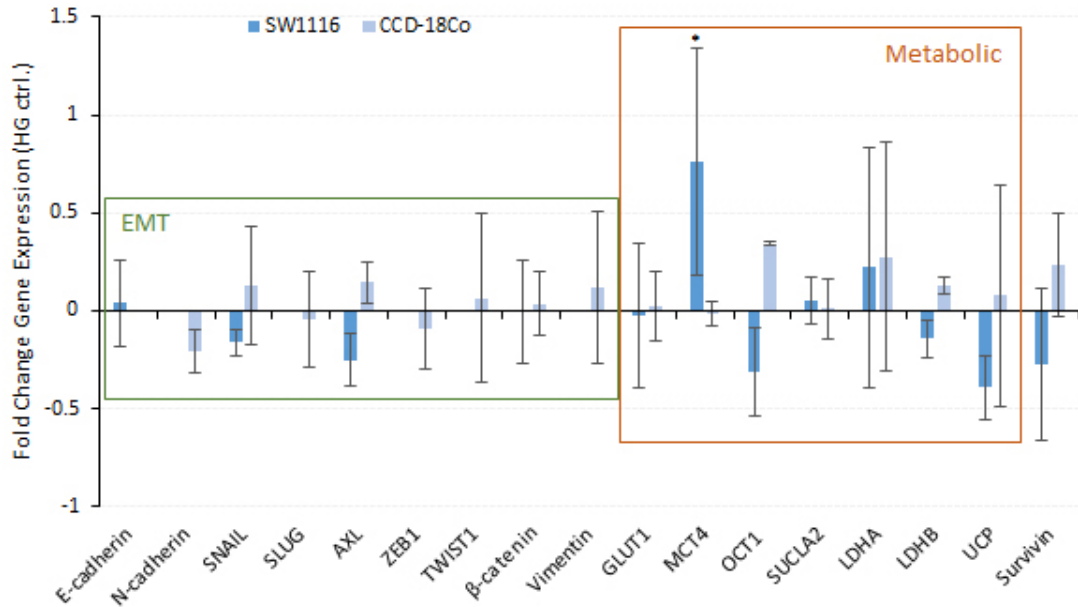


FIGURE 3.21: Relative gene expression for cells extracted after wound healing assay. qPCR data for SW1116 (P18, P19 and P14) and CCD-18Co (P16) are shown as RGE means \pm SD from 3 biological replicates, and normalized to high glucose. *, indicate $p < 0.05$ by Student t-test.

E-cadherin are only upregulated for SW1116 and N-cadherin are only upregulated for CCD-18Co. Few of the epithelial to mesenchymal transition markers, SLUG, ZEB1, TWIST1 and VIM, are only expressed in CCD-18Co. SNAIL, beta-catenin and AXL are regulated in both cell lines, as for the metabolic markers both cell lines are expressed, with varying degree of expression levels.

MCT4 (SLC16A3) are upregulated in SW1116 low glucose, and are of significant difference between high and low glucose conditions, as indicated in Figure 3.21 with a * symbol. This are calculated by a Student t-test on the genes presented in the chart.

3.4.3 Metformin Treatments

The relative gene expression of metformin treatments for SW948 and SW1116 are presented in the graphs, Figure 3.22 and Figure 3.23. The cells have been treated with (0.5 mM and 3.0 mM metformin) or without metformin for 48 hours before RNA were extracted according to section 2.2.1.8. The high and the low glucose are used as control for the treatments in the corresponding medium, but the low glucose itself are normalized to high glucose. Since high glucose are used as the overall control, it is present as 0 in the graphs, and therefore not showing up.

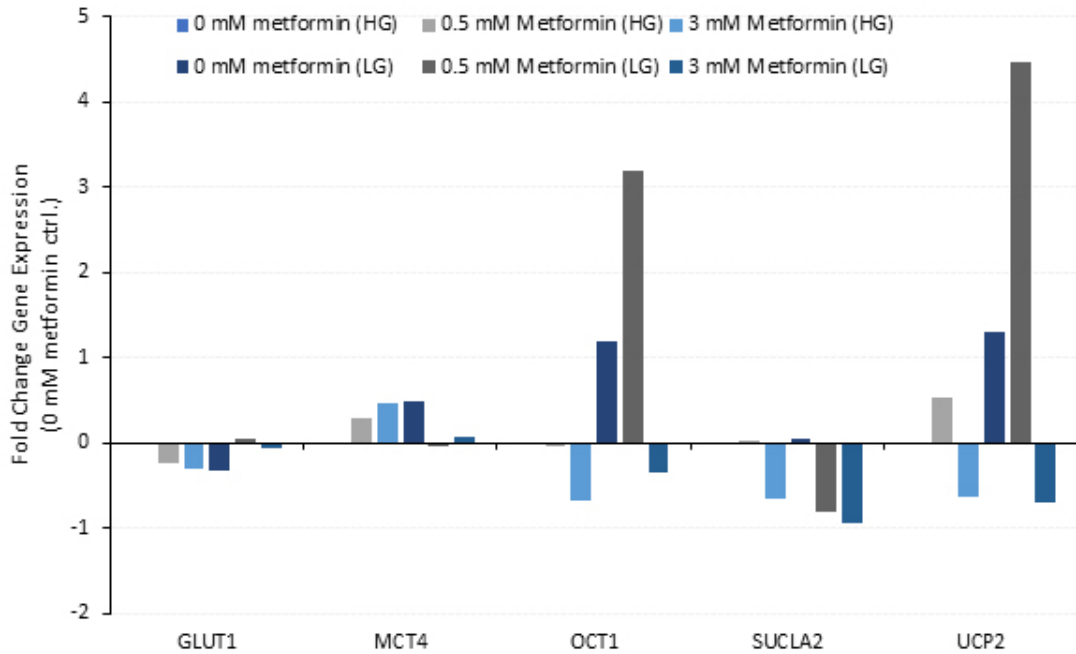


FIGURE 3.22: Relative gene expression for SW948 treated with metformin. Cells (Passage n/a, n=1) is cultured in high (4.5 g/L) and low (1.0 g/L) glucose, and treated with different concentrations of metformin (0 mM, 0.5 mM, and 3 mM) for 48 hours. The graph is normalized to high glucose with 0 mM metformin for all high glucose treatments and low glucose without metformin, low glucose treatments are normalized to low glucose. qPCR data are shown as RGE.

SW948 relative gene expression with metformin treatments (Figure 3.22) shows a relative small gene expression with GLUT1 and MCT4. OCT1, shows a high upregulation when the cells are cultured in low glucose without treatment, and even higher upregulation for 0.5 mM treatment, before a downregulation of the gene happens with 3 mM metformin treatment, this are also observed for UCP2. When SW948 are cultured in high glucose with metformin it is upregulated for MCT4, and down regulated for GLUT1 and OCT1. For SUCLA2 its only upregulated for metformin treatments with 0.5 mM (high glucose) and no treatments in low glucose.

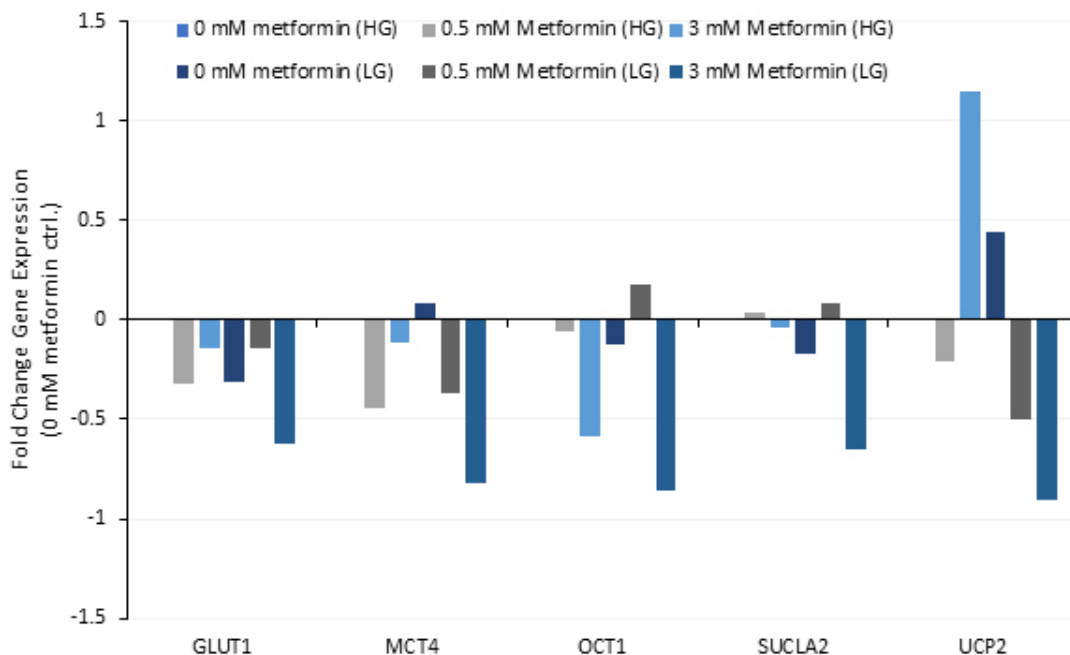


FIGURE 3.23: Relative gene expression for SW1116 treated with metformin. Cells (Passage n/a, n=1) are cultured in high (4.5 g/L) and low (1.0 g/L) glucose, and treated with different concentrations of metformin (0 mM, 0.5 mM, and 3 mM) for 48 hours. Graph is normalized to high glucose with 0 mM metformin for all high glucose treatments and low glucose without metformin, low glucose treatments are normalized to low glucose. qPCR data are shown as RGE.

The relative gene expression of SW1116 with metformin treatments (Figure 3.23) shows mostly downregulation of the different genes and different treatments, the biggest exception is UCP2, which has a high upregulation of 3 mM metformin treatment in high glucose, and a small upregulation in low glucose without treatment. MCT4, have a small upregulation for low glucose without treatment, OCT1 have a small upregulation of 0.5 mM treatment in low glucose and SUCLA2 have upregulation of 0.5 mM treatment for both high and low glucose culturing.

3.4.3.1 Cell culturing as 2D and 3D

TaqMan gene expression are used when running 2D and 3D cell lines up against each other, for both SW948 and SW1116. The graph in Figure 3.24 shows the relative gene expression of 3D cell cultures relative to 2D cultures, and are calculated according to section 2.2.11.1.

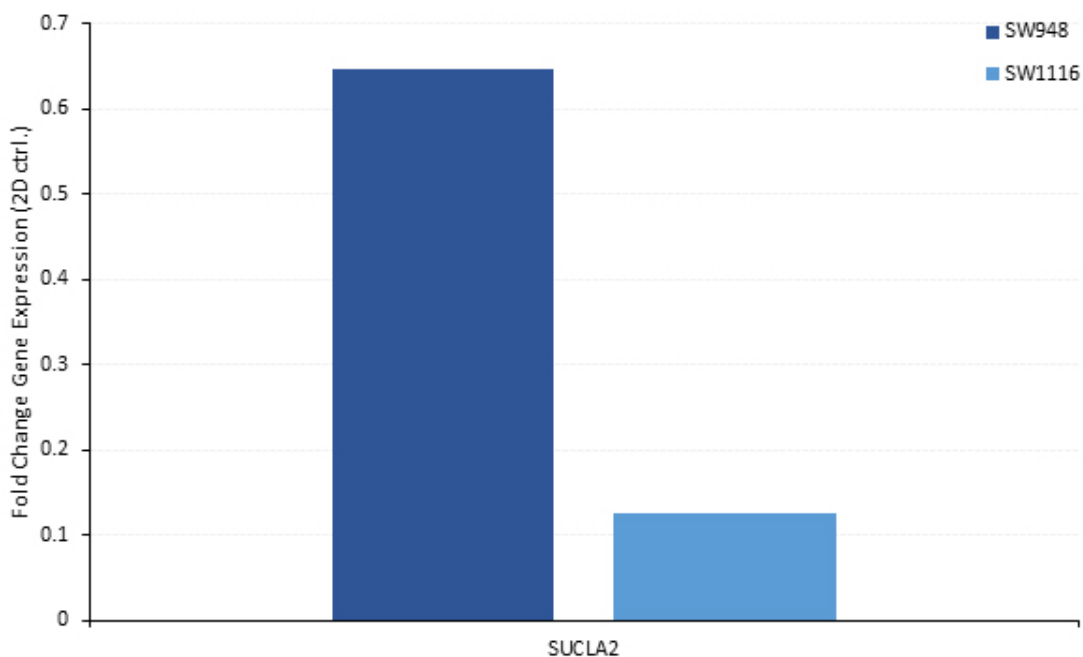


FIGURE 3.24: Relative gene expression for SW948 and SW1116 (2D and 3D). SW948 (Passage n/a, n=1) and SW1116 (Passage n/a, n=1) cultured as normal (2D) and spheroids (3D) cell cultures. The graph are normalized to 2D cultures and qPCR data are shown as RGE.

Two reference genes are used (ACTB and POLR2A) for normalization of the target gene (SUCLA2). The result shows approximately 0.5 higher fold change expression of SUCLA2 in SW948 compared to SW1116.

3.4.4 Relative Gene Expression of Patient Material

The markers validated with cell samplers were tested with patient samples under normal condition as per manufacturer [85]. Unfortunately, the result yielded no or very low amplification with a dilution from 1:5 to 1:5000. Therefore, a lower dilution was tested (1:1 to 1:1000), and still the quantification cycles (Cq) values were from 35 and up.

After exhibiting difficulties with gene expression of patient samples, possible causes were excluded by examination of kits and primers used. Two different kits were tested to check the reason behind the poor amplification of patient samples. First a reverse transcription kit (High-Capacity cDNA Reverse Transcription (Applied Biosystems)) was tested to check if the cDNA synthesis affected the quality, then a SYBR Green kit (QuantiTect SYBR Green PCR Kit) was tested. Both kits were tested by running patient material alongside cell RNA, and none of these kit

improved amplification of patient samples. To check if the primers were the reason for the low or no amplification, TaqMan assays were tested with the same sample material and cell line RNA, which also did not improve the expression of patient samples.

3.4.4.1 Patient Sample Quality

Due to the low gene expression of the patient samples, a few of them were analyzed with a bioanalyzer (Agilent 2100) as described in section 2.2.10, to check the RNA quality. The samples analyzed, were chosen based on their concentration measured with the NanoDrop (section 2.2.4); four with high concentration, four with middle range concentration and four with low concentration. In total twelve patient samples, half with normal tissue (Table 3.4), the other half with tumor tissue (Table 3.5).

TABLE 3.4: Bioanalyzer result for normal tissue samples. RNA area, RNA concentration, rRNA Ratio (28s/18s) and RNA integrity number (RIN), obtained with Agilent 2100 Bioanalyzer.

	163N	169N	162N	189N	191N	179N
RNA Area	299.6	141.7	31.7	19.9	84.8	213.3
RNA Concentration (ng/ μ l)	297	140	31	20	84	211
rRNA Ratio [28s / 18s]	0	0	1.3	1.3	0.9	0.3
RNA Integrity Number (RIN)	2.6	2.9	1.9	N/A	3.5	2.5

TABLE 3.5: Bioanalyzer result for tumor tissue samples. RNA area, RNA concentration, rRNA Ratio (28s/18s) and RNA integrity number (RIN), obtained with Agilent 2100 Bioanalyzer.

	199(M)T	168T	072T	151T	181T	062T
RNA Area	115.4	229.3	8.1	7.9	175.9	133.4
RNA Concentration (ng/ μ l)	114	227	8	8	174	132
rRNA Ratio [28s / 18s]	0.5	0.2	0.8	0.2	0.4	0.8
RNA Integrity Number (RIN)	2.4	2.6	N/A	N/A	2.6	2.7

The graphs and gel analysis from the quality analysis done with the bioanalyzer are presented in Appendix F. The Tables above (Table 3.4 and Table 3.5), present the data from the analysis, with RNA area, RNA concentration, rRNA Ratio and RNA Integrity Number (RIN). RIN is not available (N/A) for three of the samples; 189N, 072T and 151T, the rest of the RIN numbers are low, less than four, which indicate highly degraded RNA samples. This analysis shows the reason why the amplification of patient samples yielded no or very low amplification.

3.4.5 Pre-Amplification

Since the quantification of patient samples were not possible due to low amount of amplifying template, pre-amplification of cDNA was tested. To check if the pre-amplification works, the pre-amplification are done with the EMT markers, two metabolic markers (LDHA and LDHB), and BIRC5 with SW948 (P14, n=1) cultured in high glucose only. The cDNA was run with different dilutions on a plate without preamplification, and a plate with preamplification.

The differences between their Cq values are calculate and presented in Figure 3.25, with an average line. A few of the markers did not express (CDH2, TWIST1, VIM), and some of the markers did not express on the larger dilutions, but on the lower dilutions. On average the pre-amplification improved the Cq values with 8 cycles for SW948.

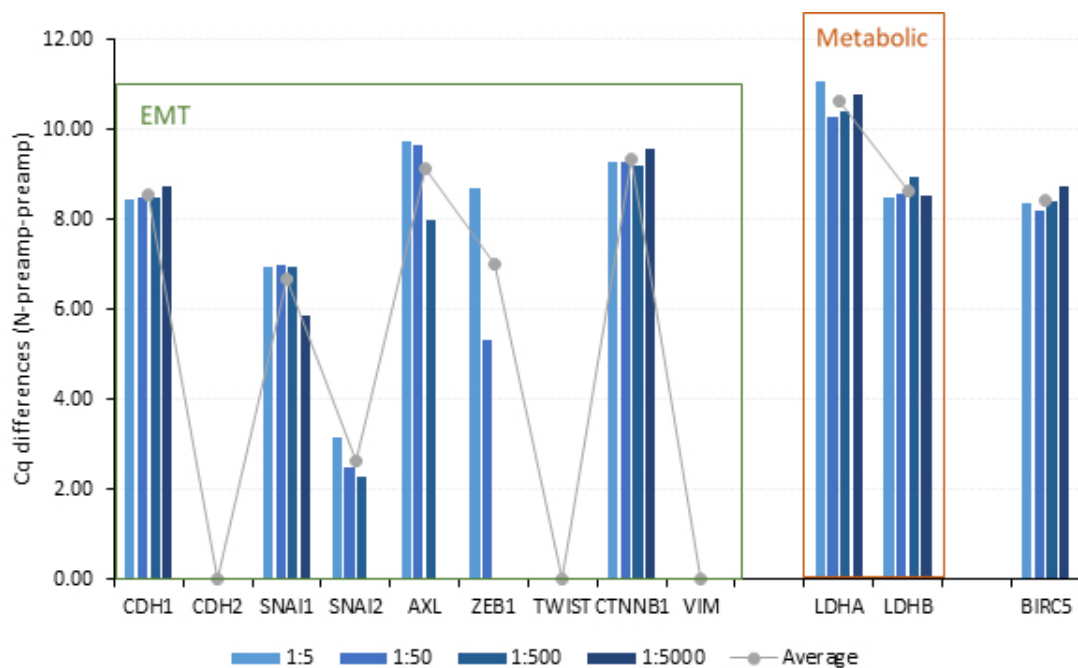


FIGURE 3.25: Cq differences for pre-amplification. Cq differences between no pre-amplification and pre-amplification dilution series (1:5-1:5000) for high glucose SW948 (P14, n=1).

The pre-amplification analysis was tested for patient samples, but it did not yield any improvement of quantification cycle, thus the pre-amplification neither did not work on patient samples used in this study.

Chapter 4

Discussion

4.1 Cell Culture

4.1.1 Viability and Proliferation Related to Glucose Levels

The analysis is done with Muse Cell Analyzer (Merck Millipore) using the Muse Count & Viability kit (Merck Millipore). The reagent contains two DNA binding dyes, a DNA-binding dye that stains cells that have lost their membrane integrity by staining the nucleus of dead and dying cells, and a membrane-permeant DNA staining dye that stains all cells with a nucleus [73].

The viability profile of the two colon cancer cell lines, SW948 and SW1116, are relative stable between themselves and different conditions, but if they are compared differences in viability are observed. SW948 have a viability percentage around 92-97%, while SW1116 have a viability percentage around 79-83%. This is probably due to their differences in metabolic characterization, SW948 are shown rely highly on glycolysis, and SW1116 relies more on oxidative phosphorylation (OXPHOS) (unpublished work from CORE research group). The glycolytic profile are often increased in cancer cells, even when oxygen is present (Warburg effect), which is required for cancer cells increased cell division, growth and migration properties [28, 86]. Even though most cancer cells mostly rely on glycolysis as their energy producing pathway. Studies have shown that some cancer cells, like glioma cells, breast carcinoma cells, pancreatic cancer cells, either can switch from aerobic glycolysis to OXPHOS, or are depended on oxidative phosphorylation for ATP formation [87–89]. Which most likely are the reason for the higher viability for SW948 cell cultured in glucose medium compared to SW1116.

According to Leibovitz *et al.* SW1116 have a generation time of 163 hours around passage 3, and SW948 have a generation time of 153 hours around passage 4, both of which have been cultured in Leibovitz's L-15 Medium [90]. The L-15 Medium substitute galactose for glucose, which is known to change the cells metabolism from being more dependent on oxidative phosphorylation (OXPHOS) to become glycolytic in several cell lines [91]. Therefore, using galactose as primary carbon source increases the proliferation rates for the different cell lines, while glucose in the media decreases the rates of proliferation [92]. The highest generation rates for SW1116 and SW948 obtained in this study are from different culturing conditions, high glucose for SW1116, and low glucose for SW948, which probably are due to their metabolic profiles, and their carbon source. SW1116 relies less on glucose in for their growth compared to the glycolytic dependent SW948. Differences in proliferation of the different glucose conditions for the various cells could be an indicator of variant activation levels of metabolic pathways involved in tumor growth, of special interest are the PI3K pathway if considering its ability to localize GLUT1 at the plasma membrane.

4.1.2 Wound Healing Related to Glucose Levels

Epithelial cells (SW1116 and SW948) forms monolayers when cultured in flasks or plates, and these cells are not mobile, while fibroblast (CCD-18Co) do not form monolayers, however, migrate slowly as individual cells. The different cell lines use different amount of time to start growing back together in the lesion made. The fibroblast uses approximately 20 hours, in both glucose concentrations, which was expected because of its migratory properties. This is lower than the results obtained by Saini *et al.* and Qiao *et al.*, where the cells needed more than 24 hours to grow back, but there is no mention of what size of pipette tip was used to make the scratch [93, 94]. Thereby, the initial scratch size might be greater than used in this study. SW1116 on the other hand used approximately one week to start grow back in to the wound inflicted, for both high and low glucose. This length of time for the wound to start repairing, are longer than 48 hours as observed by Zhao *et al.*, but they used a 10 μ l pipette tip to inflict the wound, which would make the wound smaller, and the cells grow earlier back together [95].

It seemed like the morphology of SW948 changed during wound healing, where the cells start growing on top of each other, forming multilayers, before they start detaching from the plates (Figure 3.11 in section 3.1.2). The multilayer formation are present in both high and low glucose conditions, but detaching from the wells is more frequently observed in high glucose, than low glucose. Research done by Chiricolo

et al. on wound healing for transfected SW948, with mock-transfected and untransfected SW948 used as controls, shows that both controls still have clearly visible wounds after 6 days, and also showing signs of multilayers instead of monolayers [96]. Which could indicate that formation of multilayer growth of the cells reduces the ability to heal wounds. A reasons for the multilayer growth could be that the 6-well plates (vacuum-gas plasma-treated for achieve consistent cell attachment and growth), are damaged during the scratch with the pipette tip, which seems unlikely since the other cells lines grows nicely after inflicted wound. SW948 could be more affected by the scraping, and thereby not growing together in a monolayer, but rather forming multilayers.

4.2 Multiplex PCR

EMAST markers are highly polymorphic tetranucleotides, and it is therefore important to compare the tumor sample to a corresponding normal sample. A polymorphic marker has a large number of alleles with different sizes between individuals and between alleles of the same person [97]. MSI markers are quasimonomorphic mononucleotides, which means that the markers have almost always alleles at the same size in any normal DNA [97].

The results presented in section 3.2 is a small cohort size, and it is not possible to draw any conclusions, only few indications based on the analysis. Five different EMAST and MSI markers are used with 5' fluorescently labeling to separate them by the fragment analyzer. The samples that came out as MSI-H, are also categorized as EMAST positive, which is also indicated in previous research [98, 99]. EMAST is a biomarker for loss of MSH3 function in DNA mismatch repair within cells, which can occur with mutations in MSI-H colorectal cancers [14]. MSH3 dysfunctions are often associated with advanced CRC and poorer survival rates, and it seems to develop as a consequence of inflammation [14]. Most of the samples are microsatellite stable (MSS), which means none of the markers were unstable for the tumor sample (MSI), and EMAST- denotes less than 2 unstable markers. A few were not analyzed or the analysis failed, because the analysis was inconclusive, due to no good identification of some of the markers. This can happen if the DNA sample is too small or too much diluted, and the peaks are not when performing the analysis.

4.3 Reference genes stability analysis

Stable reference genes across conditions are important for qPCR analysis. The quantification cycles (Cq) over high and low glucose are done for the three reference genes, ACTB, RRN-18S and HSP90AB, separated by different cell lines. In all cell lines the distribution of Cq values increases from RRN-18S, followed by ACTB, and lastly HSP90AB.

HSP90AB is the most stable reference gene across both colon cancer cell lines and the fibroblastic colon cell line. The two other reference genes, RRN-18S and ACTB present as the two worst, with RRN-18S as the worst for all cell lines, but especially for CCD-18Co, where the M value (geNorm algorithm) are higher than 0.5, this result are also presented in in an evaluation study by Sørby *et al.* within colon cancer [100].

4.4 Validation of Quantitative PCR analysis

In this study, a multimarker mRNA panel comprised of metabolic and EMT markers are used to cover a wide range of genes that can indicate colorectal cancer risk, presence or metastasis. The expression of markers separated on different cell lines are presented in Figure 3.15, where some of the markers are more expressed than others. Within EMT markers, fibroblast are the cell line with all but one marker expressed (E-cadherin (CDH1)), which are expressed in epithelial colon cancer cells. During cancer, the expression switches between E- and N-cadherin (CDH2), thereby exhibiting epithelial and mesenchymal phenotype, respectfully [63].

All the 20 markers were also validated for qPCR by obtaining standard curves (Appendix C) and calculating their efficiencies (Table 3.2 and Figure 3.17), as recommended in the MIQE guidelines [101]. Most of the markers had efficiencies within the range of $100 \pm 10\%$, except, LDHA (74.02%), TWIST1 (82.10%), and SLUG (87.28%). The PCR efficiency on important indicator of the performance of the assay, and therefore may inaccurate estimations leads to over- or underestimation of the relative gene expression [102].

4.5 Quantitative PCR analysis

4.5.1 Cell Samples

Normal cells primarily relies on mitochondrial oxidative phosphorylation (OXPHOS) for energy consumption, as it generates more adenosine triphosphate (ATP) than glycolysis. However, cancer cells often shift their metabolic profile, to aerobic glycolysis even under non-hypoxic conditions, which is known as the Warburg effect [103].

Glycolysis only produces two ATPs, and pyruvate is the end product, which fuels OXPHOS, thus are the two metabolic profiles tightly coupled (Figure 1.2). Under hypoxic conditions are pyruvate reduced to lactate, by lactate dehydrogenase (LDH) in the cytoplasm, before the lactate is excreted into extracellular space through monocarboxylate transporters (MCTs). While under normal aerobic conditions pyruvate enters mitochondria to be oxidized to acetyl CoA that together with oxaloacetate starts the tricarboxylic acid (TCA) cycle and OXPHOS, which can produce 36 ATPs.

Cancer cells takes up glucose at a high rate for glycolysis, but they may change their metabolic phenotype to adapt to changes in the microenvironment, giving cancer cells an advantage under unfavorable environment [104]. However, not all cancer cells primarily rely on glycolysis, some are shown to exhibit an OXPHOS phenotype [105]. The two colon cancers used in this study also exhibiting different metabolic phenotype, SW948 are highly dependent on glycolysis, and SW1116 are more OXPHOS dependent. Excess of glucose could drive cells to a metabolic shift from oxidative phosphorylation to glycolysis in cancer cells, thereby gaining invasive and rapid proliferation properties [106].

As shown in this study both GLUT1 and MCT4 exhibiting the opposite gene expressions between the two colon cancer cell lines. Meaning that one cell line upregulates the genes, while the other cell line downregulates the same gene. In SW948 the relative expression between physiological glucose and high glucose after culturing the cells for 48 hours, are significant different for GLUT1 expression. By adding the stress of an afflicted wound to SW1116 the relative gene expression of MCT4 are significant different. These observations could confirm that these cells do obtain different metabolic profile, and when GLUT1 is upregulated in low glucose for SW948 it could indicate that the cells obtain its glycolytic profile, while SW1116 being downregulated could indicate that the cells shift to a more glycolytic phenotype [107]. The monocarboxylate transporter 4 (MCT4), transport lactate from

the cytoplasm, and if glycolysis is more active, lactate dehydrogenase A and/or B (LDHA/B) more rapidly produces lactate. Thus increasing the transporter protein to remove excess lactate from cytoplasm, while compromised glycolysis induces OXPHOS [108]. Inhibition of LDHs are reported to reduce ATP levels and accumulate reactive oxygen species (ROS) and thereby inducing apoptosis [109]. A study on inhibitors of LDHs in pancreatic cancer by Maftouh and colleagues, shows that LDHA increased during anaerobic conditions, while inhibition of LDHA could offer innovative tool in hypoxic tumors [110]. LDHA experience a decrease in relative gene expression (RGE) for SW948 cells, and there is a significant different between the two culturing conditions observed. RGE of LDHA in SW1116 on the other hand changes the expression with longer culturing conditions, increasing the expression for the gene. This indicates that SW1116 are more affected by different glucose concentrations, compared to SW948. Which indicate that this cells changes to a more glycolytic pathway due to an increase in LDHA expression, while SW948 most likely obtain its glycolytic phenotype. The expression of LDHB in SW948 and SW1116 are opposite of each other, one being upregulated, the other one being downregulated. Which again support the findings of two different metabolic pathways within these cells. LDHB gets downregulated after longer culturing for SW948, while the gene are experiencing an upregulation after longer culturing for SW1116. This could be due to their metabolic phenotype shifting to address a higher glucose concentration, by either obtaining a glycolytic or OXPHOS phenotype.

An important part of the oxidative phosphorylation is the electron transport chain (ETC) where electrons are transferred from electron donors to acceptors in redox reactions, which releases energy in as ATP. The reduced form of nicotinamide adenine dinucleotide (NAD), NADH and succinate (produced by succinyl-CoA synthetase (SUCLA2) by conversion of Succinyl-CoA) are generated in the TCA cycle, and oxidized to release energy to power ATP synthase. If SUCLA2 gene are down-regulated the metabolic balance may be disturbed and increased succinate levels could be a result, and previous study have suggested a tumor promoting function [111]. The colon cancer cell lines, SW1116 and SW948, are expressing different levels of SUCLA2. SW948 shows a decreasing level of expression for this gene with longer culturing, while SW1116 shows an increasing level of expression within the same culturing time. Kim *et al.* showed that high glucose levels would lead to a decreased TCA cycle, thereby promote glycolysis, and inhibiting alternative metabolic pathways [112]. Therefore, the increasing in expression of SW1116 could indicate glycolysis are promoted. Expression of UCP2 appears to be consistent with a more glycolytic expression in cells, with an increasing glucose concentration ATP production would be decreased as a consequence of reduced membrane potential, due to the

glycolytic phenotype of the cell [113]. The glycolytic SW948 downregulates UCP2 in physiological glucose, thereby an increase in UCP2 expression are observed for high glucose concentration, indicating that the cells experience a reduction in the membrane potential and ATP production. Esteves *et al.* suggest that UCP2 over-expression are connected to change in their metabolic phenotype, from glycolysis to oxidative phosphorylation (Figure 1.3) [57].

Development of cancer are due to changes in metabolic programs to sustain the cancer cells rapid proliferation, changes connected to the Warburg effect, like up-regulation of glucose uptake and production of lactate [24, 114]. Epithelial to mesenchymal transition (EMT) represents a series of alterations and signals due to the cellular demand from rapid proliferation to survival and metastasis [115]. EMT is active in embryogenesis and tissue repair, where the epithelial cells acquire mesenchymal phenotypes [116]. Pathological EMT occurs when neoplastic epithelial cells are transition to mesenchymal cell for gaining increased mobility, invasiveness and apoptotic resistance [117].

The organic cation transporters role is uptake, intracellular inactivation and urinary/binary excretion of endogenous and exogenous substances, like metformin. OCT1 is also considered as anticancer drug [55]. Metformin diffuse rarely into the cells, but is actively taken up by OCT1 present on cell surface [118]. Decrease in metformin treatments for both cell lines, especially for higher metformin treatments could be explained by higher diffusion rate, thereby lower OCT1 expression. The glucose condition for SW948 do not express any OCT1, and for SW1116 it is down-regulated after 48 hour treatment, then it increases after 72 hours treatment. Which could be a cell response to stress of low glucose over longer periods. A study by Segal and colleagues in 2011 shows that low OCT1 levels limit metformin activity in ovarian cancers [118].

Different biomarker are used to demonstrate EMT in cancer (Figure 1.4) . The colon cancer cell lines shows diverse relative gene expression of E-cadherin and SNAIL, which again can imply their differences in metabolic profiles. E-cadherin create interactions between cells and thereby adhesion between epithelial cells [119]. Suppression of this gene may lead to mesenchymal phenotype of the cells by increasing the cells migration and invasion, thereby inducing metastasis, which are presented in breast cancer studies[120, 121]. The switch between E-cadherin to N-cadherin can be used to monitor EMT progress during cancer progression (Figure 1.1). N-cadherin are not expressed for the two colon cancer cell lines, while expressed in the fibroblastic, CCD-18Co cell line. Indicate that none of the colon cancer cell lines are suppressing E-cadherin, thereby they still contains their epithelial phenotype.

SNAIL and SLUG both represses the expression of the CDH1 gene (encodes for E-cadherin), thereby inducing EMT. SNAIL induced alteration in the cytoskeletal associated with metastasis, and is promoted by activation ERK2 in a study related to breast cancer [122]. SNAIL expression for SW948 are downregulated, while for SW1116 the expression are upregulated, most likely reasoned by their glycolytic and OXPHOS profiles, while SLUG are only upregulated for the fibroblastic CCD-18Co cell line, and not expressed for either of the colon cancer cell lines.

ZEB1 and TWIST1 were also not expressed in SW948 and SW1116, but expressed in CCD-18Co, with downregulation after 48 hour culturing, before an increased expression are observed after 72 hours of culturing. ZEB1 proteins are known to repress E-cadherin expression in breast cancer, thereby inducing EMT [123]. While TWIST1 homo- or heterodimers can bind to E-box sequences and expression of this gene are upregulated during cancer metastasis [124, 125].

Prasad and colleagues published an article in 2009 with supporting evidence that upregulation of Wnt/ β -catenin signalling induces EMT [126]. β -catenin are either located in nucleus or in cytoplasm, the latter reflects its role with E-cadherin. β -catenin have different relative expression of the epithelial cells (SW948 and SW1116) compared to CCD-18Co. The epithelial cell shows a decrease in the expression of β -catenin, while the fibroblast shows an increase in the expression of β -catenin. Reduction in β -catenin resulted in decreased ZEB1 expression and increased E-cadherin expression [127]. Vimentin are associated with migratory properties, and increased expression is a marker for EMT within cancer progression [61]. The VIM gene are not showing any expression for SW1116 and SW948, and the increased expression of CCD-18Co does not seem to change due to different growth conditions or adding of stress related factor by wound healing repair.

AXL receptor tyrosine kinase binds to the vitamin K-dependent ligase Gas6 (growth arrest-specific 6), presented in Figure 1.5XX. AXL regulate several cellular responses such as proliferation and cell survival [128]. The gene are upregulated in cell cultured with the added stress of wound healing repair. No expression are observed in in SW948, while SW1116 expression increases with longer culturing. The fibroblastic cell line shows an increase in expression for both 48 and 72 hours culturing. Activation of this gene is part of many pathways including, MAP kinases and Akt. Vajkoczy *et al.* have shown that inhibition of AXL receptor suppressor growth and invasion of tumor cells [129].

Survivin belongs to a family known as inhibitor of apoptosis protein (IAP), and has is important in regulation of apoptosis and cell division. BIRC5 are regulated highest in G2/M phase in the cell cycle, compared to G2 and S phases, and are normally

very highly expressed in colon cancer [59]. Transcriptional factors, such as p53 are investigated to regulate the expression of this gene in many cancers [130]. Both cancer cell lines expresses this gene with an upregulation after 48 hours conditions, followed by a downregulation after 72 hours treatment. This could be explained by limiting glucose levels, affect the cell cycle, and thereby inducing a downregulation of this gene.

4.5.2 Patient Samples

The RNA extracted from FFPE patient samples were found to be highly degraded by analyzing a selection of samples with a capillary gel electrophoresis. The RNA integrity is a concern when doing gene expression, and as shown in this study the RNA integrity numbers for the samples were low, less than five, which indicates highly degraded samples. Which led to no or low amplification, even with pre-amplification of the cDNA. The sample degradation are most likely due to the fixating with formalin.

Formalin-fixed paraffin-embedded (FFPE) tissue samples are a widely used method for preservation, due to well maintaining morphological features of tissues and tissue components. However, formalin often compromises the DNA and RNA integrity by chemically modifications during the fixation process [131]. N-methylol formations occurs when formaldehyde reacts with RNA, which form crosslinks between amino group due to an electrophilic attach, where the primary target are tertiary amino groups [132]. Crosslinking by formaldehyde and chemical modification of the RNA are consequences of the fixation of tissue sample, RNA fragmentation may occur from a number of different sources, like the duration of formalin fixation, which may be for extensive periods of time (no standard duration of fixation are established), and storage period at room temperature [131].

4.6 Future Perspectives

The multimarker panel chosen could be able to identify if a patient is of increased risk to develop cancer and cancer metastasis, thereby increasing the patients chance of early treatment and possible detection of cancer. A challenge with this panel was the efficiencies of some markers, especially the efficiency of LDHA, which was below 80%. A poor efficiency could be due to the marker itself, not being optimal. LDHA was tested multiple times, with different cell lines and concentrations, but still

yielded low efficiency, even though the manufacturer promise approximately 100% PCR efficiency. If the method for calculating relative gene expression was changed from Livak method [83], to Pfaffl method [133], which corrects for the differences in efficiencies, the relative gene expression values would be more correct for all markers used.

Further research could be conducted to study the metabolic alteration in colon cancer cells with different glucose conditions, by doing different Seahorse tests (Cell Energy Phenotype Test, Glycolysis Stress Test and/or Mito Stress Test). This can also be used to assess the alterations after treating the cells with metformin, or other drugs.

An interesting research topic related barely touched is the normal (2D) and spheroids (3D) cells. Growth of cell spheroids are more similar to how the cells would grow *in vivo*, since the cells are able to grow in all directions, and not only on a flat (2D) surface. By doing spheroids with the same culturing conditions and multimarker panel used in this study, the expression could be more related to the human conditions, and may yield interesting findings.

The main challenge with this study was the RNA integrity of the patient material. To further investigate the biomarker potential for the genes tested, it would be necessary to use fresh frozen tissue for RNA extraction. The preliminary analysis conducted on FFPE samples here in this project clearly shows that RNA is too degraded in formalin fixed samples to be used for gene expression studies. A possibility for FFPE fragmented RNA samples is to use miRNA studies instead, where one could find related miRNA markers to the genes of interest in this project thereby managing to perform this test.

Chapter 5

Conclusion

Based on the different cell culture assays and on the interpretation of gene expression analysis it can be concluded that there is a difference in gene expression in low glucose relative to high glucose for all three different cell lines. The E-cadherin gene can be used to identify epithelial phenotype, while the related N-cadherin, ZEB1, TWIST1 and Vimentin can identify genes with a mesenchymal phenotype, which in the future possible can be used to detect if a patient has an increased risk of cancer metastasis.

GLUT1, LDHA, and MCT4 yielded significantly upregulation of expression in low glucose relative to high glucose. All three genes could together be good biomarkers to determine if an increased dependency on glycolysis as primary energy source, which often is related to more invasive and rapid growing cells. Increased GLUT1 expression could indicate a more rapid glucose transport through the membrane, increasing pyruvate concentration in the cells. Increased pyruvate concentration in the cell could upregulate LDHA, and convert it to lactate acid thereby increasing the acidity within the cell. With accumulation of lactic acid, MCT4 could be upregulated to transport the excess lactic acid out of the cells.

References

- [1] American Cancer Society. Cancer Basics, 2015. <https://www.cancer.org/cancer/cancer-basics.html> (Accessed: 20.12.2017).
- [2] Cancer Today. Cancer Fact Sheets: All Cancers Excluding Non-Melanoma Skin. <http://gco.iarc.fr/today/fact-sheets-cancers> (Accessed: 20.12.2017).
- [3] R. A. Weinberg. *The biology of cancer*. New York: Garland Science, 2007. ISBN 9780815340768.
- [4] Kenneth F. Kiple. *The Cambridge Historical Dictionary of Disease*. Cambridge University Press: New York, 2003. ISBN 9780521808347.
- [5] NORDCAN. The NORDCAN project, 2017. <http://www-dep.iarc.fr/NORDCAN/english/frame.asp> (Accessed: 20.12.2017).
- [6] American Cancer Society. Colorectal Cancer, 2018. <https://www.cancer.org/cancer/colon-rectal-cancer.html> (Accessed: 16.01.2018).
- [7] V. Kumar, A. K. Abbas, and J. C. Aster. *Robbins Basic Pathology*. Philadelphia: Elsevier Saunders, 9 th ed., 2012. ISBN 978-1-4377-1781-6.
- [8] M. S. Wicha and D. F. Hayes. Circulating Tumor Cells: Not All Detected Cells Are Bad and Not All Bad Cells Are Detected. *Journal of Clinical Oncology*, 29(12):1508–1511, 2011. ISSN 0732-183X. doi:10.1200/JCO.2010.34.0026.
- [9] American Joint Committee on Cancer. Colon and Rectum Cancer Staging, 2009. <https://cancerstaging.org/references-tools/quickreferences/Documents/ColonMedium.pdf> (Accessed: 25.03.2018).
- [10] T. Armaghany, J. D. Wilson, Q. Chu, and G. Mills. Genetic Alterations in Colorectal Cancer. *Gastrointest Cancer Res*, 5(1):19–27, 2012. <https://www.ncbi.nlm.nih.gov/pmc/articles/PMC3348713/>.

- [11] H. R. Hagland, M. Berg, I. W. Jolma, A. Carlsen, and K. Søreide. Molecular pathways and cellular metabolism in colorectal cancer. *Digestive surgery*, 30(1):12–25, 2013. doi:10.1159/000347166. <https://www.karger.com/Article/FullText/347166>.
- [12] H. Yamagishi, H. Kuroda, Y. Imai, and H. Hiraishi. Molecular pathogenesis of sporadic colorectal cancers. *Chinese journal of cancer*, 35:4, 2016. doi:10.1186/s40880-015-0066-y. <https://www.ncbi.nlm.nih.gov/pmc/articles/PMC4704376/>.
- [13] J. M. Carethers. Microsatellite Instability Pathway and EMAST in Colorectal Cancer. *Current colorectal cancer reports*, 13(1):73–80, 2017. ISSN 1556-3790. doi:10.1007/s11888-017-0352-y. <https://www.ncbi.nlm.nih.gov/pmc/articles/PMC5373103/>.
- [14] J. M. Carethers, M. Koi, and S. S. Tseng-Rogenski. EMAST is a Form of Microsatellite Instability That is Initiated by Inflammation and Modulates Colorectal Cancer Progression. *Genes*, 6(2):185–205, 2015. ISSN 2073-4425. doi:10.3390/genes6020185. <https://www.ncbi.nlm.nih.gov/pmc/articles/PMC4488660/>.
- [15] C. R. Boland and A. Goel. Microsatellite instability in colorectal cancer. *Gastroenterology*, 138(6):2073–2087.e3, 2010. doi:10.1053/j.gastro.2009.12.064. <https://www.ncbi.nlm.nih.gov/pmc/articles/PMC3037515/>.
- [16] A. Umar *et al.* Revised Bethesda Guidelines for Hereditary Nonpolyposis Colorectal Cancer (Lynch Syndrome) and Microsatellite Instability. *Journal of the National Cancer Institute*, 96(4):261–268, 2004. <https://www.ncbi.nlm.nih.gov/pmc/articles/PMC2933058/>.
- [17] C. R. Boland *et al.* A National Cancer Institute Workshop on Microsatellite Instability for Cancer Detection and Familial Predisposition: Development of International Criteria for the Determination of Microsatellite Instability in Colorectal Cancer. *American Association for Cancer Research*, 58(22):5248–5257, 1998.
- [18] E. N. Mojarad, P. J. K. Kuppen, H. A. Aghdaei, and M. R. Zali. The CpG island methylator phenotype (CIMP) in colorectal cancer. *Gastroenterology and Hepatology*, 6(3):120–128, 2013. <https://www.ncbi.nlm.nih.gov/pmc/articles/PMC4017514/>.
- [19] Y. Komiya and R. Habas. Wnt signal transduction pathways. *Organogenesis*, 4(2):68–75, 2008. ISSN 1547-6278. doi:10.4161/org.4.2.5851.

- [20] R. Nusse. Wnt signaling in disease and in development. *Cell research*, 15(1):28–32, 2005. doi:10.1038/sj.cr.7290260. <https://www.nature.com/articles/7290260>.
- [21] T. Zhan, N. Rindtorff, and M. Boutros. Wnt signaling in cancer. *Oncogene*, 36(11):1461–1473, 2017. doi:10.1038/onc.2016.304. <https://www.nature.com/articles/onc2016304>.
- [22] B. T. MacDonald, K. Tamai, and X. He. Wnt/beta-catenin signaling: components, mechanisms, and diseases. *Developmental cell*, 17(1):9–26, 2009. doi:10.1016/j.devcel.2009.06.016. <https://www.ncbi.nlm.nih.gov/pmc/articles/PMC2861485/>.
- [23] N. Rivlin, R. Brosh, M. Oren, and V. Rotter. Mutations in the p53 Tumor Suppressor Gene: Important Milestones at the Various Steps of Tumorigenesis. *Genes & cancer*, 2(4):466–474, 2011. doi:10.1177/1947601911408889. <https://www.ncbi.nlm.nih.gov/pmc/articles/PMC3135636/>.
- [24] M. G. Vander Heiden, L. C. Cantley, and C. B. Thompson. Understanding the Warburg effect: the metabolic requirements of cell proliferation. *Science*, 324(5930):1029–1033, 2009. ISSN 0036-8075. doi:10.1126/science.1160809. <https://www.ncbi.nlm.nih.gov/pmc/articles/PMC2849637/>.
- [25] V. C. Fogg, N. J. Lanning, and J. P. Mackeigan. Mitochondria in cancer: at the crossroads of life and death. *Chinese journal of cancer*, 30(8):526–539, 2011. doi:10.5732/cjc.011.10018. <https://www.ncbi.nlm.nih.gov/pmc/articles/PMC3336361/>.
- [26] D. Hanahan and R. A. Weinberg. The Hallmarks of Cancer. *Cell*, 100(1):57–70, 2000. ISSN 1097-4172. doi:10.1016/S0092-8674(00)81683-9. [hhttps://www.cell.com/cell/fulltext/S0092-8674\(00\)81683-9](https://www.cell.com/cell/fulltext/S0092-8674(00)81683-9).
- [27] D. Hanahan and R. A. Weinberg. Hallmarks of cancer: the next generation. *Cell*, 144(5):646–674, 2011. ISSN 1097-4172. doi:10.1016/j.cell.2011.02.013. [https://www.cell.com/cell/fulltext/S0092-8674\(11\)00127-9](https://www.cell.com/cell/fulltext/S0092-8674(11)00127-9).
- [28] O. Warburg, F. Wind, and E. Negelein. The Metabolism of Tumors in the Body. *The journal of General Physiology*, 8(6):519–530, 1927.
- [29] O. Warburg. On the Origin of Cancer Cells. *Science*, 123(3191):309–314, 1956. ISSN 0036-8075. doi:10.1126/science.123.3191.309.

- [30] N. Bellance *et al.* Bioenergetics of lung tumors: alteration of mitochondrial biogenesis and respiratory capacity. *The international journal of biochemistry & cell biology*, 41(12):2566–2577, 2009. doi:10.1016/j.biocel.2009.08.012.
- [31] R. J. DeBerardinis, J. J. Lum, G. Hatzivassiliou, and C. B. Thompson. The biology of cancer: metabolic reprogramming fuels cell growth and proliferation. *Cell metabolism*, 7(1):11–20, 2008. ISSN 1550-4131. doi:10.1016/j.cmet.2007.10.002. [https://www.cell.com/cell-metabolism/fulltext/S1550-4131\(07\)00295-1](https://www.cell.com/cell-metabolism/fulltext/S1550-4131(07)00295-1).
- [32] H. R. Hagland *et al.* Targeting mitochondria in the treatment of human cancer: a coordinated attack against cancer cell energy metabolism and signalling. *Expert Opinion on Therapeutic Targets*, 11(8):1055–1069, 2007. doi:10.1517/14728222.11.8.1055.
- [33] J. Lu, L. K. Sharma, and Y. Bai. Implications of mitochondrial DNA mutations and mitochondrial dysfunction in tumorigenesis. *Cell research*, 19(7):802–815, 2009. doi:10.1038/cr.2009.69. <https://www.ncbi.nlm.nih.gov/pmc/articles/PMC4710094/>.
- [34] R. L. Trelstad, E. D. Hay, and J.-P. Revel. Cell contact during early morphogenesis in the chick embryo. *Developmental Biology*, 16(1):78–106, 1967. doi:10.1016/0012-1606(67)90018-8.
- [35] G. Greenburg and E. D. Hay. Epithelia suspended in collagen gels can lose polarity and express characteristics of migrating mesenchymal cells. *Journal of cell biology*, 95(1):333–339, 1982.
- [36] S. Lamouille, J. Xu, and R. Derynck. Molecular mechanisms of epithelial-mesenchymal transition. *Nature reviews Molecular cell biology*, 15(3):178–196, 2014. doi:10.1038/nrm3758. <https://www.ncbi.nlm.nih.gov/pmc/articles/PMC4240281/>.
- [37] H. Acloque, M. S. Adams, K. Fishwick, M. Bronner-Fraser, and M. A. Nieto. Epithelial-mesenchymal transitions: the importance of changing cell state in development and disease. *The Journal of clinical investigation*, 119(6):1438–1449, 2009. ISSN 1558-8238. doi:10.1172/JCI38019. <https://www.ncbi.nlm.nih.gov/pmc/articles/PMC2689100/>.
- [38] R. Kalluri. EMT: When epithelial cells decide to become mesenchymal-like cells. *The Journal of clinical investigation*, 119(6):1417–1419, 2009. ISSN 1558-8238. doi:10.1172/JCI39675. <https://www.ncbi.nlm.nih.gov/pmc/articles/PMC2689122/>.

- [39] R. Kalluri and R. A. Weinberg. The basics of epithelial-mesenchymal transition. *The Journal of clinical investigation*, 119(6):1420–1428, 2009. ISSN 1558-8238. doi:10.1172/JCI39104. <https://www.ncbi.nlm.nih.gov/pmc/articles/PMC2689101/>.
- [40] A. Marble. Diabetes and Cancer. *N Engl J Med*, 211(8):339–349, 1934. doi:10.1056/NEJM193408232110801.
- [41] M. Inoue, M. Iwasaki, T. Otani, S. Sasazuki, and M. Noda. Diabetes Mellitus and the Risk of Cancer: Results From a Large-Scale Population-Based Cohort Study in Japan. *Arch Intern Med*, 166(17):1871–1877, 2006. doi:10.1001/archinte.166.17.1871. <https://jamanetwork.com/journals/jamainternalmedicine/fullarticle/410967>.
- [42] J. A. Meyerhardt *et al.* Impact of diabetes mellitus on outcomes in patients with colon cancer. *Journal of Clinical Oncology*, 21(3):433–440, 2003. ISSN 0732-183X. doi:10.1200/JCO.2003.07.125.
- [43] M.-S. Lee *et al.* Type 2 diabetes increases and metformin reduces total, colorectal, liver and pancreatic cancer incidences in Taiwanese: a representative population prospective cohort study of 800,000 individuals. *BMC cancer*, 11:20, 2011. doi:10.1186/1471-2407-11-20. <https://www.ncbi.nlm.nih.gov/pmc/articles/PMC3031263/>.
- [44] C. J. Currie *et al.* Mortality after incident cancer in people with and without type 2 diabetes: impact of metformin on survival. *Diabetes care*, 35(2):299–304, 2012. doi:10.2337/dc11-1313. <https://www.ncbi.nlm.nih.gov/pmc/articles/PMC3263862/>.
- [45] P. Vigneri, F. Frasca, L. Sciacca, G. Pandini, and R. Vigneri. Diabetes and cancer. *Endocrine-related cancer*, 16(4):1103–1123, 2009. doi:10.1677/ERC-09-0087. <http://erc.endocrinology-journals.org/content/16/4/1103.long>.
- [46] National Cancer Institute. NCI Dictionary of Cancer Terms: Biomarker. <https://www.cancer.gov/publications/dictionaries/cancer-terms/def/biomarker> (Accessed: 19.04.2018).
- [47] Research Advocacy Network. Biomarkers in Cancer: An Introductory Guide for Advocates. http://www.researchadvocacy.org/sites/default/files/resources/BiomarkerinCancer_WebDownloadVersion.pdf (Accessed: 19.04.2018).

- [48] Y.-M. Shen, G. Arbman, B. Olsson, and X.-F. Sun. Overexpression of GLUT1 in colorectal cancer is independently associated with poor prognosis. *The International journal of biological markers*, 26(3):166–172, 2011. doi:10.5301/JBM.2011.8550.
- [49] R. S. Brown and R. L. Wahl. Overexpression of Glut-1 Glucose Transporter in Human Breast Cancer: An Immunohistochemical Study. *Cancer*, 72(10):2979–2985, 1993.
- [50] T. Yamamoto *et al.* Over-expression of facilitative glucose transporter genes in human cancer. *Biochem Biophys Res Commun*, 170(1):223–230, 1990.
- [51] F.-Y. Chung *et al.* GLUT1 gene is a potential hypoxic marker in colorectal cancer patients. *BMC cancer*, 9:241, 2009. doi:10.1186/1471-2407-9-241. <https://www.ncbi.nlm.nih.gov/pmc/articles/PMC3087329/>.
- [52] T. N. Price, N. V. Jackson, and P. A. Halestrap. Cloning and sequencing of four new mammalian monocarboxylate transporter (MCT) homologues confirms the existence of a transporter family with an ancient past. *Biochemical Journal*, 329(2):321–328, 1998. doi:10.1042/bj3290321. <https://www.ncbi.nlm.nih.gov/pmc/articles/PMC1219047/>.
- [53] P. Miao, S. Sheng, X. Sun, J. Liu, and G. Huang. Lactate dehydrogenase A in cancer: a promising target for diagnosis and therapy. *International Union of Biochemistry and Molecular Biology*, 65(11):904–910, 2013. doi:10.1002/iub.1216.
- [54] E. Desideri, R. Vegliante, and M. R. Ciriolo. Mitochondrial dysfunctions in cancer: genetic defects and oncogenic signaling impinging on TCA cycle activity. *Cancer letters*, 356(2 Pt A):217–223, 2015. doi:10.1016/j.canlet.2014.02.023.
- [55] M. Heise *et al.* Downregulation of organic cation transporters OCT1 (SLC22A1) and OCT3 (SLC22A3) in human hepatocellular carcinoma and their prognostic significance. *BMC cancer*, 12:109, 2012. doi:10.1186/1471-2407-12-109. <https://bmccancer.biomedcentral.com/articles/10.1186/1471-2407-12-109>.
- [56] R. Pryor and F. Cabreiro. Repurposing metformin: an old drug with new tricks in its binding pockets. *The Biochemical journal*, 471(3):307–322, 2015. doi:10.1042/BJ20150497. <https://www.ncbi.nlm.nih.gov/pmc/articles/PMC4613459/>.

- [57] P. Esteves, C. Pecqueur, and M.-C. Alves-Guerra. UCP2 induces metabolic reprogramming to inhibit proliferation of cancer cells. *Molecular & cellular oncology*, 2(1):e975024, 2015. ISSN 2372-3556. doi:10.4161/23723556.2014.975024. <https://www.ncbi.nlm.nih.gov/pmc/articles/PMC4905249/>.
- [58] D. Robbins and Y. Zhao. New aspects of mitochondrial Uncoupling Proteins (UCPs) and their roles in tumorigenesis. *International journal of molecular sciences*, 12(8):5285–5293, 2011. doi:10.3390/ijms12085285. <https://www.ncbi.nlm.nih.gov/pmc/articles/PMC3179165/>.
- [59] N. K. Sah, Z. Khan, G. J. Khan, and P. S. Bisen. Structural, functional and therapeutic biology of survivin. *Cancer letters*, 244(2):164–171, 2006. doi:10.1016/j.canlet.2006.03.007.
- [60] G. Ambrosini, C. Adida, and D. C. Altieri. A novel anti-apoptosis gene, survivin, expressed in cancer and lymphoma. *Nature Medicine*, 3:917–921, 1997. doi:10.1038/nm0897-917.
- [61] M. Zeisberg and E. G. Neilson. Biomarkers for epithelial-mesenchymal transitions. *The Journal of clinical investigation*, 119(6):1429–1437, 2009. ISSN 1558-8238. doi:10.1172/JCI36183. <https://www.ncbi.nlm.nih.gov/pmc/articles/PMC2689132/>.
- [62] P. J. Morin. β -catenin signaling and cancer. *BioEssays*, 21(12):1021–1030, 1999. doi:10.1002/(SICI)1521-1878(199912)22:1<1021::AID-BIES6>3.0.CO;2-P.
- [63] R. B. Hazan, R. Qiao, R. Keren, I. Badano, and K. Suyama. Cadherin Switch in Tumor Progression. *Annals of the New York Academy of Sciences*, 1014(1):155–163, 2004. ISSN 00778923. doi:10.1196/annals.1294.016.
- [64] D. Olmeda *et al.* Snail and Snai2 collaborate on tumor growth and metastasis properties of mouse skin carcinoma cell lines. *Oncogene*, 27:4690–4701, 2008. doi:10.1038/onc.2008.118. <https://www.nature.com/articles/onc2008118>.
- [65] Y. Chen and T. Gridley. The SNAI1 and SNAI2 proteins occupy their own and each other’s promoter during chondrogenesis. *Biochemical and Biophysical Research Communications*, 435(3):356–360, 2013. ISSN 0006291X. doi:10.1016/j.bbrc.2013.04.086. <https://www.ncbi.nlm.nih.gov/pmc/articles/PMC3717576/>.

- [66] R. Ganesan, E. Mallets, and J. Gomez-Cambronero. The transcription factors Slug (SNAI2) and Snail (SNAI1) regulate phospholipase D (PLD) promoter in opposite ways towards cancer cell invasion. *Molecular oncology*, 10(5):663–676, 2016. doi:10.1016/j.molonc.2015.12.006. <https://www.ncbi.nlm.nih.gov/pmc/articles/PMC4870114/>.
- [67] P. Zhang, Y. Sun, and L. Ma. ZEB1: At the crossroads of epithelial-mesenchymal transition, metastasis and therapy resistance. *Cell cycle (Georgetown, Tex.)*, 14(4):481–487, 2015. doi:10.1080/15384101.2015.1006048. <https://www.ncbi.nlm.nih.gov/pmc/articles/PMC4614883/>.
- [68] Q. Qin, Y. Xu, T. He, C. Qin, and J. Xu. Normal and disease-related biological functions of Twist1 and underlying molecular mechanisms. *Cell research*, 22(1):90–106, 2012. doi:10.1038/cr.2011.144. <https://www.nature.com/articles/cr2011144>.
- [69] A. Satelli and S. Li. Vimentin as a potential molecular target in cancer therapy Or Vimentin, an overview and its potential as a molecular target for cancer therapy. *Cellular and molecular life sciences*, 68(18):3033–3046, 2011. doi:10.1007/s00018-011-0735-1. <https://www.ncbi.nlm.nih.gov/pmc/articles/PMC3162105/>.
- [70] E. B. Rankin and A. J. Giaccia. The Receptor Tyrosine Kinase AXL in Cancer Progression. *Cancers*, 8(11), 2016. ISSN 2072-6694. doi:10.3390/cancers8110103. <https://www.ncbi.nlm.nih.gov/pmc/articles/PMC5126763/>.
- [71] G. Zhang, M. Wang, H. Zhao, and W. Cui. Function of Axl receptor tyrosine kinase in non-small cell lung cancer. *Oncology letters*, 15(3):2726–2734, 2018. ISSN 1792-1074. doi:10.3892/ol.2017.7694. <https://www.ncbi.nlm.nih.gov/pmc/articles/PMC5778882/>.
- [72] Laboroptik. Information about Counting Chamber (Hemocytometer). <http://www.lo-laboroptik.de/englisch/info/info.html> (Accessed: 17.03.18).
- [73] M. Millipore. Muse™ Count & Viability Kit User’s Guide. 2013.
- [74] QIAGEN. RNeasy® Mini Handbook: For purification of total RNA from animal cells, animal tissues, bacteria, and yeast, and for RNA cleanup. 2012.
- [75] QIAGEN. AllPrep DNA/RNA FFPE Kit Handbook: For simultaneous purification of genomic DNA and total RNA (including small RNAs) from formalin-fixed, paraffin-embedded tissue sections. 2017.

- [76] Thermo Fisher Scientific. NanoDrop One User Guide: NanoDrop Micro-UV/Vis Spectrophotometers. 2016.
- [77] QIAGEN. QuantiTect® Reverse Transcription Handbook: For cDNA synthesis with integrated removal of genomic DNA contamination. For use in real-time two-step RT-PCR. 2009.
- [78] QIAGEN. Type-it® Microsatellite PCR Handbook: For reliable multiplex PCR-based analysis of microsatellites without the need for optimization. 2009.
- [79] Bio-Rad. SsoAdvanced PreAmp Supemix. 2000.
- [80] J. Vandesompele *et al.* Accurate normalization of real-time quantitative RT-PCR data by geometric averaging of multiple internal control genes. *Genome Biology*, 3(7), 2002. <https://www.ncbi.nlm.nih.gov/pmc/articles/PMC126239/>.
- [81] B. Kozera and M. Rapacz. Reference genes in real-time PCR. *Journal of applied genetics*, 54(4):391–406, 2013. doi:10.1007/s13353-013-0173-x. <https://www.ncbi.nlm.nih.gov/pmc/articles/PMC3825189/>.
- [82] Agilent Technologies. Agilent RNA 6000 Nano Kit Guide. 2013.
- [83] K. J. Livak and T. D. Schmittgen. Analysis of relative gene expression data using real-time quantitative PCR and the 2(-Delta Delta C(T)) Method. *Methods*, 25(4):402–408, 2001. ISSN 10462023. doi:10.1006/meth.2001.1262.
- [84] J. E. N. Jonkman *et al.* An introduction to the wound healing assay using live-cell microscopy. *Cell Adhesion & Migration*, 8(5):440–451, 2014. ISSN 1933-6926. doi:10.4161/cam.36224. <https://www.ncbi.nlm.nih.gov/pmc/articles/PMC5154238/>.
- [85] QIAGEN. QuantiTect® SYBR® Green PCR Handbook: For quantitative, real-time PCR and two-step RT-PCR using SYBR Green I. 2011.
- [86] T. Shiraishi *et al.* Glycolysis is the primary bioenergetic pathway for cell motility and cytoskeletal remodeling in human prostate and breast cancer cells. *Oncotarget*, 6(1), 2015. doi:10.18632/oncotarget.2766. <https://www.ncbi.nlm.nih.gov/pmc/articles/PMC4381583/>.
- [87] C. E. Griguer, C. R. Oliva, and G. Y. Gillespie. Glucose Metabolism Heterogeneity in Human and Mouse Malignant Glioma Cell Lines. *Journal of Neuro-Oncology*, 74(2):123–133, 2005. ISSN 0167-594X. doi:10.1007/s11060-004-6404-6.

- [88] R. Rossignol *et al.* Energy Substrate Modulates Mitochondrial Structure and Oxidative Capacity in Cancer Cells. *Cancer research*, 64:985–993, 2004. ISSN 1538-7445. doi:10.1158/0008-5472.CAN-03-1101. <http://cancerres.aacrjournals.org/content/64/3/985.long>.
- [89] K. Smolková *et al.* Mitochondrial bioenergetic adaptations of breast cancer cells to aglycemia and hypoxia. *Journal of Bioenergetics and Biomembranes*, 42(1):55–67, 2010. ISSN 0145-479X. doi:10.1007/s10863-009-9267-x.
- [90] A. Leibovitz *et al.* Classification of Human Colorectal Adenocarcinoma Cell Lines. *Cancer research*, 36(12):4562–4569, 1976. ISSN 1538-7445. <http://cancerres.aacrjournals.org/content/36/12/4562.long>.
- [91] C. Aguer *et al.* Galactose Enhances Oxidative Metabolism and Reveals Mitochondrial Dysfunction in Human Primary Muscle Cells. *PloS one*, 6(12):e28536, 2011. doi:10.1371/journal.pone.0028536. <https://www.ncbi.nlm.nih.gov/pmc/articles/PMC3240634/>.
- [92] A. N. Brodsky, J. Zhang, R. P. Visconti, and S. W. Harcum. Expansion of mesenchymal stem cells under atmospheric carbon dioxide. *Biotechnology Progress*, 29(5):1298–1306, 2013. doi:10.1002/btpr.1782. <https://www.ncbi.nlm.nih.gov/pmc/articles/PMC3902052/>.
- [93] J. Qiao, Z. Liu, C. Yang, L. Gu, and D. Deng. SRF promotes gastric cancer metastasis through stromal fibroblasts in an SDF1-CXCR4-dependent manner. *Oncotarget*, 7(29):46088–46099, 2016. doi:10.18632/oncotarget.10024. <https://www.ncbi.nlm.nih.gov/pmc/articles/PMC5216783/>.
- [94] S. Saini, T. Liu, and J. Yoo. TNF- α stimulates colonic myofibroblast migration via COX-2 and Hsp27. *Journal of Surgical Research*, 204(1):145–152, 2016. ISSN 00224804. doi:10.1016/j.jss.2016.04.034. <https://www.ncbi.nlm.nih.gov/pmc/articles/PMC5391874/>.
- [95] J. Zhao *et al.* Cadherin-12 contributes to tumorigenicity in colorectal cancer by promoting migration, invasion, adhesion and angiogenesis. *Journal of translational medicine*, 11:288, 2013. doi:10.1186/1479-5876-11-288. <https://www.ncbi.nlm.nih.gov/pmc/articles/PMC3879717/>.
- [96] M. Chiricolo, N. Malagolini, S. Bonfiglioli, and F. Dall’Olio. Phenotypic changes induced by expression of beta-galactoside alpha2,6 sialyltransferase I in the human colon cancer cell line SW948. *Glycobiology*, 16(2):146–154, 2006. ISSN 0959-6658. doi:10.1093/glycob/cwj045. <https://academic.oup.com/glycob/article/16/2/146/592345>.

- [97] O. Buhard, N. Suraweera, A. Lectard, A. Duval, and R. Hamelin. Quasi-monomorphic Mononucleotide Repeats for High-Level Microsatellite Instability Analysis. *Disease Markers*, 20(4-5):251–257, 2004. ISSN 0278-0240. doi:10.1155/2004/159347. <https://www.ncbi.nlm.nih.gov/pmc/articles/PMC3888729/>.
- [98] K. Yamada *et al.* Microsatellite instability at tetranucleotide repeats in sporadic colorectal cancer in Japan. *Oncol Rep*, 23(2):551–561, 2010. doi:10.3892/or.00000669. <https://www.ncbi.nlm.nih.gov/pmc/articles/PMC2846616/>.
- [99] Y. Hamaya *et al.* Efficacy of Adjuvant 5-Fluorouracil Therapy for Patients with EMAST-Positive Stage II/III Colorectal Cancer. *PLOS ONE*, 10(5):e0127591, 2015. doi:10.1371/journal.pone.0127591. <https://www.ncbi.nlm.nih.gov/pmc/articles/PMC4440728/>.
- [100] L. A. Sørby, S. N. Andersen, I. R. K. Bukholm, and M. B. Jacobsen. Evaluation of suitable reference genes for normalization of real-time reverse transcription PCR analysis in colon cancer. *Journal of experimental & clinical cancer research : CR*, 29:144, 2010. doi:10.1186/1756-9966-29-144. <https://www.ncbi.nlm.nih.gov/pmc/articles/PMC2988724/>.
- [101] S. A. Bustin *et al.* The MIQE guidelines: Minimum Information for Publication of Quantitative Real-Time PCR Experiments. *Clinical chemistry*, 55(4):611–622, 2009. doi:10.1373/clinchem.2008.112797. <http://clinchem.aaccjnl.org/content/55/4/611.long>.
- [102] D. Svec, A. Tichopad, V. Novosadova, M. W. Pfaffl, and M. Kubista. How good is a PCR efficiency estimate: Recommendations for precise and robust qPCR efficiency assessments. *Biomolecular Detection and Quantification*, 3:9–16, 2015. ISSN 22147535. doi:10.1016/j.bdq.2015.01.005. <https://www.sciencedirect.com/science/article/pii/S2214753515000169>.
- [103] W. H. Koppenol, P. L. Bounds, and C. V. Dang. Otto Warburg’s contributions to current concepts of cancer metabolism. *Nature Reviews Cancer*, 11(5):325–337, 2011. ISSN 1474-175X. doi:10.1038/nrc3038.
- [104] A. Marusyk and K. Polyak. Tumor heterogeneity: Causes and consequences. *Biochimica et Biophysica Acta (BBA) - Reviews on Cancer*, 1805(1):105–117, 2010. ISSN 0304419X. doi:10.1016/j.bbcan.2009.11.002. <https://www.ncbi.nlm.nih.gov/pmc/articles/PMC2814927/>.

- [105] J. I. ZHENG. Energy metabolism of cancer: Glycolysis versus oxidative phosphorylation (Review). *Oncology letters*, 4(6):1151–1157, 2012. ISSN 1792-1074. doi:10.3892/ol.2012.928. <https://www.ncbi.nlm.nih.gov/pmc/articles/PMC3506713/>.
- [106] P. S. Ward and C. B. Thompson. Metabolic Reprogramming: A Cancer Hallmark Even Warburg Did Not Anticipate. *Cancer Cell*, 21(3):297–308, 2012. ISSN 15356108. doi:10.1016/j.ccr.2012.02.014. <https://www.ncbi.nlm.nih.gov/pmc/articles/PMC3311998/>.
- [107] M. Liu, J. Gao, Q. Huang, Y. Jin, and Z. Wei. Downregulating microRNA-144 mediates a metabolic shift in lung cancer cells by regulating GLUT1 expression. *Oncology letters*, 11(6):3772–3776, 2016. ISSN 1792-1074. doi:10.3892/ol.2016.4468. <https://www.ncbi.nlm.nih.gov/pmc/articles/PMC4888127/>.
- [108] G. Baek *et al.* MCT4 Defines a Glycolytic Subtype of Pancreatic Cancer with Poor Prognosis and Unique Metabolic Dependencies. *Cell Reports*, 9(6):2233–2249, 2014. ISSN 22111247. doi:10.1016/j.celrep.2014.11.025. <https://www.sciencedirect.com/science/article/pii/S2211124714009917>.
- [109] A. Le *et al.* Inhibition of lactate dehydrogenase A induces oxidative stress and inhibits tumor progression. *Proceedings of the National Academy of Sciences*, 107(5):2037–2042, 2010. ISSN 0027-8424. doi:10.1073/pnas.0914433107. <http://www.pnas.org/content/107/5/2037>.
- [110] M. Maftouh *et al.* Synergistic interaction of novel lactate dehydrogenase inhibitors with gemcitabine against pancreatic cancer cells in hypoxia. *British Journal of Cancer*, 110(1):172–182, 2014. ISSN 0007-0920. doi:10.1038/bjc.2013.681. <https://www.ncbi.nlm.nih.gov/pmc/articles/PMC3887288/>.
- [111] A. King, M. A. Selak, and E. Gottlieb. Succinate dehydrogenase and fumarate hydratase: linking mitochondrial dysfunction and cancer. *Oncogene*, 25(34):4675–4682, 2006. doi:10.1038/sj.onc.1209594. <https://www.nature.com/articles/1209594>.
- [112] E. S. Kim, F. Isoda, I. Kurland, and C. V. Mobbs. Glucose-induced metabolic memory in Schwann cells: prevention by PPAR agonists. *Endocrinology*, 154(9):3054–3066, 2013. doi:10.1210/en.2013-1097. <https://www.ncbi.nlm.nih.gov/pmc/articles/PMC5393331/>.
- [113] F. Bouillaud. UCP2, not a physiologically relevant uncoupler but a glucose sparing switch impacting ROS production and glucose sensing. *Biochimica et Biophysica Acta (BBA) - Bioenergetics*, 1787(5):377–383, 2009. ISSN

00052728. doi:10.1016/j.bbabbio.2009.01.003. <https://www.sciencedirect.com/science/article/pii/S0005272809000103>.
- [114] L. K. Boroughs and R. J. DeBerardinis. Metabolic pathways promoting cancer cell survival and growth. *Nature Cell Biology*, 17(4):351–359, 2015. ISSN 1465-7392. doi:10.1038/ncb3124. <https://www.ncbi.nlm.nih.gov/pmc/articles/PMC4939711/>.
- [115] F. Liu, L.-N. Gu, B.-E. Shan, C.-Z. Geng, and M.-X. Sang. Biomarkers for EMT and MET in breast cancer: An update. *Oncology letters*, 12(6):4869–4876, 2016. ISSN 1792-1074. doi:10.3892/ol.2016.5369. <https://www.ncbi.nlm.nih.gov/pmc/articles/PMC5228449/>.
- [116] J. P. Thiery, H. Acloque, R. Y. J. Huang, and M. A. Nieto. Epithelial-mesenchymal transitions in development and disease. *Cell*, 139(5):871–890, 2009. ISSN 1097-4172. doi:10.1016/j.cell.2009.11.007. [https://www.cell.com/cell/fulltext/S0092-8674\(09\)01419-6](https://www.cell.com/cell/fulltext/S0092-8674(09)01419-6).
- [117] K. Polyak and R. A. Weinberg. Transitions between epithelial and mesenchymal states: acquisition of malignant and stem cell traits. *Nature Reviews Cancer*, 9(4):265–273, 2009. ISSN 1474-175X. doi:10.1038/nrc2620.
- [118] E. D. Segal *et al.* Relevance of the OCT1 transporter to the antineoplastic effect of biguanides. *Biochemical and Biophysical Research Communications*, 414(4):694–699, 2011. ISSN 0006291X. doi:10.1016/j.bbrc.2011.09.134.
- [119] U. Cavallaro and G. Christofori. Cell adhesion and signalling by cadherins and Ig-CAMs in cancer. *Nature Reviews Cancer*, 4(2):118–132, 2004. ISSN 1474-175X. doi:10.1038/nrc1276.
- [120] H. Oka *et al.* Expression of E-Cadherin Cell Adhesion Molecules in Human Breast Cancer Tissues and Its Relationship to Metastasis. *Cancer research*, 53(7):1696–1701, 1993. ISSN 1538-7445.
- [121] R. Heimann, F. Lan, R. McBride, and S. Hellman. Separating Favorable from Unfavorable Prognostic Markers in Breast Cancer: The Role of E-Cadherin. *Cancer research*, 60:298–304, 2000. ISSN 1538-7445. <http://cancerres.aacrjournals.org/content/60/2/298.long>.
- [122] B. N. Smith *et al.* Snail Promotes Epithelial Mesenchymal Transition in Breast Cancer Cells in Part via Activation of Nuclear ERK2. *PloS one*, 9(8):e104987, 2014. doi:10.1371/journal.pone.0104987. <https://www.ncbi.nlm.nih.gov/pmc/articles/PMC4133359/>.

- [123] A. Eger *et al.* DeltaEF1 is a transcriptional repressor of E-cadherin and regulates epithelial plasticity in breast cancer cells. *Oncogene*, 24(14):2375–2385, 2005. doi:10.1038/sj.onc.1208429. <https://www.nature.com/articles/1208429>.
- [124] M.-H. Yang *et al.* Direct regulation of TWIST by HIF-1 α promotes metastasis. *Nature Cell Biology*, 10(3):295–305, 2008. ISSN 1465-7392. doi:10.1038/ncb1691.
- [125] W. Yu, H. Kamara, and K. K. H. Svoboda. The role of twist during palate development. *Developmental Dynamics*, 237(10):2716–2725, 2008. ISSN 10588388. doi:10.1002/dvdy.21627.
- [126] C. P. Prasad *et al.* Expression analysis of E-cadherin, Slug and GSK3beta in invasive ductal carcinoma of breast. *BMC cancer*, 9:325, 2009. doi:10.1186/1471-2407-9-325. <https://www.ncbi.nlm.nih.gov/pmc/articles/PMC2753637/>.
- [127] L. Li, C. Liu, R. J. Amato, J. T. Chang, and W. Li. CDKL2 promotes epithelial-mesenchymal transition and breast cancer progression. *Oncotarget*, 5(21), 2014. doi:10.18632/oncotarget.2535. <https://www.ncbi.nlm.nih.gov/pmc/articles/PMC4279414/>.
- [128] R. M. Linger, A. K. Keating, H. S. Earp, and D. K. Graham. TAM Receptor Tyrosine Kinases: Biologic Functions, Signaling, and Potential Therapeutic Targeting in Human Cancer. *Advanced Cancer Research*, 100:35–83, 2008. doi:10.1016/S0065-230X(08)00002-X. <https://www.ncbi.nlm.nih.gov/pmc/articles/PMC3133732/>.
- [129] P. Vajkoczy *et al.* Dominant-negative inhibition of the Axl receptor tyrosine kinase suppresses brain tumor cell growth and invasion and prolongs survival. *Proceedings of the National Academy of Sciences*, 103(15):5799–5804, 2006. ISSN 0027-8424. doi:10.1073/pnas.0510923103. <https://www.ncbi.nlm.nih.gov/pmc/articles/PMC1458653/>.
- [130] A. Mirza *et al.* Human survivin is negatively regulated by wild-type p53 and participates in p53-dependent apoptotic pathway. *Oncogene*, 21:2613 EP–, 2002. doi:10.1038/sj.onc.1205353. <https://www.nature.com/articles/1205353>.
- [131] S. K. Nam *et al.* Effects of Fixation and Storage of Human Tissue Samples on Nucleic Acid Preservation. *Korean Journal of Pathology*, 48(1):36,

2014. ISSN 1738-1843. doi:10.4132/KoreanJPathol.2014.48.1.36. <https://www.ncbi.nlm.nih.gov/pmc/articles/PMC3950233/>.
- [132] M. Srinivasan, D. Sedmak, and S. Jewell. Effect of Fixatives and Tissue Processing on the Content and Integrity of Nucleic Acids. *The American Journal of Pathology*, 161(6):1961–1971, 2002. ISSN 00029440. doi:10.1016/S0002-9440(10)64472-0. <https://www.ncbi.nlm.nih.gov/pmc/articles/PMC1850907/>.
- [133] M. W. Pfaffl. A new mathematical model for relative quantification in real-time RT-PCR. *Nucleic Acids Research*, 29(9):45e–45, 2001. ISSN 0022-1554. doi:10.1093/nar/29.9.e45. <https://www.ncbi.nlm.nih.gov/pmc/articles/PMC55695/>.

Appendix A

Proliferation and Viability

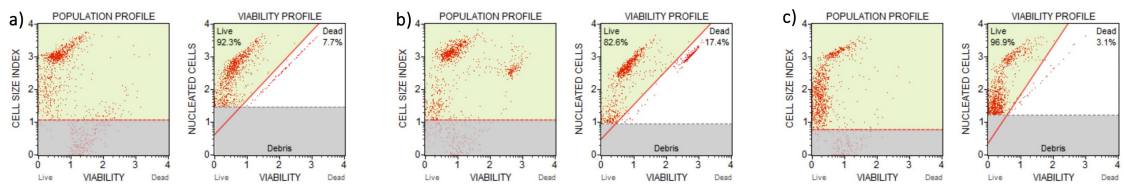


FIGURE 1: Example of population and viability profile for the different cell lines. a) SW948, b) SW1116, c) CCD-18Co, obtained with MUSE cell analyzer and MUSE count and viability kit.

Wound healing

Time	Measurements (%)	
	High glucose	Low glucose
0 h	100 ± 25.10	100 ± 17.81
24 h	75.77 ± 19.65	88.51 ± 15.83
96 h	34.29 ± 20.77	45.09 ± 15.94
~ 192 h	17.03 ± 7.36	19.37 ± 6.17

(A) SW1116 (P18, P19, P14, n=9)

Time	Measurements (%)	
	High glucose	Low glucose
0 h	100 ± 26.65	100 ± 20.20
24 h	86.46 ± 23.87	88.12 ± 18.67
~ 96 h	58.04 ± 16.48	60.86 ± 13.68
~ 188 h	42.53 ± 13.65	17.07 ± 6.40

(B) SW948 (P25, P26, P13, n=9)

Time	Measurements (%)	
	High glucose	Low glucose
0 h	100 ± 15.35	100 ± 13.86
6 h	95.49 ± 10.10	92.60 ± 10.71
20 h	66.38 ± 17.62	52.06 ± 10.15

(c) CCD-18Co (P16, n=6)

TABLE 1: Wound healing measurements. Results are normalized to high (4.5 g/L) and low (1.0 g/L) glucose at 0 hours, a) SW1116, b) SW948, and c) CCD-18Co. Measurements are obtain by analyzing images with ImageJ (wound healing tool).

Appendix B

EMAST analysis

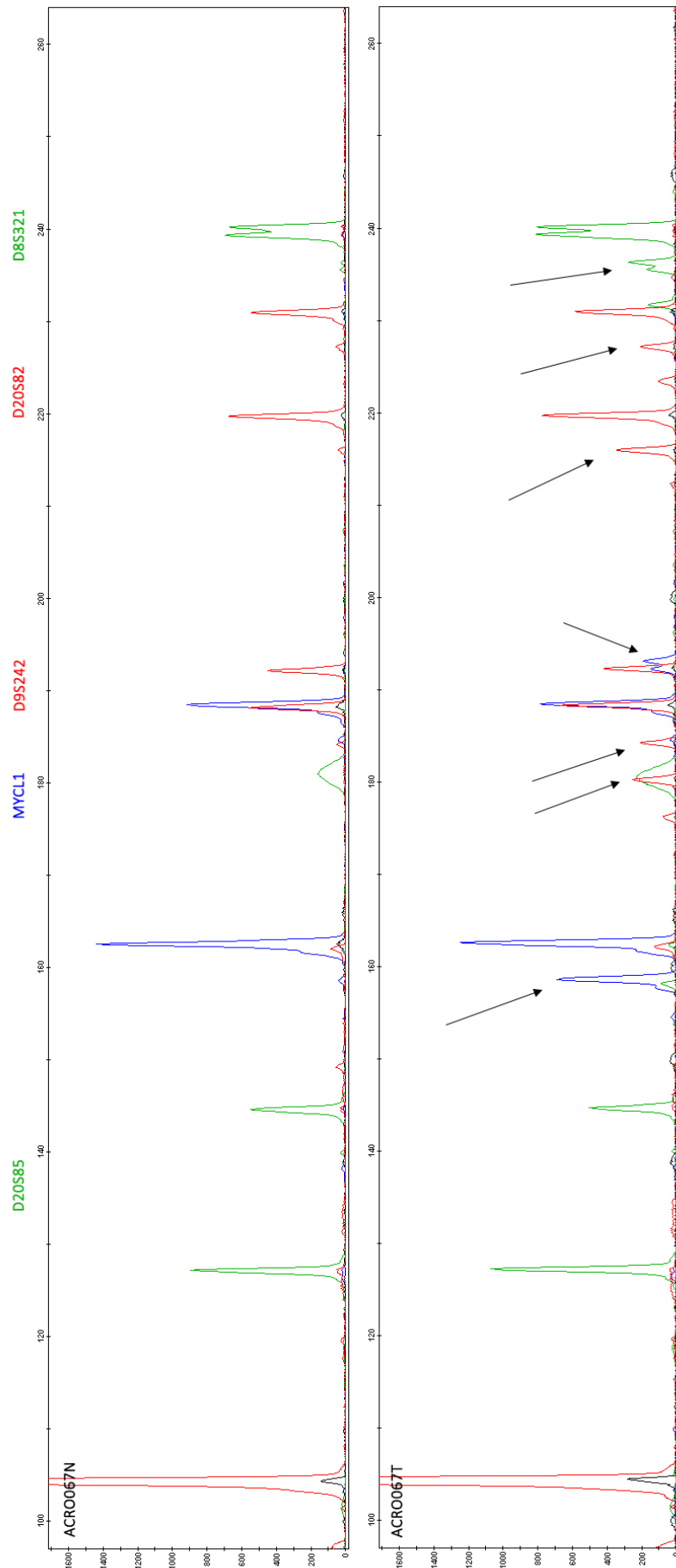


FIGURE 2: EMMAST positive for ACRO067. Arrows presents unstable tetranucleotide markers by extra peaks coming up for tumor sample compared with normal sample. Arrows point at unstable markers.

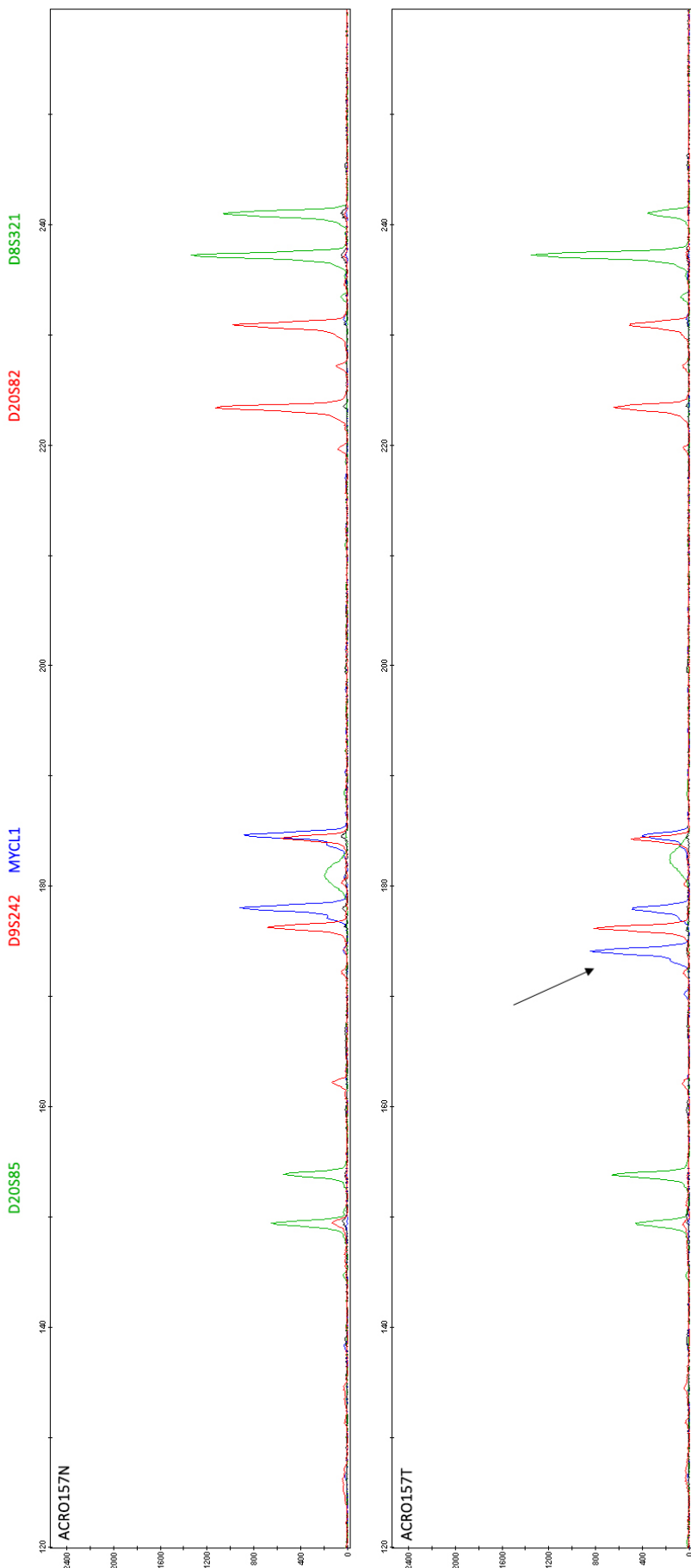


FIGURE 3: EMMA negative for ACRO157. Arrows presents unstable tetranucleotide marker by extra peak coming up for tumor sample compared with normal sample. Arrow point at unstable marker.

MSI analysis

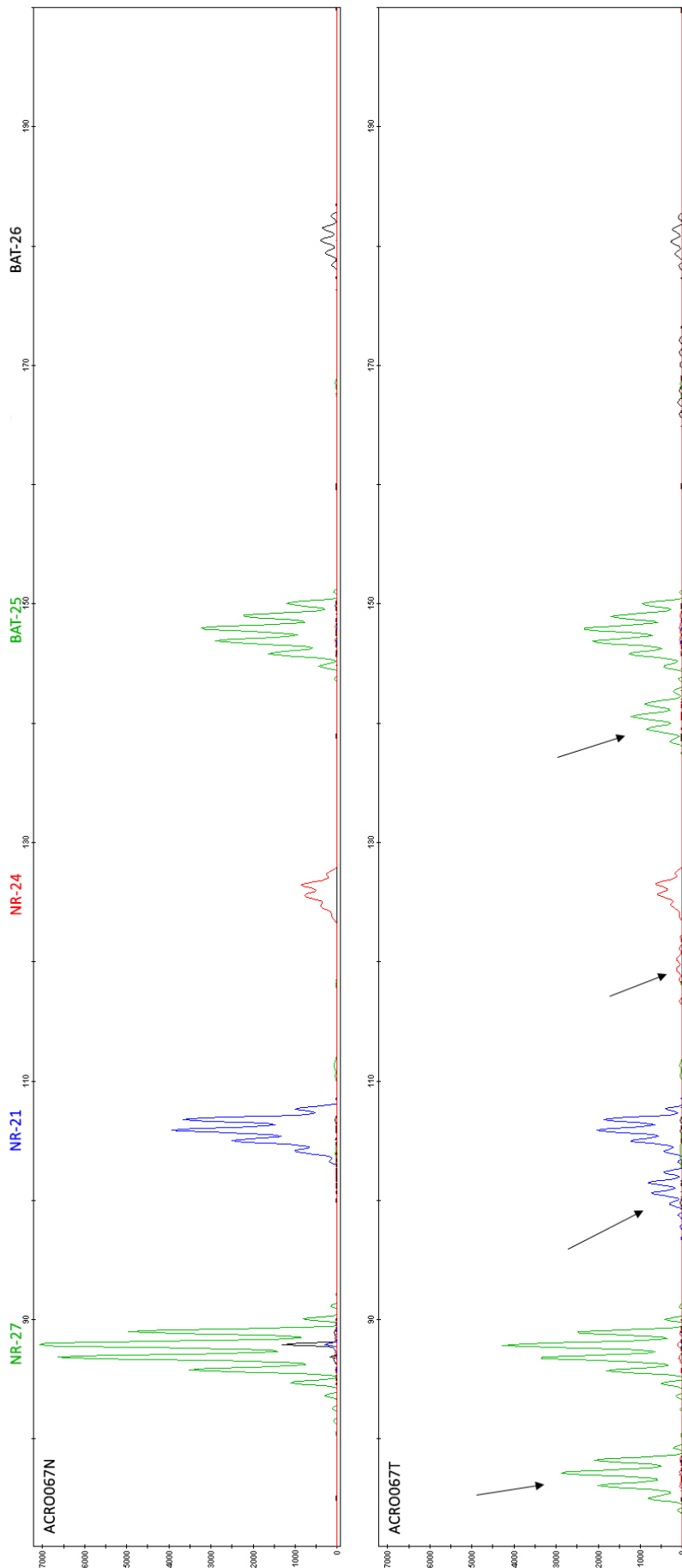


FIGURE 4: MSI-High for ACRO067. Arrows presents unstable mono- and dinucleotide markers by extra peaks coming up for tumor sample compared with normal sample. Arrows point at unstable markers.

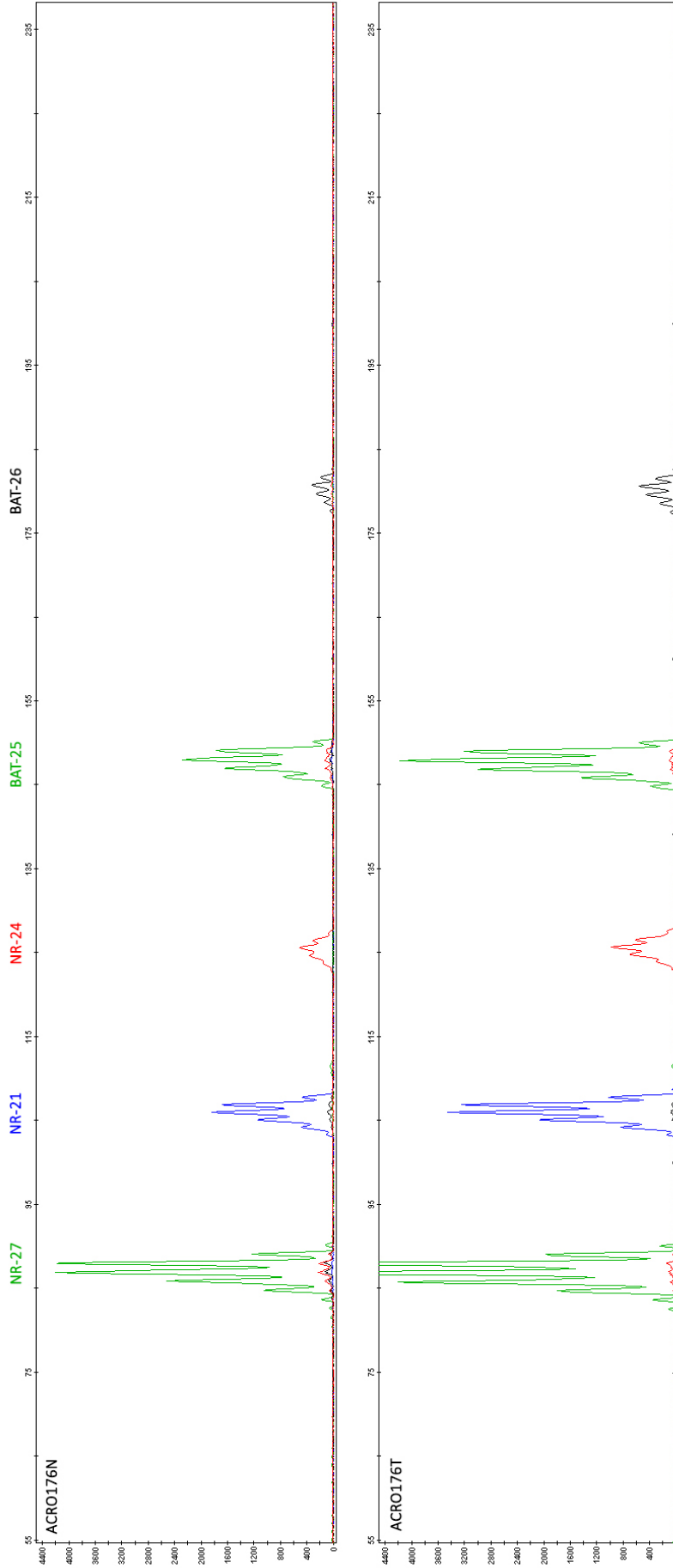


FIGURE 5: Microsatellite stable (MSS) for ACRO067. Normal sample are compared with tumor sample with MSI markers.

Appendix C

TABLE 2: Average expression stability (M) value and coefficient of variation (CV). Obtained for reference genes over different cell lines used in this study, as well as their mean values. Calculated with geNorm from qbase+ software.

Cell type	Gene	M	CV%	Mean M	Mean CV (%)
SW948	RRN	0.394	17.4	0.373	14.8
	ACTB	0.31	9		
	HSP	0.414	18.1		
SW1116	RRN	0.345	15.3	0.341	13.5
	ACTB	0.276	7.5		
	HSP	0.4	17.7		
CCD-18Co	RRN	0.465	18.4	0.487	20.1
	ACTB	0.46	17.2		
	HSP	0.537	24.9		

Appendix D

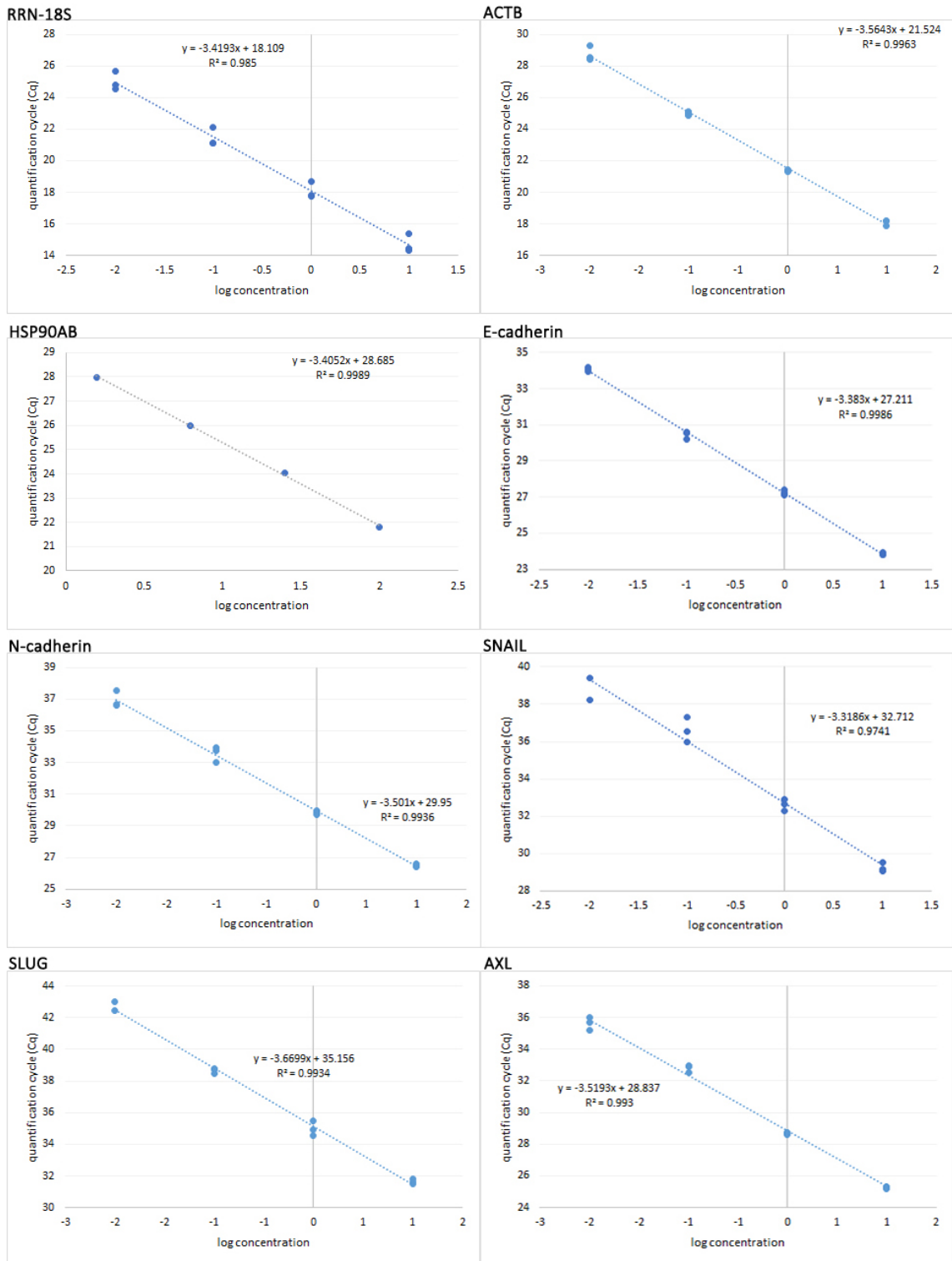


FIGURE 6: Standard curves for SYBR green markers amplification efficiencies (1).

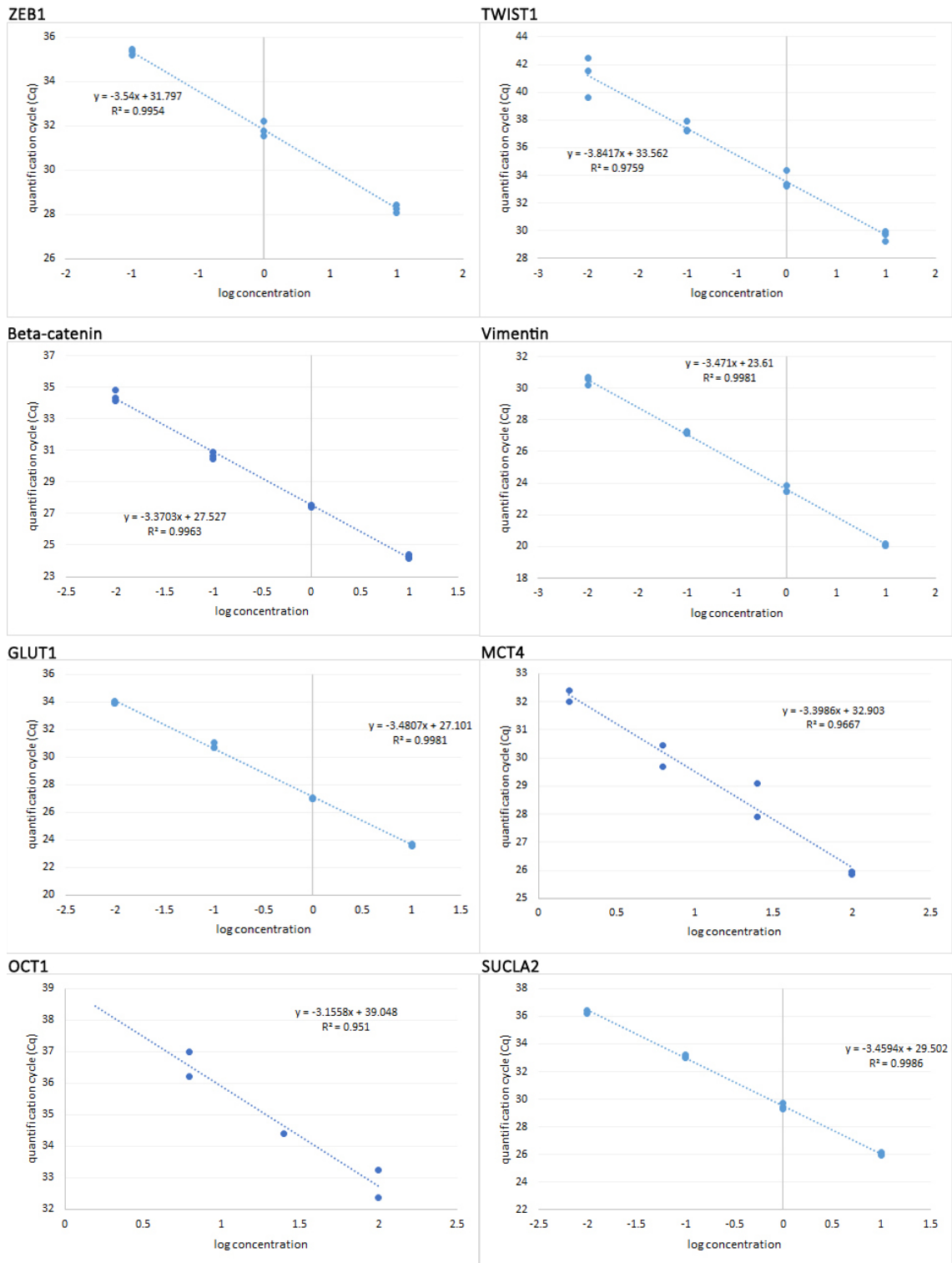


FIGURE 7: Standard curves for SYBR green markers amplification efficiencies (2).

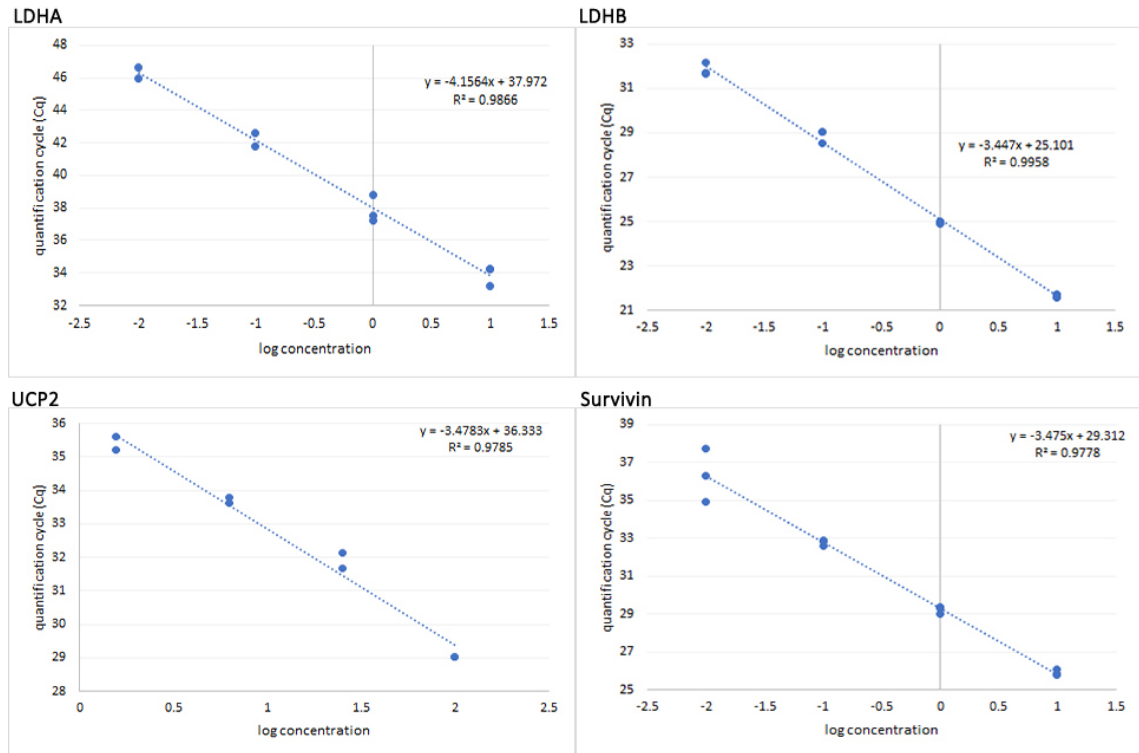


FIGURE 8: Standard curves for SYBR green markers amplification efficiencies (3).

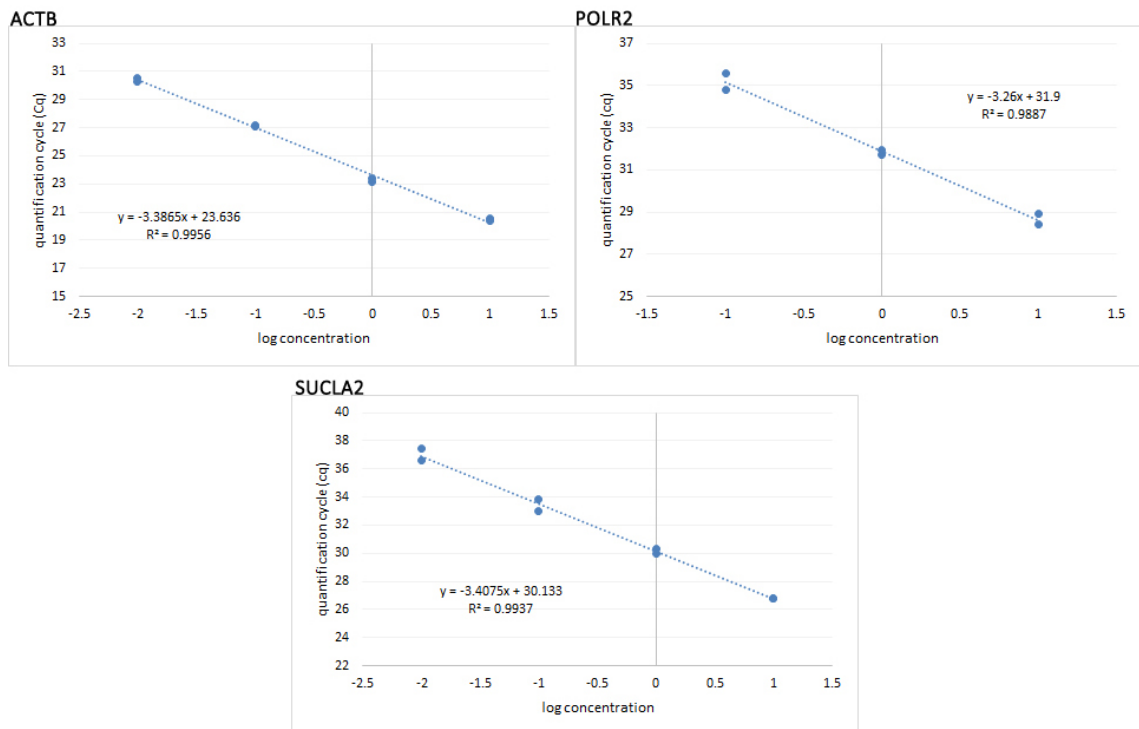


FIGURE 9: Standard curves for TaqMan assays amplification efficiencies

Appendix E

TABLE 3: Relative gene expression of cell lines after 48 hours. Mean RGE, standard deviation and thresholds (3SD above mean) of SW948 (P22, P23, P15, n=3), SW1116 (P20, P22, P17, n=3) and CCD-18Co (P17, only technical replicates) cultured in high (4.5 g/L) and low (1.0 g/L) glucose.

Assay	SW948			SW1116			CCD-18Co		
	Mean	SD	Threshold	Mean	SD	Threshold	Mean	SD	Threshold
E-cadherin	-2.90E-01	1.96E-01	2.97E-01	1.50E-01	1.81E-01	6.93E-01	N/A	N/A	N/A
N-cadherin	N/A	N/A	N/A	N/A	N/A	N/A	-1.57E-03	1.59E-01	4.76E-01
SNAIL	-4.63E-01	2.81E-01	3.79E-01	2.59E-01	8.93E-01	2.94E+00	-1.81E-01	3.20E-01	7.78E-01
SLUG	N/A	N/A	N/A	N/A	N/A	N/A	2.53E-01	5.91E-01	2.03E+00
AXL	N/A	N/A	N/A	-4.46E-02	9.27E-02	2.34E-01	5.04E-02	1.22E-01	4.17E-01
ZEB1	N/A	N/A	N/A	N/A	N/A	N/A	-9.10E-02	1.47E-01	3.49E-01
TWIST1	N/A	N/A	N/A	N/A	N/A	N/A	-2.20E-02	9.93E-02	2.76E-01
β -catenin	-2.53E-01	2.95E-01	6.32E-01	-8.46E-02	3.09E-01	8.44E-01	1.50E-02	8.97E-02	2.84E-01
Vimentin	N/A	N/A	N/A	N/A	N/A	N/A	2.25E-01	1.79E-02	2.79E-01
GLUT1	5.72E-01	7.84E-01	2.92E+00	-5.93E-02	1.89E-01	5.07E-01	-7.26E-02	5.79E-02	1.01E-01
MCT4	-2.15E-01	5.17E-01	1.34E+00	4.91E-01	6.51E-01	2.44E+00	-3.74E-02	6.64E-02	1.62E-01
OCT1	N/A	N/A	N/A	-3.47E-02	4.20E-01	1.23E+00	2.18E-01	7.60E-01	2.50E+00
SUCLA2	3.20E-01	8.18E-01	2.77E+00	-1.28E-01	1.58E-01	3.45E-01	1.07E-03	1.98E-01	5.94E-01
LDHA	-2.05E-01	6.33E-01	1.69E+00	-1.54E-01	1.41E-01	2.70E-01	-3.43E-02	1.00E-01	2.66E-01
LDHB	1.95E-01	6.01E-01	2.00E+00	-1.45E-01	2.26E-01	5.34E-01	1.31E-01	7.20E-02	3.47E-01
UCP2	-5.46E-01	2.14E-01	9.69E-02	3.01E-01	4.59E-01	1.68E+00	4.25E-01	8.03E-01	2.83E+00
Survivin	-2.23E-01	2.98E-01	6.71E-01	-9.79E-02	1.26E-01	2.80E-01	1.59E-01	3.32E-02	2.59E-01

TABLE 4: Relative gene expression of cell lines after 48 hours. Mean RGE, standard deviation and thresholds (3SD above mean) of SW948 (P22, P23, P15, n=3), SW1116 (P20, P22, P17, n=3) and CCD-18Co (P17, only technical replicates) in high (4.5 g/L) and low (1.0 g/L) glucose.

Assay	SW948			SW1116			CCD-18Co		
	Mean	SD	Threshold	Mean	SD	Threshold	Mean	SD	Threshold
E-cadherin	8.91E-02	3.25E-01	1.06E+00	-1.32E-01	3.03E-01	7.76E-01	N/A	N/A	N/A
N-cadherin	N/A	N/A	N/A	N/A	N/A	N/A	3.69E+00	5.56E+00	2.04E+01
SNAIL	-4.74E-01	4.61E-01	9.10E-01	9.81E-02	4.93E-01	1.58E+00	2.52E+00	3.73E+00	1.37E+01
SLUG	N/A	N/A	N/A	N/A	N/A	N/A	1.14E+01	1.88E+01	6.78E+01
AXL	N/A	N/A	N/A	6.58E-02	2.27E-01	7.48E-01	5.08E+00	7.99E+00	2.91E+01
ZEB1	N/A	N/A	N/A	N/A	N/A	N/A	3.94E+00	5.99E+00	2.19E+01
TWIST1	N/A	N/A	N/A	N/A	N/A	N/A	2.06E+00	3.19E+00	1.16E+01
β -catenin	-2.31E-02	4.92E-01	1.45E+00	-1.52E-01	2.58E-01	6.22E-01	4.52E+00	6.72E+00	2.47E+01
Vimentin	N/A	N/A	N/A	N/A	N/A	N/A	4.22E+00	6.67E+00	2.42E+01
GLUT1	3.02E-01	3.46E-01	1.34E+00	-1.89E-01	3.12E-01	7.48E-01	4.53E+00	7.16E+00	2.60E+01
MCT4	1.23E-01	1.05E+00	3.27E+00	-9.28E-02	9.64E-02	1.96E-01	3.76E+00	6.21E+00	2.24E+01
OCT1	N/A	N/A	N/A	1.19E+00	1.12E+00	4.56E+00	-2.09E-01	1.87E-01	3.53E-01
SUCLA2	-2.65E-02	5.59E-01	1.65E+00	2.92E-03	5.29E-01	1.59E+00	4.33E+00	6.93E+00	2.51E+01
LDHA	-7.08E-02	8.47E-01	2.47E+00	2.09E-02	8.84E-01	2.67E+00	2.88E+00	4.26E+00	1.57E+01
LDHB	-2.82E-01	3.94E-01	9.00E-01	1.31E-01	4.71E-01	1.54E+00	4.34E+00	6.84E+00	2.49E+01
UCP2	-4.57E-01	3.60E-01	6.23E-01	-2.30E-02	2.65E-01	7.71E-01	4.58E+00	7.04E+00	2.57E+01
Survivin	-3.25E-01	3.28E-01	6.58E-01	-6.80E-02	2.39E-01	6.48E-01	3.53E+00	4.98E+00	1.85E+01

TABLE 5: Relative gene expression of cell lines after wound healing assay. Mean RGE, standard deviation and thresholds (3SD above mean) of SW1116 (P18, P19, P14, n=3) and CCD-18Co (P16, n=3) cultured for in high (4.5 g/L) and low (1.0 g/L) glucose.

<i>Assay</i>	SW1116			CCD-18Co		
	<i>Mean</i>	<i>SD</i>	<i>Threshold</i>	<i>Mean</i>	<i>SD</i>	<i>Threshold</i>
E-cadherin	3.87E-02	2.22E-01	7.05E-01	N/A	N/A	N/A
N-cadherin	N/A	N/A	N/A	-2.10E-01	1.10E-01	1.21E-01
SNAIL	-1.61E-01	6.71E-02	4.03E-02	1.26E-01	3.05E-01	1.04E+00
SLUG	N/A	N/A	N/A	-4.31E-02	2.43E-01	6.85E-01
AXL	-2.54E-01	1.33E-01	1.46E-01	1.45E-01	1.05E-01	4.59E-01
ZEB1	N/A	N/A	N/A	-9.24E-02	2.08E-01	5.32E-01
TWIST1	N/A	N/A	N/A	6.41E-02	4.32E-01	1.36E+00
β -catenin	-5.26E-03	2.62E-01	7.80E-01	3.34E-02	1.62E-01	5.19E-01
Vimentin	N/A	N/A	N/A	1.20E-01	3.88E-01	1.28E+00
GLUT1	-2.32E-02	3.72E-01	1.09E+00	2.34E-02	1.77E-01	5.53E-01
MCT4	7.62E-01	5.80E-01	2.50E+00	-1.24E-02	6.28E-02	1.76E-01
OCT1	-3.09E-01	2.26E-01	3.68E-01	3.42E-01	9.86E-03	3.71E-01
SUCLA2	4.95E-02	1.22E-01	4.16E-01	1.12E-02	1.54E-01	4.73E-01
LDHA	2.20E-01	6.11E-01	2.05E+00	2.74E-01	5.85E-01	2.03E+00
LDHB	-1.45E-01	9.59E-02	1.43E-01	1.31E-01	4.48E-02	2.65E-01
UCP2	-3.93E-01	1.61E-01	9.07E-02	7.56E-02	5.69E-01	1.78E+00
Survivin	-2.76E-01	3.86E-01	8.83E-01	2.34E-01	2.61E-01	1.02E+00

Appendix F

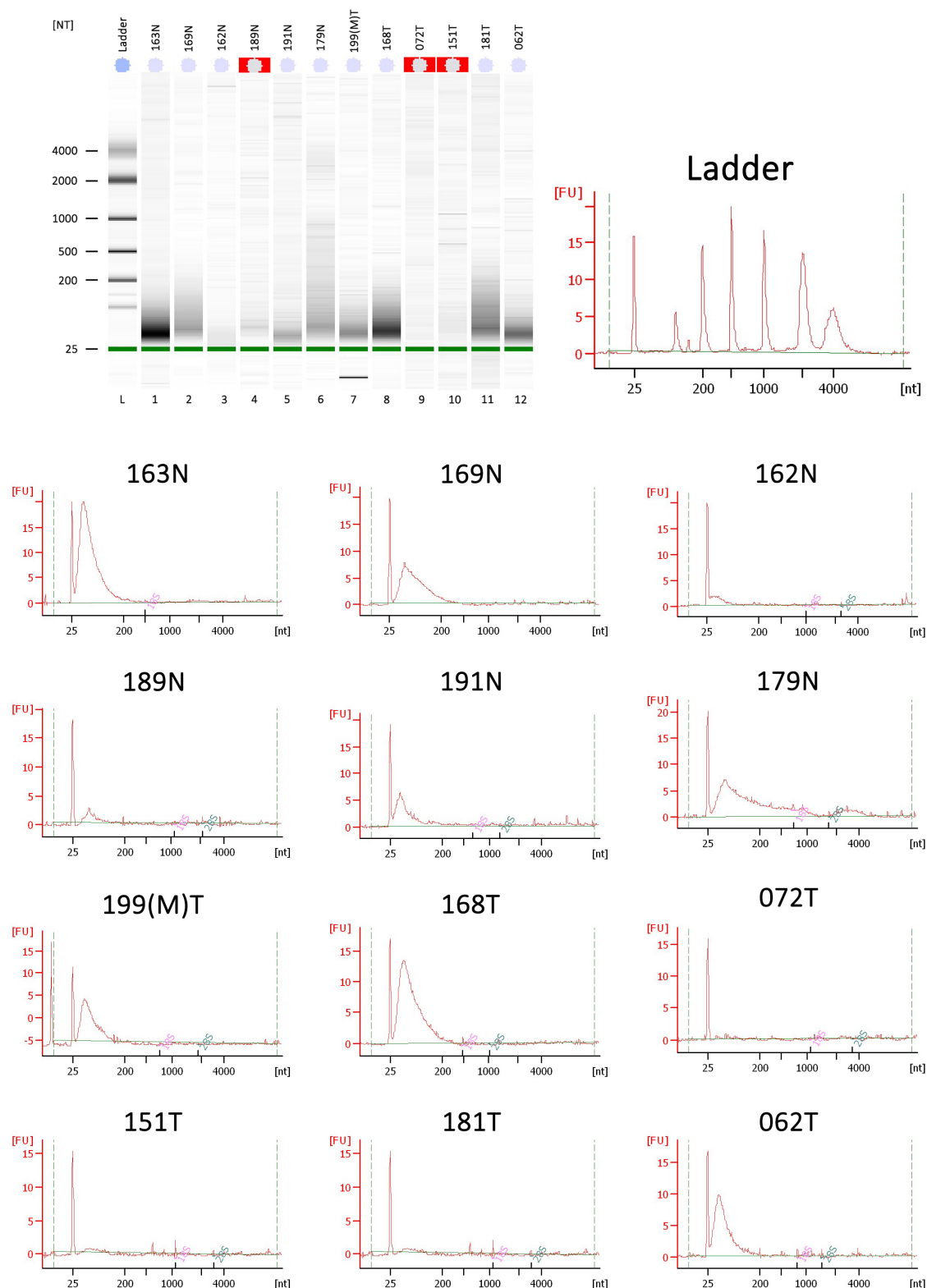


FIGURE 10: RNA integrity analysis. Result of a 12 RNA extracted from FFPE tissue sample blocks, 4 of "good" quality, 4 of "middle" quality and 4 of "bad" quality (determined by NanoDrop measurements).